SPECTROLAB, INC.
Subsidiary of Hughes Aircraft Company

NASA Contractor Report 189215

DEVELOPMENT OF ADVANCED SILICON SOLAR CELLS FOR SPACE STATION FREEDOM

David R. Lillington
Report # 240-746
Spectrolab, Inc.
Sylmar, California

August 9, 1990

Prepared for Lewis Research Center

12500 Gladstone Avenue, Sylmar, California 91342-5373
Telephone: (818) 365-4611; TLX II: 910-496-1750 SPECTILLM SYLM
Telecopier (FAX): (818) 361-5102. (818) 365-7680

REPORT DOCUMENTATION PAGE

Form Approved
OMB No. 0704-0188

1. AGENCY USE ONLY (*Leave blank*)	2. REPORT DATE	3. REPORT TYPE AND DATES COVERED
	August 1990	Final Contractor Report

4. TITLE AND SUBTITLE

Development of Advanced Silicon Solar Cells for Space Station Freedom

5. FUNDING NUMBERS

NAS3-24672

6. AUTHOR(S)

D.R. Lillington

7. PERFORMING ORGANIZATION NAME(S) AND ADDRESS(ES)

Spectrolab, Inc.
12500 Gladstone Ave.
Sylmar, CA 91342

8. PERFORMING ORGANIZATION REPORT NUMBER

240-746

9. SPONSORING/MONITORING AGENCY NAMES(S) AND ADDRESS(ES)

National Aeronautics and Space Administration
Lewis Research Center
Cleveland, Ohio 44135-3191

10. SPONSORING/MONITORING AGENCY REPORT NUMBER

NASA CR- 189215

11. SUPPLEMENTARY NOTES

12a. DISTRIBUTION/AVAILABILITY STATEMENT

Unclassified - Unlimited
Subject Category 44

12b. DISTRIBUTION CODE

13. ABSTRACT (*Maximum 200 words*)

This report describes the development of large area high efficiency wrapthrough solar cells for Space Station FREEDOM. The goal of this contract was the development and fabrication of 8cm x 8cm coplanar back contact solar cells with a minimum output of 1.039 watts/cell.

The first task in this program was a modeling study to determine the optimum configuration of the cell and to study the effects of surface passivation, substrate resistivity and back surface field on the BOL and EOL performances. In addition the optical stack, including the cell cover, AR coatings and Kapton blanket, was modeled to optimize "on orbit" operation.

The second phase was a manufacturing development phase to develop high volume manufacturing processes for the reliable production of low recombination velocity boron back surface fields, techniques to produce smooth, low leakage wrapthrough holes, passivation, photoresist application methods and metallization schemes.

The final portion of this program was a pilot production phase. Seven hundred solar cells were delivered in this phase. At the end of the program, cells with average efficiencies over 13% were being produced with power output in excess of 1.139 watts/cell, thus substantially exceeding the program goal.

14. SUBJECT TERMS	15. NUMBER OF PAGES	16. PRICE CODE
	105	

17. SECURITY CLASSIFICATION OF REPORT	18. SECURITY CLASSIFICATION OF THIS PAGE	19. SECURITY CLASSIFICATION OF ABSTRACT	20. LIMITATION OF ABSTRACT
Unclassified	Unclassified	Unclassified	

TABLE OF CONTENTS

TABLE OF CONTENTS

1.0 INTRODUCTION

This final report describes the development of large area high efficiency wrapthrough solar cells for Space Station FREEDOM under NASA development contract NAS3-24672.

The contract was awarded in September 1985 in which Spectrolab was tasked with developing a 8cm x 8cm coplanar back contact solar cell with a minimum output of 1.039 watts/cell (approximately 12.3% AM0 efficiency taking into account the cropped corners of the cell). The goal for thermal absorptance was 0.63. Specific areas to be addressed were high efficiency, low cost and the ability to manufacture the cell in quantities of 200kw/year or greater.

The program was divided into 3 tasks.

Task 1, which was completed in February 1986 was a modeling study to determine the optimum configuration of the cell and to study the effects of surface passivation, substrate resistivity, and back surface field on the BOL and EOL performances. The merits and demerits of wraparound vs wrapthrough contacts were also evaluated. The task also involved an empirical study to determine the lower limits of thermal absorptance achievable with either a planar or sculptured surface cell. This task was also later modified to include a study to optimize the complete optical stack (cell cover, cell, AR coatings, and Kapton blanket) for "on orbit" operation.

Task II was a manufacturing development phase to develop manufacturing processes compatible with high volume and high efficiency. Specific areas addressed in this task were methods for the reliable production of low recombination velocity boron

back surface fields, techniques to produce smooth, low leakage wrapthrough holes, passivation, photoresist application methods and metallization schemes. In addition work was performed on this application of coverglass considering cost as an important production consideration.

Task III which commenced in June 1987 was originally intended to be a pilot production phase in which 1000 wafers would be started on the manufacturing line to give a minimum of 100 cells with power output greater than 1.039 watts/cell. During this period the software was developed for computer acquisition of I-V curves.

The contract was later modified several times to reflect an increased number of deliverables. Ultimately 700 solar cells were delivered at various times throughout Task III. Some of these cells were filtered with a 6 mil thick borosilicate cover.

Problems associated with process induced minority carrier lifetime degradation in 2 ohm-cm silicon also led to a change from 2 ohm-cm to 10 ohm-cm substrates in the middle of Task III. This resulted in a substantial increase in performance with improved yields. At the end of the program, cells with average efficiencies of over 13% were being produced with power output in excess of 1.139 watts/cell, thus substantially exceeding the program goal.

In Figures 1-1 through 1-3 show the major subtasks in which the program milestones and deliverables are shown. These are discussed in more detail in the sections which follow.

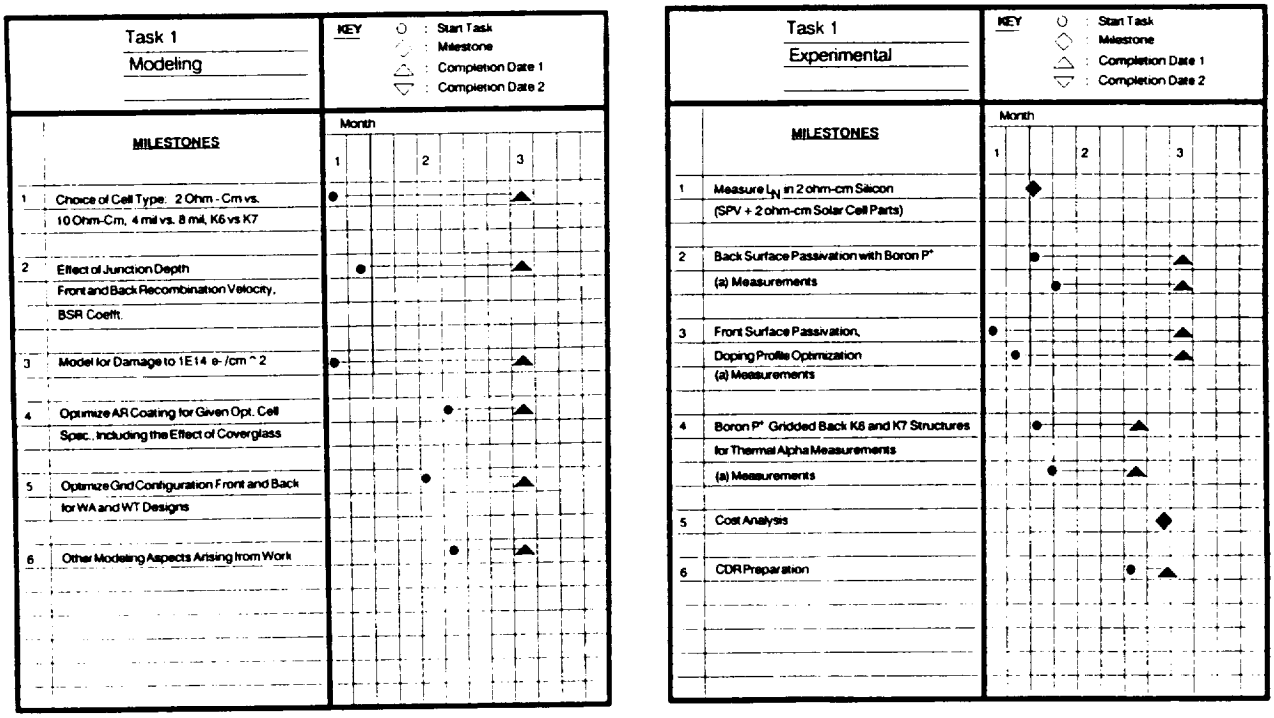

Figure 1-1 MILESTONE SCHEDULE AND DELIVERABLES FOR TASK 1

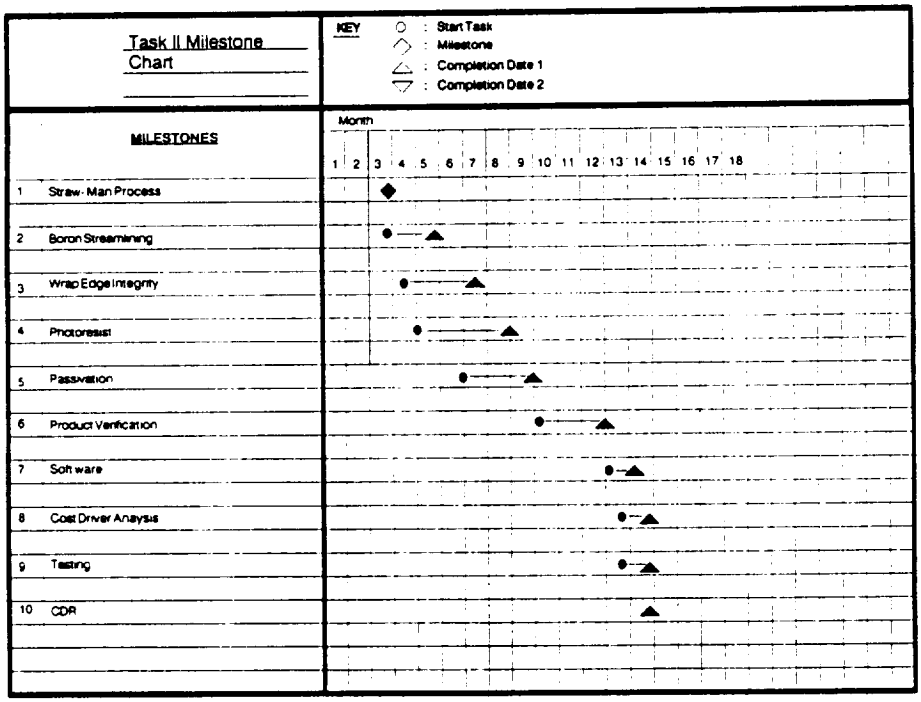

Figure 1-2 MILESTONE SCHEDULE AND DELIVERABLES FOR TASK 2

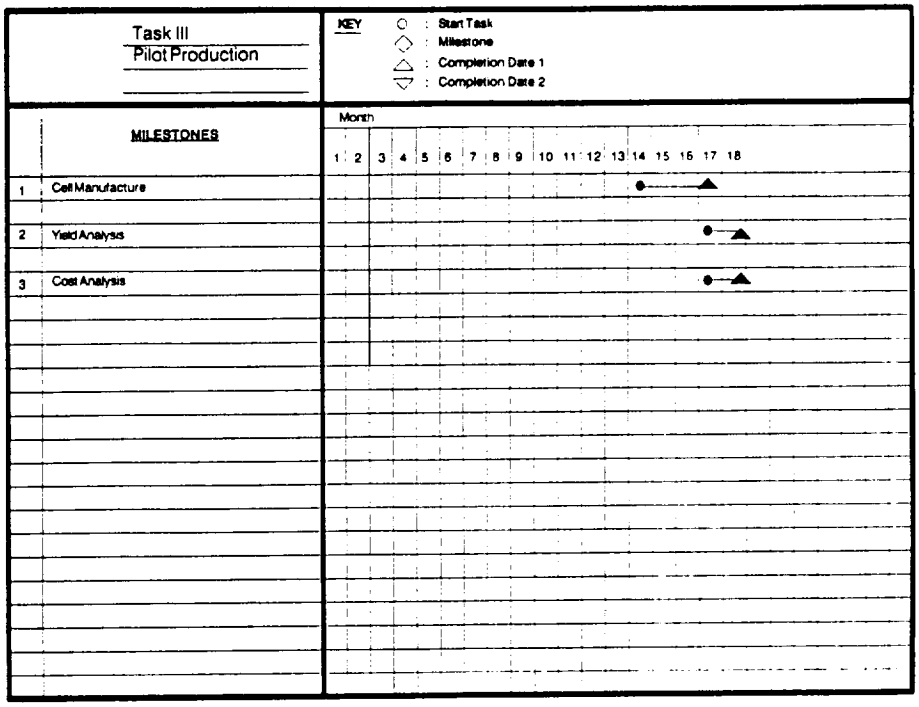

Figure 1-3 MILESTONE SCHEDULE AND DELIVERABLES FOR TASK 3

2.0 TASK I CELL OPTIMIZATION

During this task, cell models were set-up to accurately predict the optimum design for performance over a 10 year period of operation, although modelling was performed up to 1MeV electron fluences of 1E14 cm^{-2} (equivalent to approximately 30 years in orbit). Based on those detailed models it was possible to determine the optimum thickness, resistivity and generic type of cell (i.e. wraparound, wrapthrough, BSF, no BSF etc.) for the Space Station FREEDOM Array.

Experimental work was also performed to develop techniques for surface passivation to increase blue response although the use

of passivation oxides were found to produce only a marginal increase in performance due to the already high blue response of the emitter.

During Task I a substantial dependence of the thermal absorptance of sculptured cells on emitter surface doping concentration was noted. The contract was therefore amended to investigate this phenomenon further since sculptured surface cells were projected to produce higher efficiencies than planar surface cells. There was thus a trade off between higher efficiency at 28°C and higher thermal absorptance since the latter increased "on orbit" operating temperature.

Task I was also later amended to include a study to determine the optimum optical stack for incorporation into the Space Station Freedom Kapton blanket array.

This study, performed by OCLI, included cell optimization under both front and back (albedo illumination) and took into account absorption and reflection losses in the Kapton blanket, adhesive and in each layer of the cell. A coverglass study was also performed under this contract to determine the most cost effective cover to use for the FREEDOM cell.

Finally front and back grid line optimization was performed to reduce resistive and distributed sheet resistance losses to a minimum.

2.1 CHOICE OF GENERIC CELL TYPE (K4, K5, K6 or K7)

A systematic study was performed to determine the optimum generic cell type. This included studies of the effects of junction depth, wafer resistivity, surface finish (planar or textured) and back surface field on BOL and EOL performance.

The cell base resistivity is an important factor in obtaining higher efficiencies and lower resistivity should lead to higher efficiency. Unfortunately, higher damage coefficients are also associated with lower resistivity. Because of this a balance must be struck such that the ratio of EOL performance to BOL performance is as high as possible. Another variable that can be introduced is the base thickness. Using the criterion that the EOL diffusion length must be greater than the base thickness, one can use somewhat lower resistivities by using smaller base thickness. As an example, the use of a 100 micron thick base might permit the use of 1-2 ohm-cm silicon material whereas this is not possible for a 200 micron thick cell.

In order to facilitate the discussion in this report, we show in Figure 2-1 the four different Spectrolab generic types of cell considered in this study. They are designated K4 through K7 and are described below.

A) Type K4 — This cell has planar front and back surfaces. There is no back surface field.

B) Type K5 — This cell has a sculptured or textured front surface for increased light absorption and radiation hardness. The back is also considered to be sculptured for this program.

C) Type K6 — This cell is similar in surface design to the K4 cell but has a P^+ BSF region at the back surface.

D) Type K7 — This cell is similar to the K5 design but has a P^+ BSF region at the back surface.

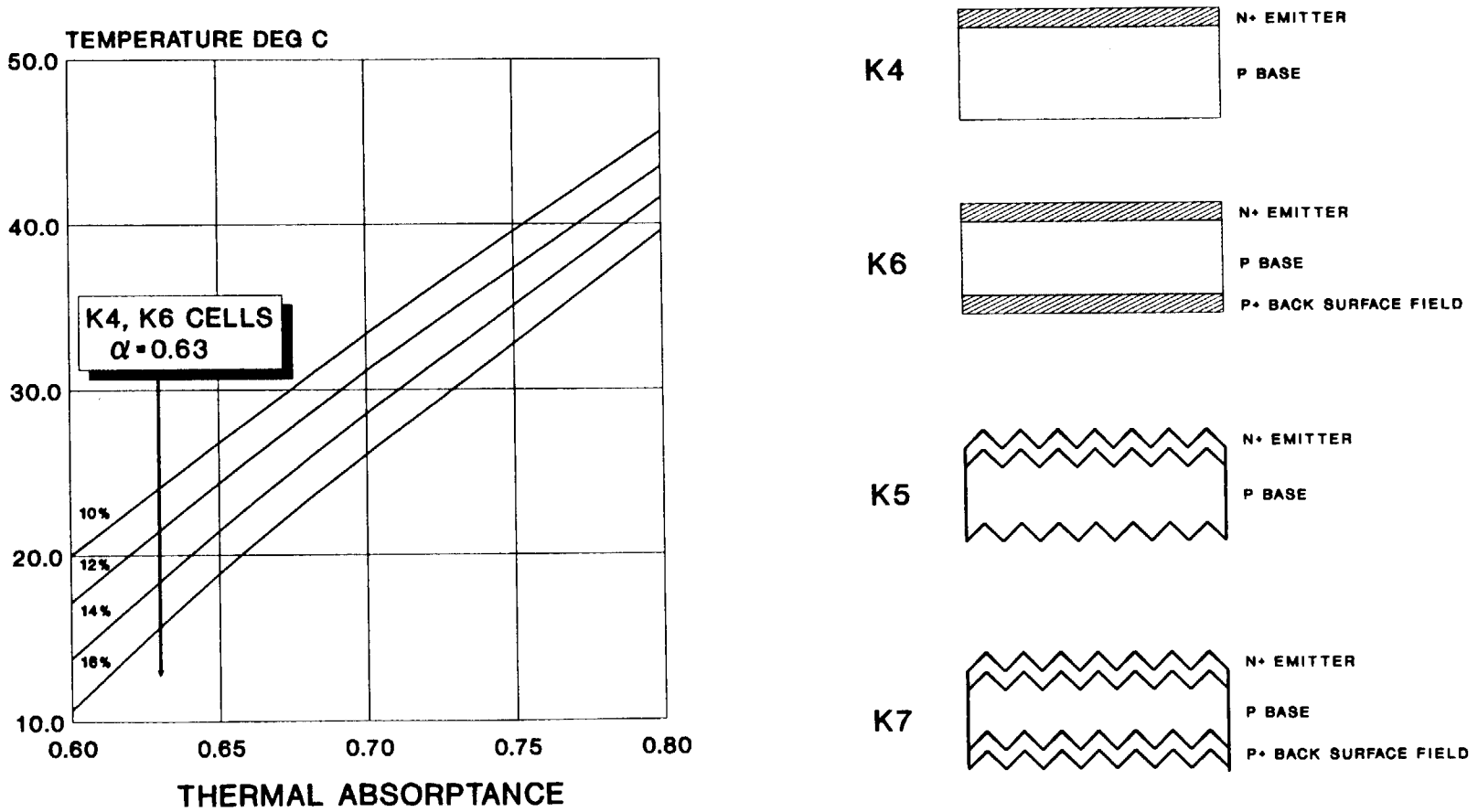

Figure 2-1 SPECTROLAB GENERIC CELL TYPES, K4, K5, K6 AND K7

The choice of cell type for a particular mission depends to a great extent on the radiation fluence experienced during that mission. For very high fluence missions, where fluences exceed 10^{15} 1 MeV electron/cm^2, 10 ohm-cm K4 or K5 cells are generally used; for lower fluence missions K6 or K7 structures give higher BOL and EOL efficiency since the back surface field remains effective over the lifetime of the device. For low fluence missions, K4 or K5 parts based on lower resistivity 1-3 ohm-cm silicon may also be considered since high efficiency may be achieved without back surface fields. It was shown in this study, however, that a back surface field may also be beneficial on a 1-3 ohm-cm cell if low back surface recombination velocities may be achieved.

The effect of various cell parameters on cell performance is described below.

2.1.1 Radiation Damage Modeling

Radiation damage modeling was performed using proprietary Spectrolab codes based on closed form solutions of standard semiconductor equations. These models have been verified on many flight programs. Input data for the models was derived from data bases found to be accurate in predicting performance of other cell designs. Radiation damage induced degradation of diffusion length was assumed to proceed according to the equation:

$$\frac{1}{L(o)^2} = \frac{1}{L(\phi)^2} + K_B \phi$$

where $L(o)$ and $L(\phi)$ are the diffusion length at BOL and at EOL (after ϕ fluence) respectively and
K_B is the damage coefficient.

The value of K_B was derived from actual radiation data on flight quality 2 ohm and 10 ohm-cm top/bottom contact cells and was determined to be 5×10^{-11} per electron and 3×10^{-11} per electron for 2 ohm-cm and 10 ohm-cm silicon respectively. The damage coefficient in the heavily doped N^+ emitter region of the cell was assumed to be 3×10^{-9} per electron.

A summary of all parameters used in the modeling is given in Table 2-1.

In order to be able to make a meaningful comparison in performance between textured (K5 or K7) and planar (K4 or K6) cells, it was necessary to include the effects of operating temperature on cell performance. Obviously it was impossible to determine accurately the "on-orbit" operating temperature of the array since the array design was undetermined at this time. Nevertheless the Stefan Boltzman relation was used in an idealized model to obtain a first order approximation, based on the known emissivity and thermal absorptance of the cells alone.

This idealized model assumed the cell to be operating in a totally transparent array with a hemispherical emittance of 0.82. Based on this assumption we show in Figure 2-2 the computed "on-orbit" operating temperature for K4, K5, K6 and K7 cells of different efficiencies. For a planar cell (K4 or K6) thermal absorptance is approximately 0.63 giving an operating temperature of between 15°C and 24°C depending on cell efficiency, while for a textured surface cell with a thermal absorptance of approximately 0.81 the operating temperature is between 37°C and 46°C.

Table 2-1 SUMMARY OF ALL PARAMETERS USED IN MODELLING

MODELING PARAMETERS FOR 10 OHM-CM CELL	
EMITTER THICKNESS uM	0.15
EMITTER DIFF LENGTH uM	2.34
EMITTER DIFF COEFFT cm2/S	1.74
EMITTER SURFACE REC VELOCITY cm/S	50000
EMITTER DOPING CM-3	5.0E+18
BASE WIDTH um	200
BASE DIFF LENGTH um (10 Ohm-cm)	600
BASE DIFF COEFFT cm2/S (10 Ohm-cm)	33
BACK SURFACE REC VELY cm/S	10
BASE DOPING CM-3 (10 Ohm-cm)	1.5E+15
TEMP DEG C	28

MODELING PARAMETERS FOR 2 OHM-CM CELL	
EMITTER THICKNESS uM	0.15
EMITTER DIFF LENGTH uM	2.34
EMITTER DIFF COEFFT cm2/S	1.74
EMITTER SURFACE REC VELOCITY cm/S	50000
EMITTER DOPING CM-3	5.0E+18
BASE WIDTH um	200
BASE DIFF LENGTH um (2 Ohm-cm)	300
BASE DIFF COEFFT cm2/S (2 Ohm-cm)	28
BACK SURFACE REC VELY cm/S	10
BASE DOPING CM-3 (2 Ohm-cm)	8.0E+15
TEMP DEG C	28

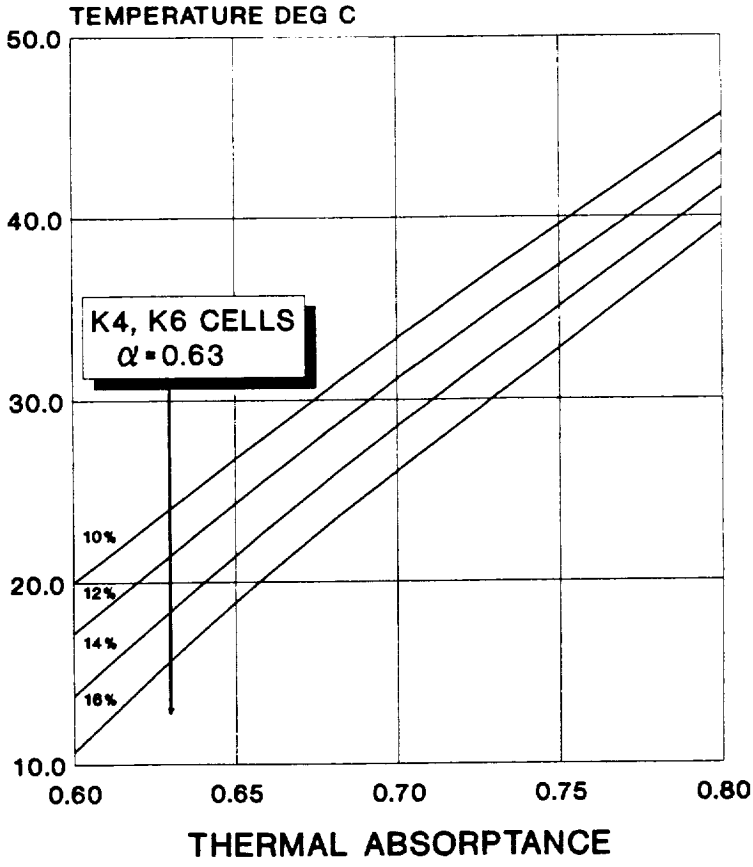

Figure 2-2 CALCULATED CELL OPERATING TEMPERATURE AS A FUNCTION OF THERMAL ABSORPTANCE AND AM0, 28°C CONVERSION EFFICIENCY

In Table 2-2 we summarize the results of the radiation modeling study. At this point in the program the modeling study had shown that substantial increases in performance could be achieved using 2 ohm-cm silicon; hence the data in Table 2-2 is confined to 2 ohm-cm. (Later experimental work showed, however, that 10 ohm-cm wafers were required to overcome the effects of boron-oxygen precipitate formations.) Also, 8 mil thick, K7 or K6 cells were not considered since the effect of the BSF on such a thick cell, bearing in mind the 300 micron diffusion length, would only be small at BOL and negligible at EOL.

Table 2-2 COMPUTED AM0, CELL CHARACTERISTICS FOR DIFFERENT CELL TYPES AS A FUNCTION OF 1 MeV ELECTRON FLUENCE

Cell Type	Fluence	Voc mV	Jsc mA/cm^2	Effy @ 25C %	P/P(0)	FF	Thermal Alpha	Effy on Orbit
2 ohm-cm, 8 mil, K4	0	595.00	38.30	13.1	1.0	0.780	0.63	13.50
2 ohm-cm, 8 mil, K4	5E13	583.00	37.60	12.5	1.0	0.775	0.63	12.80
2 ohm-cm, 8 mil, K4	1E14	576.10	37.10	12.2	0.9	0.773	0.63	12.60
2 ohm-cm, 8 mil, K5	0	583.30	42.10	14.0	1.0	0.770	0.81	12.50
2 ohm-cm, 8 mil, K5	5E13	571.30	41.30	13.2	1.0	0.761	0.81	12.00
2 ohm-cm, 8 mil, K5	1E14	564.30	40.80	13.0	0.9	0.763	0.81	11.60
2 ohm-cm, 4 mil, K6	0	618.60	38.60	13.8	1.0	0.783	0.63	14.10
2 ohm-cm, 4 mil, K6	5E13	596.30	38.00	13.0	0.9	0.777	0.63	13.20
2 ohm-cm, 4 mil, K6	1E14	585.50	37.60	12.6	0.9	0.774	0.63	12.90
2 ohm-cm, 4 mil, K7	0	606.70	42.20	14.7	1.0	0.774	0.81	13.20
2 ohm-cm, 4 mil, K7	5E13	584.40	41.60	13.8	0.9	0.768	0.81	12.30
2 ohm-cm, 4 mil, K7	1E14	573.50	41.10	13.3	0.9	0.763	0.81	12.00

As seen from the data of Table 2-2 the highest efficiency at 25°C is achieved using a 2 ohm-cm, 4 mil thick, K7 cell although this is not true at the estimated on-orbit operating temperature.

Generally higher efficiencies were predicted for 4 mil thick cells due to the lower bulk related dark current losses which give high predicted V_{OC}s.

When operating temperature was taken into account the highest BOL efficiency was achieved using a 2 ohm-cm, 4 mil, K6 cell. This also achieved the highest EOL efficiency. However, 4 mil cells were later discounted at the Critical Design Review (CDR), at which it was concluded by NASA and others that the risks of manufacturing a large area 4 mil cell were too high.

2.1.2 Effect of Junction Depth on Cell Performance

Computer modeling was performed to investigate the sensitivity of cell efficiency to junction depth.

There are several trade-offs involved in junction depth, substrate resistivity and thickness. Shallow junctions diminish emitter loss associated with recombination centers in the emitter and on the cell surface by reducing the absorption volume of the emitter. In reducing the emitter thickness, however, higher doping and/or higher gridline densities must be introduced. Higher doping leads to band-gap narrowing and Auger recombination which in turn increases the emitter saturation current and decreases the open circuit voltage. If a deeper junction is used then fewer gridlines are required. This reduces shadowing, but, unless emitter recombination can be reduced the shadow gain is lost.

The model used specifically included the effects of radiation damage in the solar cell emitter, which has been found to be non-trivial at higher fluence levels, even when the junction was shallow ($X_j \sim 0.15\ \mu m$). We chose to investigate cell performance when the emitter junction depth was increased to 0.3 microns. In this case the surface was assumed to be somewhat passivated, (i.e., with surface recombination velocity reduced to 10^3 cm sec^{-1}), since an unpassivated deep junction cell would yield very poor efficiencies. Otherwise, the junction depth was assumed to be 0.15 microns with a surface recombination velocity of 5×10^4 cm sec^{-1}. These parameters were considered appropriate for the standard Spectrolab emitter on production cells.

Table 2-3 shows the results of our modeling for both 2 and 10 ohm-cm cells of 4 and 8 mils thickness. The figures in parentheses represent the data for a cell with the standard Spectrolab emitter (0.15μm). Other data for the base region which was used in the modeling are shown in Table 2-1. It should be noted that the results indicate that, for 10 ohm-cm cells, a fractional gain in efficiency is obtained by making the junction deeper without deterioration of P/P_o. For 2 ohm-cm cells the small efficiency gain at BOL is somewhat offset by a decrease in P/P_o at EOL (i.e., 5 x 10^{13} 1 MeV electrons cm^2). In both cases it is not considered cost effective to change the junction depth to 0.3 microns, bearing in mind the very small gain in efficiency in comparison to the high cost of reoptimizing the emitter.

Table 2-3 COMPUTED BOL AND EOL EFFICIENCIES OF VARIOUS CELL TYPES WITH 0.3 MICRONS JUNCTION DEPTH. COMPUTED VALUES FOR 0.15 MICRON JUNCTION DEPTH SHOWN IN PARENTHESES

Substrate Resistivity Ohm-cm	Substrate Thickness (mil)	Surface Type	Efficiency (BOL) %	Efficiency (EOL) %	P/P(0)
2	8	Planar	16.05 (15.83)	13.58 (13.80)	.846 (.889)
2	4	Planar	15.95 (15.39)	13.81 (13.99)	.865 (.909)
2	8	Sculptured	16.34 (15.75)	13.93 (14.09)	.855 (.895)
2	4	Sculptured	16.30 (15.66)	14.19 (14.29)	.871 (.912)
10	8	Planar	15.82 (15.32)	14.21 (13.76)	.898 (.898)
10	4	Planar	15.46 (14.95)	14.24 (13.79)	.920 (.922)
10	8	Sculptured	16.07 (15.51)	14.47 (13.97)	.901 (.901)
10	4	Sculptured	15.78 (15.21)	14.55 (14.03)	922 (.923)

Assumes 1E15 1 Mev electrons cm^-2 EOL

2.1.3 Thermal Absorptance (Alpha) Measurements

The goal of this program was to develop a cell with a thermal absorptance of 0.63 or less to operate in a transparent array design. Because a data base of thermal absorptance did not exist for gridded back contact cells, the following cell structures were fabricated:

a) Planar gridded back n+p cell (no BSF) (K4)
b) Textured gridded back n+p cell (no BSF) (K5)
c) Planar gridded back n+pp+ cell with boron p+ BSF (K6)
d) Textured gridded back n+pp+ cell with boron p+ BSF (K7)

The structures had grid lines on both front and back surfaces and the wafer was AR coated on both sides with a standard dual AR coating of 570Å TiO_2/870Å Al_2O_3. These thicknesses were later changed as a result of the OCLI study to optimize the optical stack for the collection of albedo.

Each wafer was mounted in a Beckman DKZ Spectrophotometer with a Gier Dunkel integrating sphere in such a way that both Reflectance plus Transmittance (R+T) could simultaneously be measured. This meant mounting the sample at about 10° off normal incidence to the light beam. Measurements were made over the wavelength range 0.28μm to 2.50μm and thermal absorptance calculated using conventional techniques. The thermal absorption was calculated from the R+T curves assuming $R+T+\alpha=1$. Figure 2-3 shows the sum of reflectance plus transmittance measured on these K7 cells. The spectral reflectance of both planar and sculptured surface cells with full back metallization are also shown for comparison.

It is clear that both K4 and K6 planar cells have excellent IR rejection and show the absorptance goal of 0.63 to be achievable. The difference between K5 and K7 parts in the IR

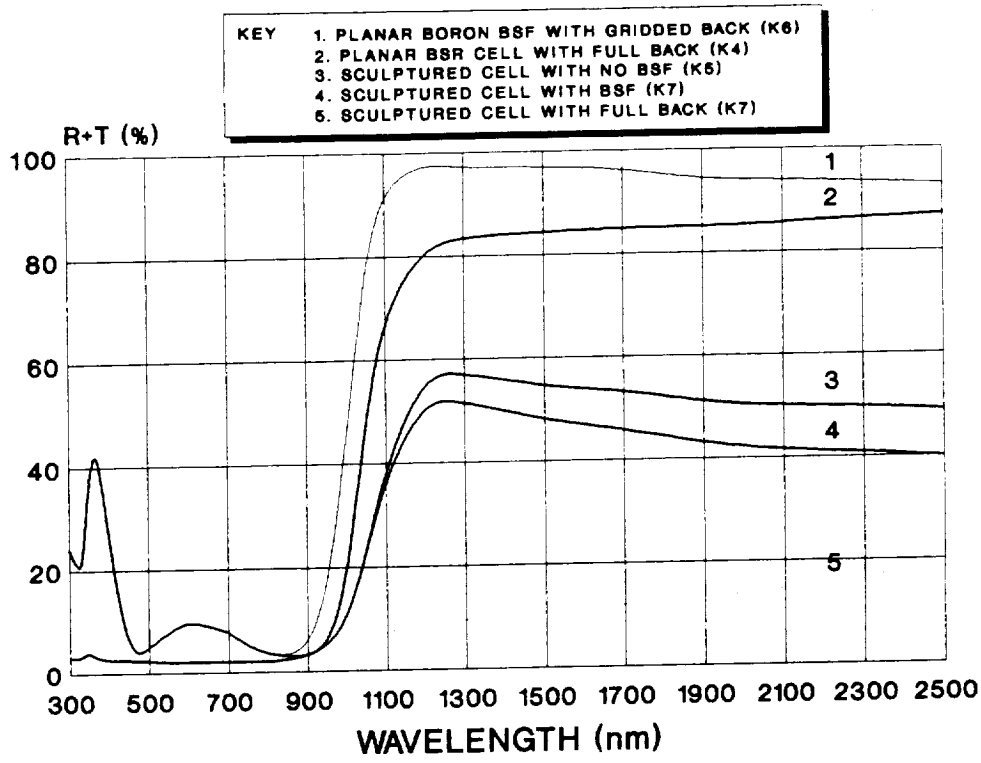

Figure 2-3 SUM OF REFLECTANCE PLUS TRANSMITTANCE FOR GRIDDED BACK BARE CELLS OF DIFFERENT CELL TYPE. CELLS ARE AR COATED BOTH SIDES

region was initially somewhat surprising and was investigated further under an amendment to this contract. The phenomenon was later attributed to free electron absorption in the heavily doped p+ regions of the cell due to the many light passes made through the cell as a result of light scattering by the textured surface. Similar effects were noted in the n+ junction region and resulted in a technique to reduce the thermal absorptance of sculptured surface cells by emitter doping profile modification as described further in Section 2.1.3.1 below.

2.1.3.1 Effect of Surface Doping Concentration on Thermal Absorptance

A modification to the contract was made to investigate, in more detail, the cause of the anomaly in I.R. reflectance between textured cells with and without the p+ BSF.

This difference was also evident in textured samples with and without the n+ emitter diffusion as shown in Figure 2-4.

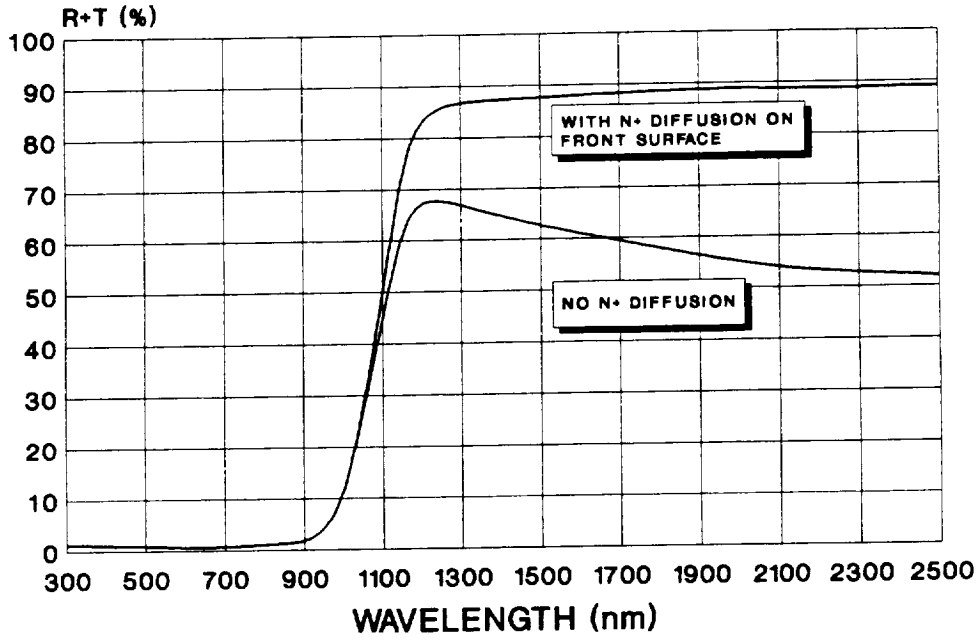

Figure 2.4 REFLECTANCE PLUS TRANSMITTANCE OF SCULPTURED WAFER (NO GRIDS), WITH AND WITHOUT N+ JUNCTION DIFFUSION

Since there was no difference between samples, other than the heavily doped region, the difference in I.R. thermal absorptance was attributed to free electron absorption in the emitter, caused by multiple light passes in the latter.

The importance of this result was that it allowed the possibility of making sculptured surface cells with thermal absorptance substantially lower than had hitherto been possible. Because of the inherently higher modeled efficiencies of sculptured compared to planar cells this would provide substantial cost savings on the photovoltaic array and the contract was amended to investigate this phenomenon in more detail.

The amendment was divided into two parts.

1. Identification of the absorption mechanism.
2. Development of techniques to reduce the thermal absorptance of sculptured cells and to fabricate prototype cells for process verification.

2.1.3.1.1 Theory of Free Carrier Absorption

At wavelengths beyond that of the interband electronic transition limit, absorption in a semiconductor can occur due to both excitation of lattice vibrations and/or intraband excitation of free carriers (electrons and/or holes). The absorption due to the latter mechanism is proportional to the number of free carriers along the light path in the solid and is independent of the carrier concentration along the path.

Semiclassical modeling suffices to give the relation

$$\alpha = \frac{\lambda_o^2 g^3}{4\pi^2 \varepsilon_o c^3 \eta} \left[\frac{n}{M_n^2 \mu_n} + \frac{p}{M_p^2 \mu_p} \right]$$

where	n and p	are the free electron and hole concentrations
	λ o	is the free space wavelength of the radiation
	g	is a number close to unity
	Mp and Mn	are the effective masses for holes and electrons respectively
	μp and μn	are the hole and electron mobilities respectively
	η	is the refractive index of the solid

It is clear that the absorption coefficient increases as the square of wavelength. For silicon with an absorption edge at approximately 1.1 microns for interband transitions, free carrier absorption is conveniently observed in the 1.5 micron to 10 micron range. In the case of silicon space cells the free carrier effect is likely in both the n+ emitter and p+ BSF where free carrier concentrations are around 5 x $10^{18}cm^{-3}$ but can be locally $10^{20}cm^{-3}$ close to the surface.(2) As an example, a simple calculation shows that at 1.5 microns wavelength, approximately 10% absorption takes place in a 2 micron thick emitter with N = $10^{19}cm^{-3}$. This may be higher in sculptured cells since the light beam makes many more passes through the heavily doped region. Significant free carrier absorption in regions of the cell where the doping concentration is less than approximately 5 x $10^{18}cm^{-3}$ to $10^{19}cm^{-3}$ (i.e., deeper within the junction and throughout the base) would not be expected.

2.1.3.1.2 Identification of I.R. Absorption Mechanism

Silicon substrates with a wide range of doping concentration were obtained from Aurel Corporation. These substrates were etched down to 10 mils thickness and a dual AR coating of TiO_2/Al_2O_3 was applied to the front surface to maximize the amount of light reaching the cell. The sum of reflectance plus transmittance was then measured using the Beckman DK2 with Gier Dunkel integrating sphere.

In Figures 2-5 and 2-6 we show the sum of R+T for both n and p type substrates.

Over at least part of the wavelength range, the absorption characteristic appears to follow a square law as predicted by theory. The absorption in low doped substrates is negligible. In Figures 2-7 and 2-8 we also show the computed absorption coefficients at "sub-bandgap" energies computed from the R+T data of Figures 2-5 and 2-6. These data are consistent with the absorption seen in approximately 1 micron deep heavily doped junctions of sculptured cells if approximately 10 light passes through the junction are assumed.

Having established the relationship between absorptance and doping level, five lots of 2cm x 2cm, 2 ohm-cm cells, with different doping levels at the emitter surface were fabricated. The method of profile modification involved the successive oxidation and reduction of the silicon surface using an oxidation-reduction cycle utilizing HNO_3 followed by HF. In order to monitor the removal of material from the junction the sheet resistance of the diffused layer was also recorded after each material removal step and the doping profile determined

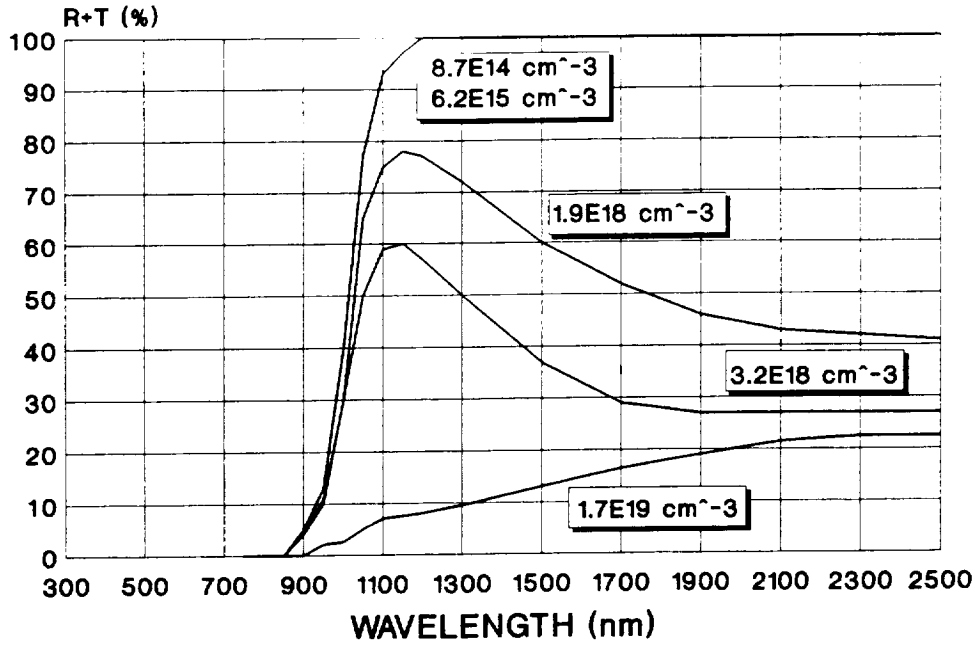

Figure 2-5 EXPERIMENTALLY DETERMINED REFLECTANCE PLUS TRANSMITTANCE AT "BELOW BAND GAP ENERGIES" FOR 10 MIL PLANAR N-TYPE WAFERS OF DIFFERENT BASE DOPING CONCENTRATION

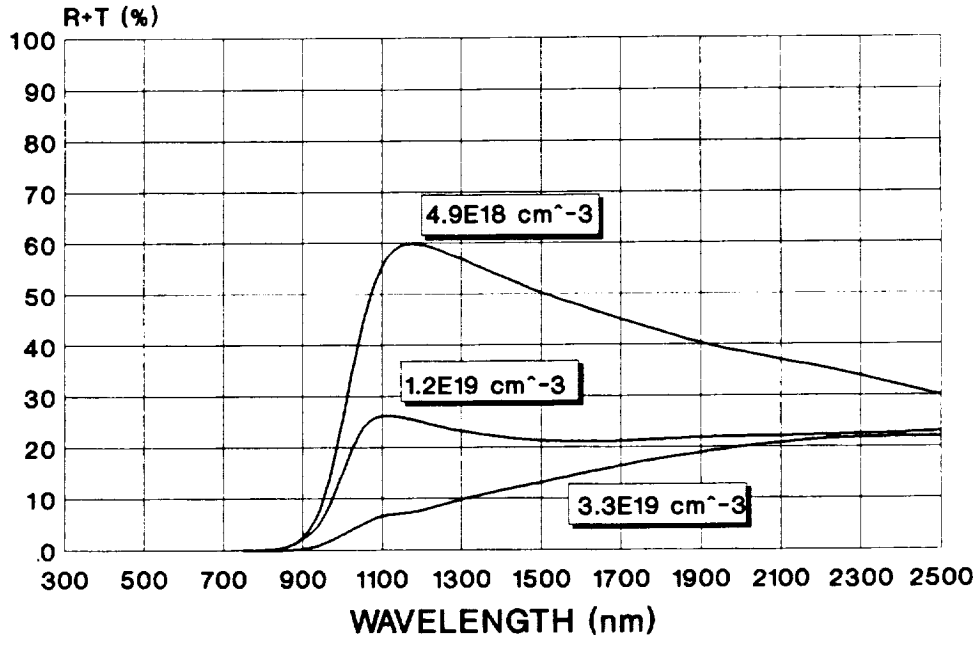

Figure 2-6 EXPERIMENTALLY DETERMINED REFLECTANCE PLUS TRANSMITTANCE AT "BELOW BAND GAP ENERGIES" FOR 10 MIL PLANAR P-TYPE WAFERS OF DIFFERENT BASE DOPING CONCENTRATION

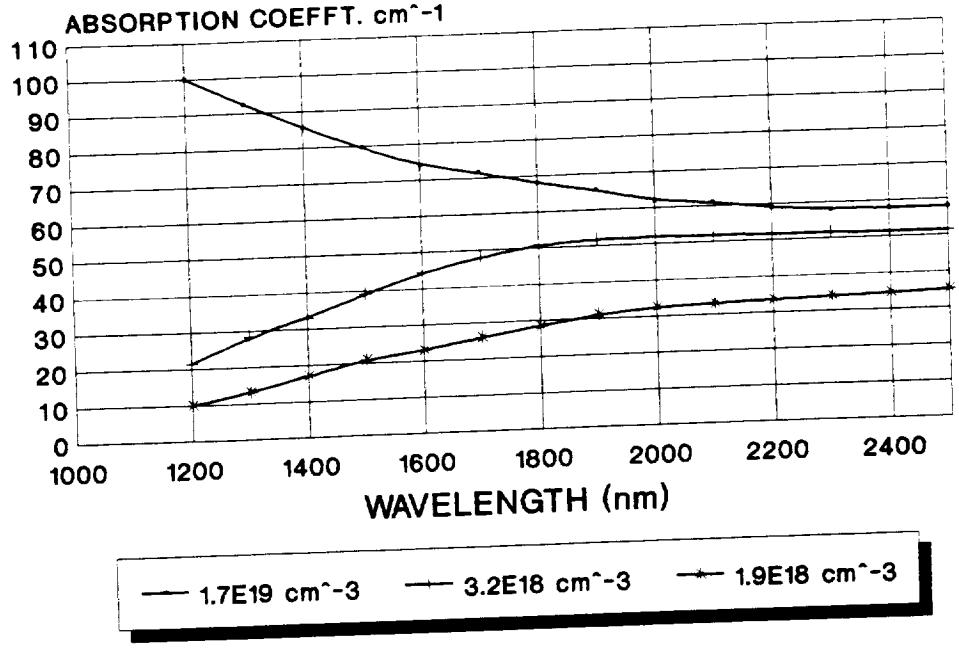

Figure 2-7 "BELOW BAND GAP ENERGY" ABSORPTION COEFFICIENTS DERIVED FROM ABSORPTION DATA FOR N TYPE WAFERS

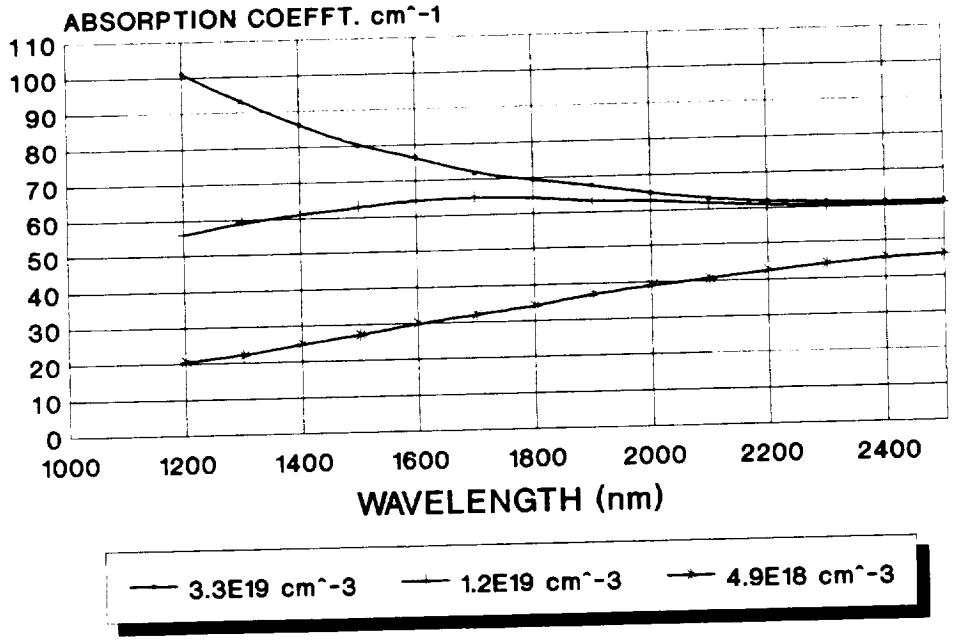

Figure 2-8 "BELOW BAND GAP ENERGY" ABSORPTION COEFFICIENTS DERIVED FROM ABSORPTION DATA FOR P TYPE WAFERS

using a spreading resistance technique at Solecon Labs. In order to expedite the investigation, both front and back metallization was performed by evaporation through a mechanical mask. This resulted in a grid obscuration of approximately 7%, about 3% higher than with a conventional photoresist lift-off process. Each side of the cell was coated with a dual AR coating of TiO_2/Al_2O_3.

Table 2-4 and Figures 2-9, and 2-10 summarize the electrical and optical data on these cells. Increasing the emitter n+ sheet resistance from 25 to 55 ohms per square did not apparently markedly increase I_{SC} but a small decrease in V_{OC} was observed on the higher sheet resistance samples. This was presumably due to the increasing effect of recombination velocity beneath the front contact as the emitter became progressively thinner. There was no apparent effect on power density within the small group of cells tested. The effect of increased sheet resistance on thermal absorptance was significant however as seen from Figure 2-11. An increase in sheet resistance from 25 to 55 ohms/square produced a decrease of approximately 3 alpha points from 0.82 to 0.79 respectively. The current densities measured for these cells was almost in complete agreement with our model for a 2 ohm-cm K5 solar cell.

2.1.3.1.3 Summary

This study clearly showed that the thermal absorptance of textured surface cells could be reduced by reducing the doping concentration at the emitter surface, without effecting cell efficiency. However the process of chemical oxidation/reduction was found to cause a decrease in Voc as the emitter sheet resistance increased. This limited the number of oxidation/ reduction cycles to about twenty.

Table 2-4 ILLUMINATED IV DATA FOR GRIDDED BACK SCULPTURED SURFACE 2 OHM-CM CELLS (NO BSF) WITH DIFFUSED EMITTERS OF DIFFERENT SHEET RESISTANCE

Sheet Resistance Ohms/sq	Voc mV	Jsc mA/cm^2	Jsc mA/cm^2 (Normalized)	Jsc mA/cm^2 (Model)	Effy @ 28C % (Actual)*	Effy @ 25C % ** (Normalized)	Effy @ 25C % (Model)
20	583.5	39.8	41.1	41.1	13.2	13.2	13.9
30	581.9	39.7	41.0	41.1	13.2	13.2	13.9
46	580.4	39.8	41.1	41.1	13.2	13.2	13.9
55	579.8	40.0	41.3	41.1	13.2	13.2	13.9

* Gridlines on these cells were defined by mechanical masking resulting in 7% obscuration Total cell area was 4.12 cm^2

** Normalized to a more usual 4% obscuration

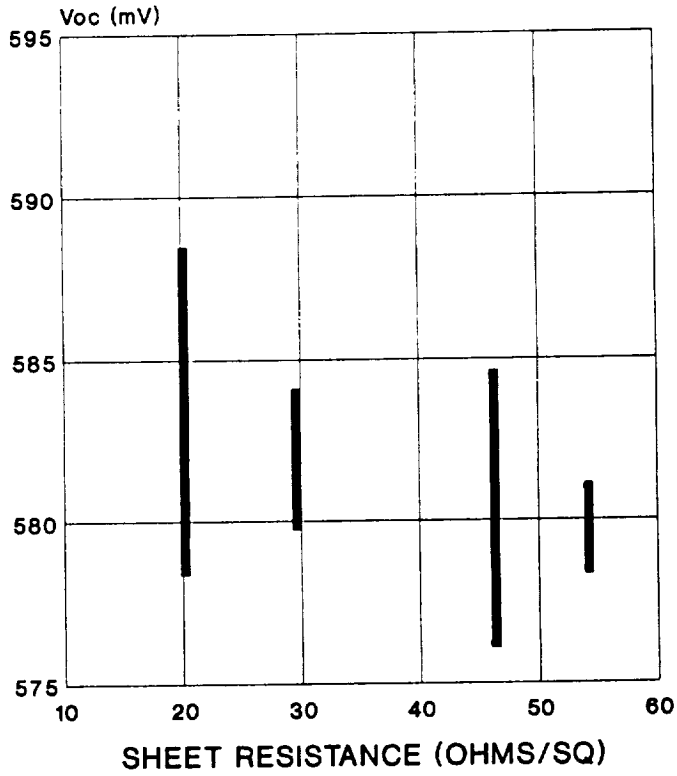

Figure 2-9 OPEN CIRCUIT VOLTAGE DISTRIBUTION OF SCULPTURED CELLS AS A FUNCTION OF EMITTER SHEET RESSITANCE

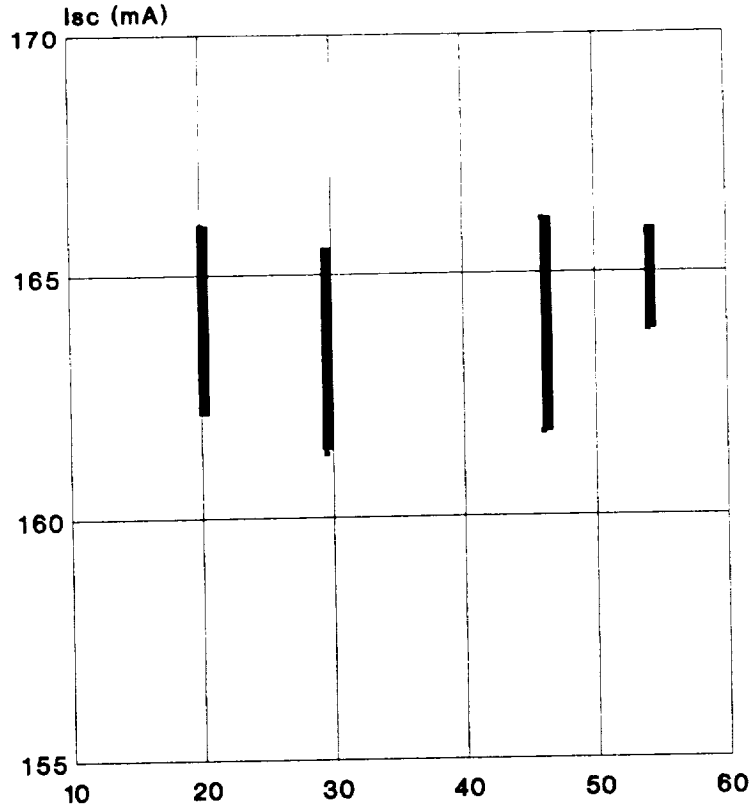

Figure 2-10 SHORT CIRCUIT CURRENT DISTRIBUTION OF SCULPTURED CELLS AS A FUNCTION OF EMITTER SHEET RESISTANCE

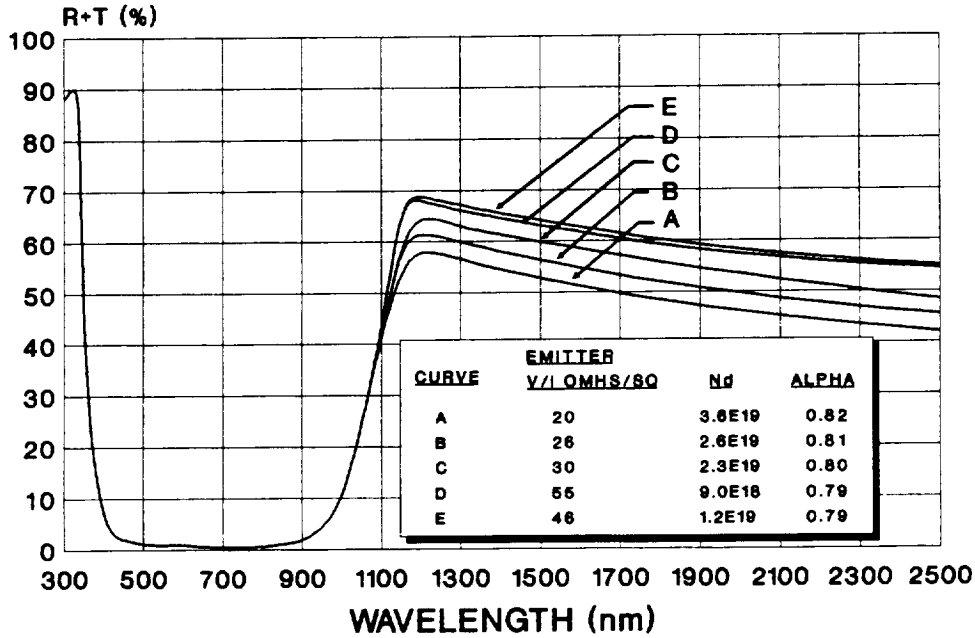

Figure 2-11 MEASURED REFLECTANCE PLUS TRANSMITTANCE AS A FUNCTION OF EMITTER SURFACE DOPING CONCENTRATION FOR 8 MIL 2 OHM-CM SCULPTURED SURFACE SOLAR CELLS. CELLS ARE DAR COATED ON BOTH SIDES.

After considerable discussion at the CDR at which all the major Aerospace companies were represented, it was decided that the reduction in thermal absorptance was not sufficiently high to warrant further investigation on this program and that the planar surface cell would be pursued.

2.2 FRONT SURFACE PASSIVATION

In order to increase the cell's blue response and reduce the saturation current in the emitter the use of a thin thermal oxide was investigated to passivate the emitter front surface. This oxide, typically 100Å thick and grown at 800°C in dry O_2 has been shown by other researchers to be an effective means of emitter surface passivation to increase Jsc and Voc on emitter limited cells.

Experiments consisted of dry thermal oxidation (in O_2 at 800°C), of emitters in which the surface concentration had been carefully and reproducibly altered by successive oxidation and reduction of the surface using HNO_3 and HF acid respectively.

Figure 2-12 shows the doping profile measured by a spreading resistance technique on a "standard" Spectrolab emitter of sheet resistance equal to 141 ohms per square. The surface doping concentration of approximately $10^{20}cm^{-3}$ is sufficiently high that the first few hundred angstroms of the surface may be considered to be "dead". If this is the case then the emitter is no longer transparent to minority carriers and will not benefit from the presence of surface passivation by thin thermal oxides. Figure 2-13 shows that this is experimentally the case where we show the effect of 100Å of dry thermal oxide on quantum efficiency. Both curves represent an average of five measurements made on cells picked at random from the lot. It is clear

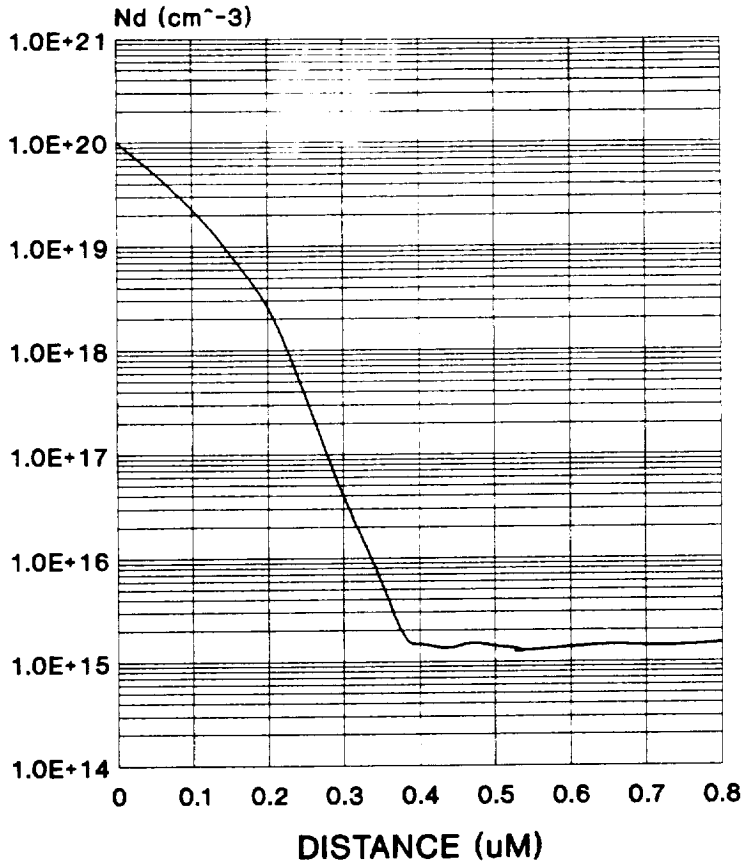

Figure 2-12 SPREADING RESISTANCE PROFILE OF "STANDARD DIFFUSION"

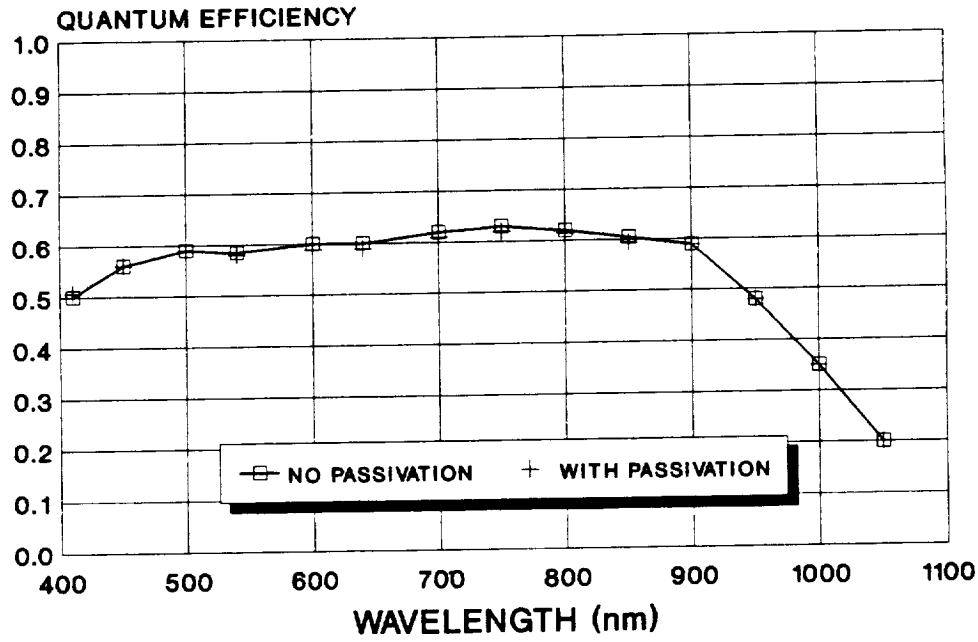

Figure 2-13 MEASURED EXTERNAL QE OF 2cm X 2cm CELLS WITH AND WITHOUT PASSIVATION OXIDE. STANDARD EMITTER DIFFUSION

from the similarity of blue spectral response that no passivation has taken place. This was to be expected, bearing in mind the high surface concentration of phosphorus atoms.

In contrast, Figure 2-14 shows the difference in quantum efficiency between passivated and unpassivated solar cells which had approximately 300-400Å of silicon removed from the surface prior to passivation by a thin thermal oxide 100Å thick. No AR coating was applied. The doping profile prior to oxidation is shown in Figure 2-15. The quantum efficiency data was obtained from the averaged quantum efficiency data of four cells taken from the lot. The parts were then dipped in 10% HF to remove the passivation oxide and were then retested. In this case there was a significant difference in blue response, indicating that passivation had taken place.

In order to check that the decrease in blue response after removal of the SiO_2 layer was not due to any antireflection effect of the passivation layer, the spectral reflectance between 350-1100 nm was measured on several parts with and without the passivation oxide. There was no difference in reflectance at wavelengths down to 350 nm. Additionally, dark I-V measurements were performed on several parts before and after removal of the passivation oxide. A typical dark I-V curve on a 2cm x 2cm cell is shown in Figure 2-16. The change in dark I-V characteristics is a clear indication of passivation having taken place and results in an increase in approximately 15 mV in open circuit voltage. Measurements of the first diode saturation current I_{01} before and after removal of the oxide layer indicated that the emitter saturation current (I_{01E}) increased by approximately 2×10^{-12} A cm^{-2} after the oxide was removed.

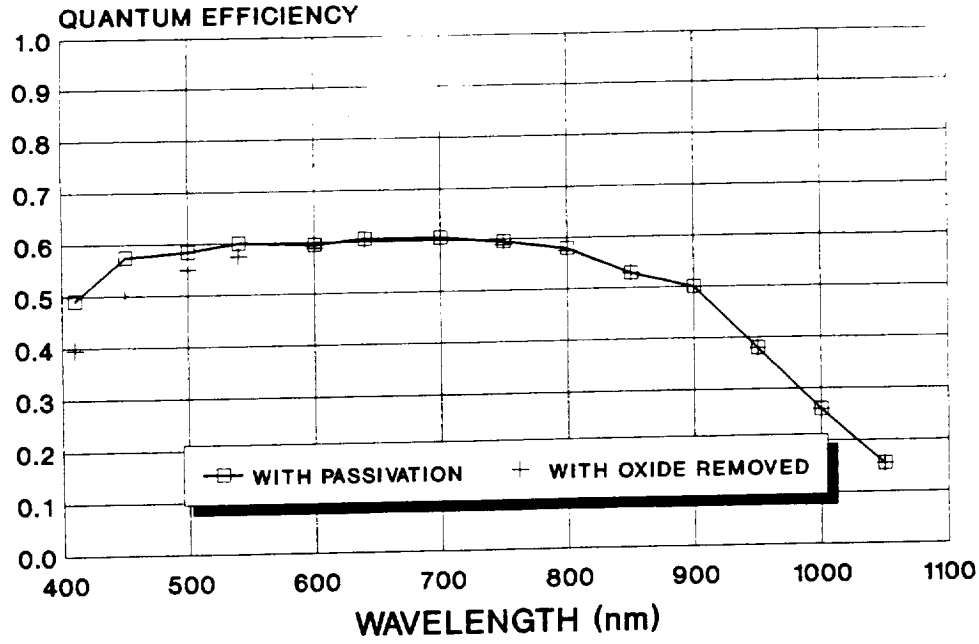

Figure 2-14 MEASURED EXTERNAL QE OF 2cm X 2cm CELLS WITH AND WITHOUT PASSIVATION OXIDE. MODIFIED EMITTER DIFFUSION

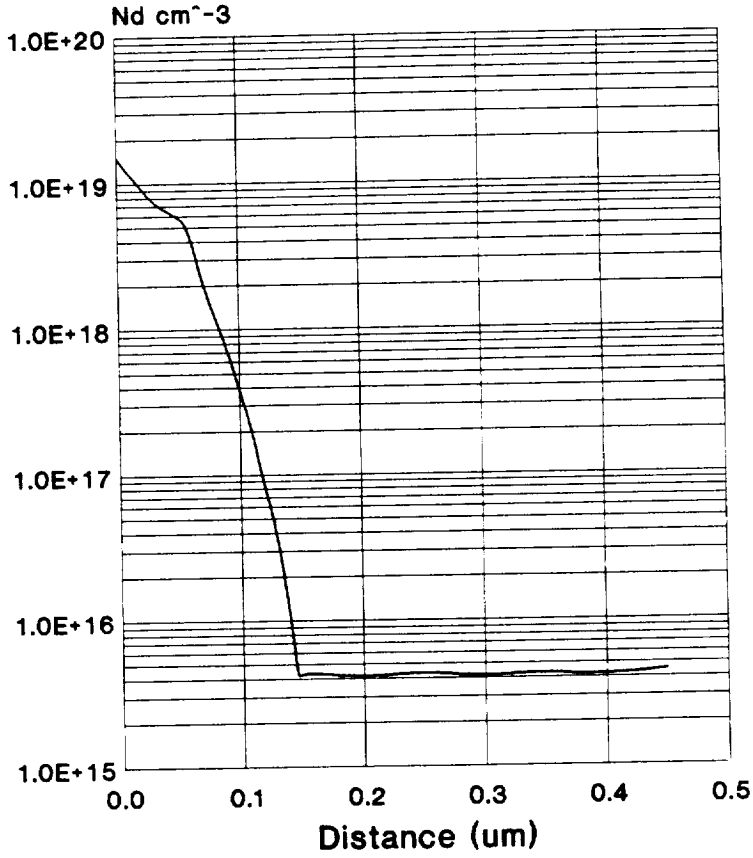

Figure 2-15 SPREADING RESISTANCE PROFILE OF "MODIFIED EMITTER DIFFUSION"

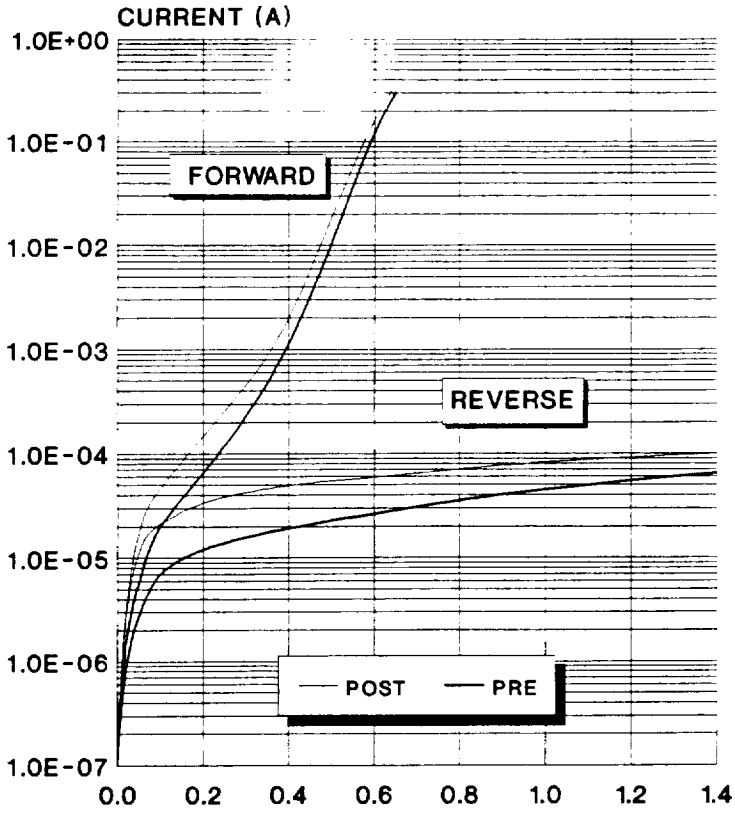

Figure 2-16 DARK IV CURVE OF 2cm X 2cm CELL PRE AND POST REMOVAL OF PASSIVATION OXIDE

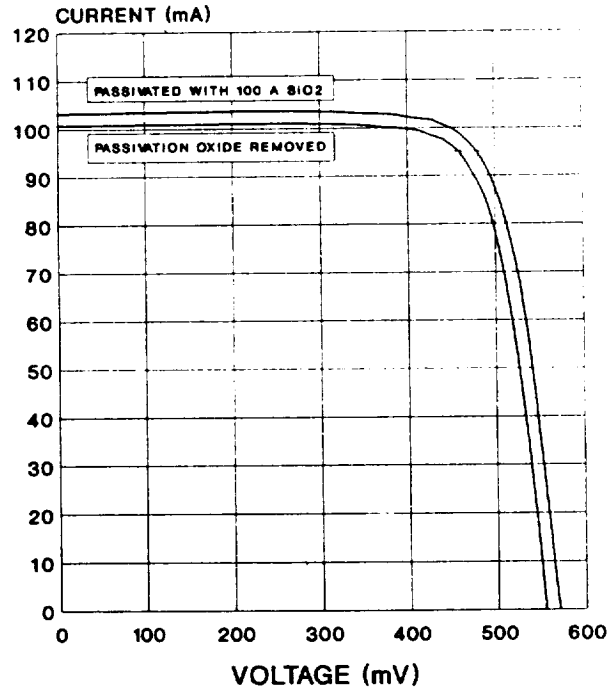

Figure 2-17 ILLUMINATED IV CURVE OF 2cm X 2cm CELL PRE AND POST REMOVAL OF PASSIVATION OXIDE

Figure 2-17 shows the difference in illuminated I-V output characteristic before and after removal of the passivation oxide. It is clear that both current and voltage are enhanced by the presence of the oxide. The measurement of I_{SC} on a number of parts indicated that it was reduced by 2-3 mA on a 2cm x 2cm cell when the oxide was removed and that the open circuit voltage difference was 10-15 mV.

Although it was clear that the 100Å thick oxide was playing a role in surface passivation of modified emitter profiles we were unable to increase blue response above that obtained for the best "standard" Spectrolab emitters with high surface concentration. In other words, when the surface concentration was deliberately reduced it was essential to passivate the surface but with the "standard" diffusion profile no additional increase in performance was achieved by passivation.

In order to ascertain whether or not further improvements to the already good blue response were possible the internal QE was measured by deconvoluting the external QE from the reflectance.

Figure 2-18 shows the measured internal and external quantum efficiency for a K4 cell with standard emitter profile. The internal quantum efficiency approached unity at short wavelengths and was an indication that no significant further passivation could be accomplished.

2.3 OPTIMIZATION OF THE THERMO-OPTICAL STACK

As part of Task 1 a study was undertaken to optimize the total optical stack including cell, cell cover, and all coatings present on the cell and on the blanket itself. The study was subcontracted to Optical Coating Laboratory, Inc. (OCLI).

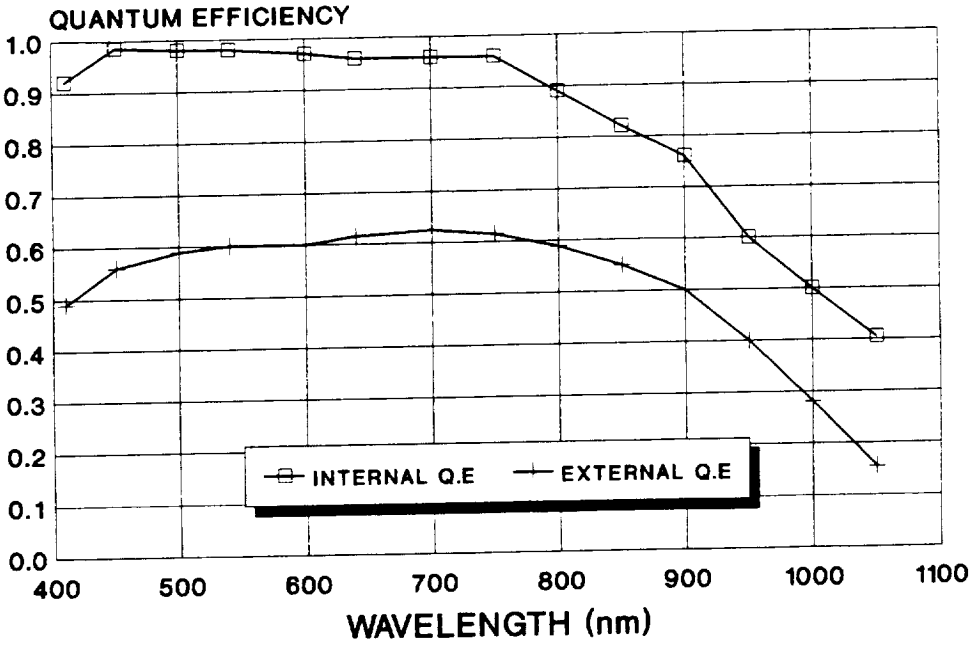

Figure 2-18 INTERNAL AND EXTERNAL QE OF 2cm X 2cm CELL WITH STANDARD DIFFUSION

OCLI had extensive experience in design of thin film coatings and a unique thin film design and analysis program had already been developed in-house to provide capability for novel customer requirements. The Space Station FREEDOM photovoltaic array was unusual in that the basic design had seven thin film coatings, a glass cover, layers of adhesives, the silicon cell, and two layers of Kapton.

OCLI had already started work on a separate contract to develop coatings to protect the Kapton array from erosion in low earth orbit by Atomic Oxygen. Calculations of the optical properties

of the specified Kapton array concept were therefore available and hence provided a starting point for the design study.

The study was broken into two major tasks, the first being to optimize the cell to accept albedo radiation from backside illumination, the second to consider a trade between the different OCLI cell covers available at that time.

Traditional solar array panels only generate power from solar energy incident on the front surface. A high reflector is coated on the back cell surface to reflect unwanted infrared energy back into space. The Space Station FREEDOM Kapton array is largely transparent to infrared energy. Albedo energy incident on the rear surface of the array may therefore be converted to power by use of the gridded back silicon cells. Since the gridded back cell with BSF has a high internal spectral response on both sides it was important to consider the additional power contributed from albedo.

The first task was to optimize thin film coatings for the rear surface of the silicon cells. A model of the Kapton support structure was used to determine the spectral content of albedo energy reflected from the earth, incident on the rear surface of the silicon cell. Numerous calculations were made to optimize cell power generation from incident albedo energy at the beginning of life (BOL) and end of life (EOL). Other coatings were designed to provide maximum transmittance of infrared energy out the back of the cell. The effects of these coatings on front surface power generation from AM0 solar irradiation was also considered. The theoretical model used for these calculations is discussed in Section 2.3.1 below and the results are discussed in Section 2.3.2.1 and 2.3.2.2 following.

The second task was to compare the optical properties and costs of available solar cell covers. Theoretical and experimental data were collected on the optical properties of these products from the ultraviolet to infrared wavelengths. These data were used in conjunction with silicon cell response data to determine cell efficiency, solar absorptance, normal emittance, near infrared transmittance and cost for various configurations. The results are discussed in Section 2.3.3.

2.3.1 Solar Array Model for Back Surface Cell Coating

The model used to optimize the coatings for the rear surface of the cell is shown in Figure 2-19. The optical effects of the solar cell cover were neglected and light was assumed to enter the cell from an adhesive of refractive index n=1.41. The cell front surface DAR was assumed to be fixed for this study, this being 870Å Al_2O_3/570Å TiO_2. This DAR coating is well established as being optimum for the maximum transmission of the AM0 spectrum into silicon.

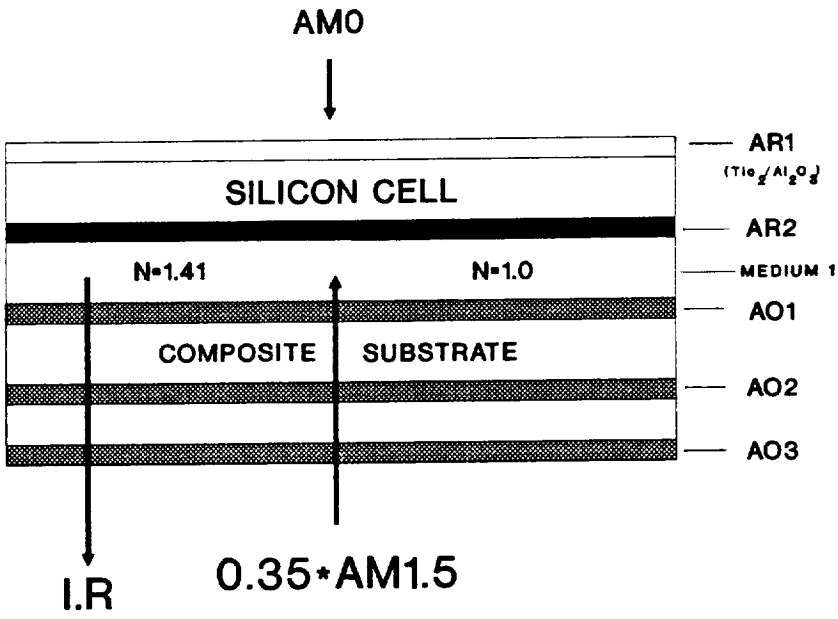

Figure 2-19 MODEL USED FOR OPTICAL STACK OPTIMIZATION

The cell was assumed to be operating in a composite Kapton blanket array as shown in Figure 2-19. The AR coating labelled AR2 was the variable optimized in this study. The region adjacent to AR2 may be filled either with adhesive (n=1.41) or may be empty (n = 1.0). Both cases were considered in this study as the optimum thickness of AR2 was strongly affected by the refractive index of this medium. The Kapton blanket itself was assumed to be a composite of atomic oxygen resistant coatings A01, A02 and A03, adhesives, interconnects and Kapton sheets.

The optical transmittance of the composite structure affects the amount and spectral composition of albedo energy incident on the cell from the rear. No effort was made to change the optical properties of this baseline design which was proprietary to LMSC. Short circuit current under front and back illumination was obtained from modeled internal QE data for the 2 ohm cm K6 cell. Figures 2-20 and 2-21 show typical calculated internal spectral response data at fluences up to 6 x 10^{14} 1MeV electrons cm^{-2} for both frontside and backside illumination. The substrate resistivity was assumed to be 2 ohm-cm although this was later changed to 10 ohm-cm for experimental devices due to processing related problems (see Section 3.2.5). Radiation damage coefficients used in the model were derived from empirical data from radiation damage studies on 2 ohm-cm solar cells. The damage coefficient was 5E-11 per electron in the base and 3 x 10^{-8} per electron in the emitter.

Following calculation of internal spectral response from the internal QE, the short circuit of the cell was computed by convolving the former with the illuminating spectrum reaching the cell. For the case of frontside illumination the spectrum reaching the cell was the AM0 spectrum (modified to take into account the reflectance of the frontside DAR coating). For backside illumination the light reaching the cell was assumed to

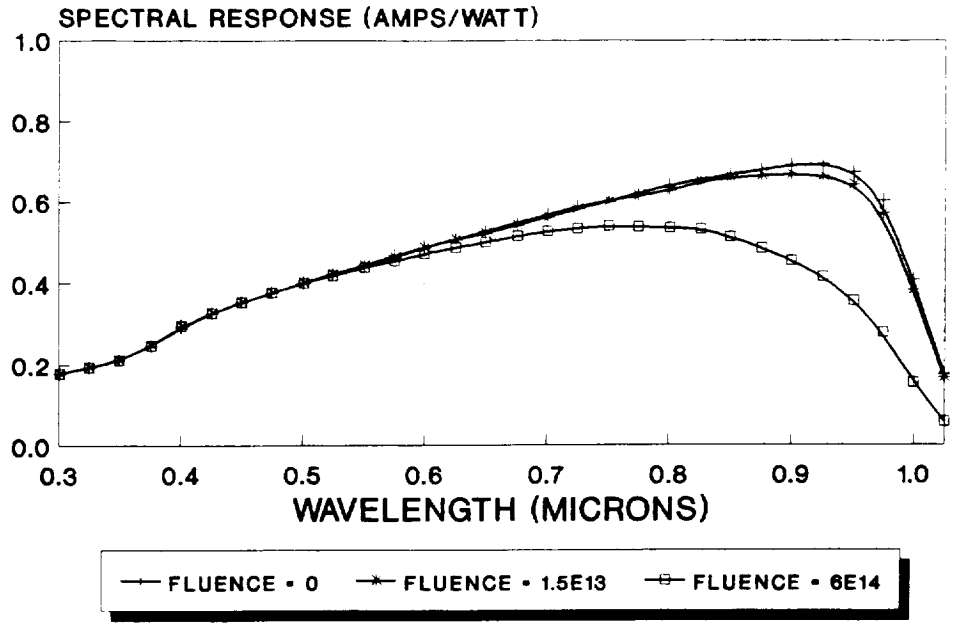

Figure 2-20 COMPUTED SPECTRAL RESPONSE (UNDER FRONT ILLUMINATION) OF GRIDDED BACK 2 OHM-CM K6 CELL AS A FUNCTION OF 1 MeV ELECTRON FLUENCE

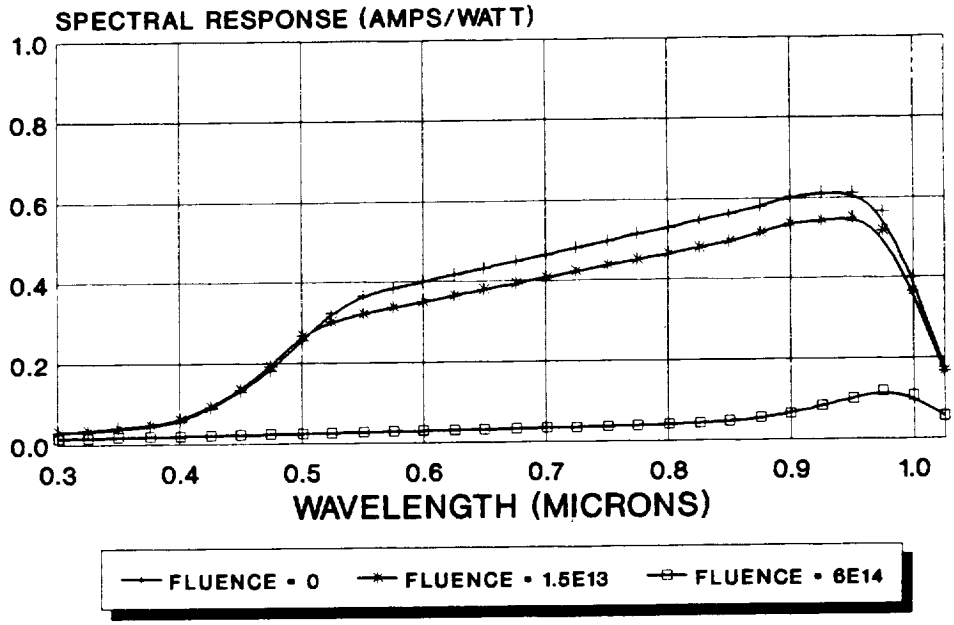

Figure 2-21 COMPUTED SPECTRAL RESPONSE (UNDER BACK SIDE ILLUMINATION) OF GRIDDED BACK 2 OHM-CM K6 CELL AS A FUNCTION OF 1 MeV ELECTRON FLUENCE

be a 35% AM1.5 spectrum[1], modified to take into account reflection and absorption losses in the Kapton blanket and backside DAR coating AR2. The AR coating thickness was then varied systematically until maximum J_{sc} conditions were obtained.

In some instances the backside DAR coating AR2 was optimized for maximum transmission of infrared (IR) radiation out through the back of the array. This amounted to optimizing the transmission at 1.5 microns wavelength. This was performed for medium 1 refractive indices of both n=1.41 (adhesive) or n=1.0 (space). The albedo produced short circuit current was then calculated for each optimum thickness of AR2. In this way it was possible to perform a sensitivity analysis to determine how different backside AR coatings optimized for different operating conditions (i.e. IR transmission or albedo collection) affected overall backside illumination performance.

2.3.2 Cell Performance

2.3.2.1 Modeled

As mentioned earlier two distinct scenarios were considered; one in which the backside AR coating was optimized for IR transmission and one in which it was optimized for the collection of albedo. In each case calculations were performed for a medium 1 refractive index of n=1.41 (adhesive) or n=1.0 (space) and gave rise to a large matrix of data shown in Tables 2-5 and 2-6. Typical data extracted from Tables 2-5 and 2-6 are shown in Figures 2-22 and 2-23 where we show modeled J_{sc} vs fluence for a dual AR coating of TiO_2/Al_2O_3 optimized for

---

[1]The intensity of the AM1.5 spectrum used during the OCLI study was 22.75 $mWcm^{-2}$. Subsequent work performed by Cleveland State University showed that albedo intensity on a feathered array may be up to 50 $mWcm^{-2}$ at certain times during the orbit.

Table 2-5 ALBEDO Jsc (mA CM^{-2}) CALCULATED AT BOL, AND FLUENCES OF 1.5E13 AND 6E14 1 MeV ELECTRONS CM^{-2}, FOR BACKSIDE AR COATINGS OPTIMIZED FOR ALBEDO COLLECTION

Designed for	Back Side AR Coating (Type, Thickness A)	DESIGNS OPTIMIZED FOR ALBEDO TRANSMITTANCE BOL n=1.0	BOL n=1.41	1.5E13 n=1.0	1.5E13 n=1.41	6E14 n=1.0	6E14 n=1.41
BOL	AO 746/T2 523	3.59	3.64	3.18	3.23	0.34	0.35
n=1.0	T2 758	3.44	3.69	3.05	3.27	0.33	0.35
	AO 1085	3.43	3.30	3.04	2.93	0.33	0.32
	TA 822	3.50	3.67	3.10	3.25	0.33	0.35
BOL	AO 973/T2 728	3.51	3.70	3.11	3.29	0.34	0.35
n=1.41	T2 746	3.43	3.69	3.04	3.27	0.33	0.34
	AO 1095	3.43	3.30	3.04	2.93	0.33	0.34
	TA 816	3.50	3.67	3.10	3.25	0.33	0.34
1.5E13	AO 748/T2 522	3.58	3.63	3.18	3.23	0.35	0.35
n=1.0	T2 757	3.44	3.69	3.05	3.27	0.33	0.35
	AO 1085	3.43	3.30	3.04	2.93	0.33	0.32
	TA 822	3.50	3.67	3.11	3.25	0.33	0.35
1.5E13	AO 973/T2 727	3.51	3.70	3.12	3.29	0.34	0.36
n=1.41	T2 746	3.43	3.69	3.04	3.27	0.33	0.35
	AO 1095	3.43	3.30	3.04	2.93	0.33	0.32
	TA 817	3.50	3.67	3.10	3.25	0.34	0.35
6E14	AO 810/T2 563	3.58	3.66	3.17	3.25	0.35	0.35
n=1.0	T2 793	3.44	3.69	3.05	3.27	0.33	0.35
	AO 1139	3.43	3.30	3.04	2.93	0.33	0.32
	TA 860	3.50	3.67	3.11	3.25	0.34	0.35
6E14	AO 982/T2 755	3.50	3.70	3.11	3.29	0.34	0.36
n=1.41	T2 780	3.44	3.69	3.05	3.27	0.33	0.36
	AO 1154	3.43	3.30	3.04	2.93	0.33	0.32
	TA 854	3.50	3.67	3.11	3.25	0.34	0.35

NOTE

AO Denotes Aluminum oxide
T2 Denotes Titanium dioxide
TA Denotes Tantalum oxide
All thicknesses in angstroms

Table 2-6 ALBEDO Jsc (mA CM^{-2} CALCULATED AT BOL, AND FLUENCES OF 1.5E13 AND 6E14 1 MeV ELECTRONS CM^{-2} FOR BACKSIDE AR COATINGS OPTIMIZED FOR IR TRANSMITTANCE AT 1.5 MICRONS

Designed for	Back Side AR Coating (Type, Thickness A)	DESIGNS OPTIMIZED FOR IR TRANSMITTANCE AT 1.5 MICRONS					
		BOL n=1.0	BOL n=1.41	1.5E13 n=1.0	1.5E13 n=1.41	6E14 n=1.0	6E14 n=1.41
BOL n=1.0	AO 1497/T2 1064	3.38	3.58	3.00	3.18	0.33	0.35
	T2 1558	2.75	3.23	2.45	2.87	0.27	0.32
	AO 1938	2.81	3.13	2.50	2.78	0.28	0.31
	TA 1688	2.76	3.22	2.45	2.86	0.27	0.32
BOL n=1.41	AO 2409/T2 1616	3.02	3.31	2.69	2.94	0.30	0.33
	T2 1574	2.75	3.23	2.45	2.87	0.27	0.32
	AO 1937	2.81	3.13	2.50	2.78	0.28	0.31
	TA 1696	2.76	3.22	2.45	2.86	0.27	0.32

NOTE

AO Denotes Aluminum oxide
T2 Denotes Titanium dioxide
TA Denotes Tantalum oxide
All thicknesses in angstroms

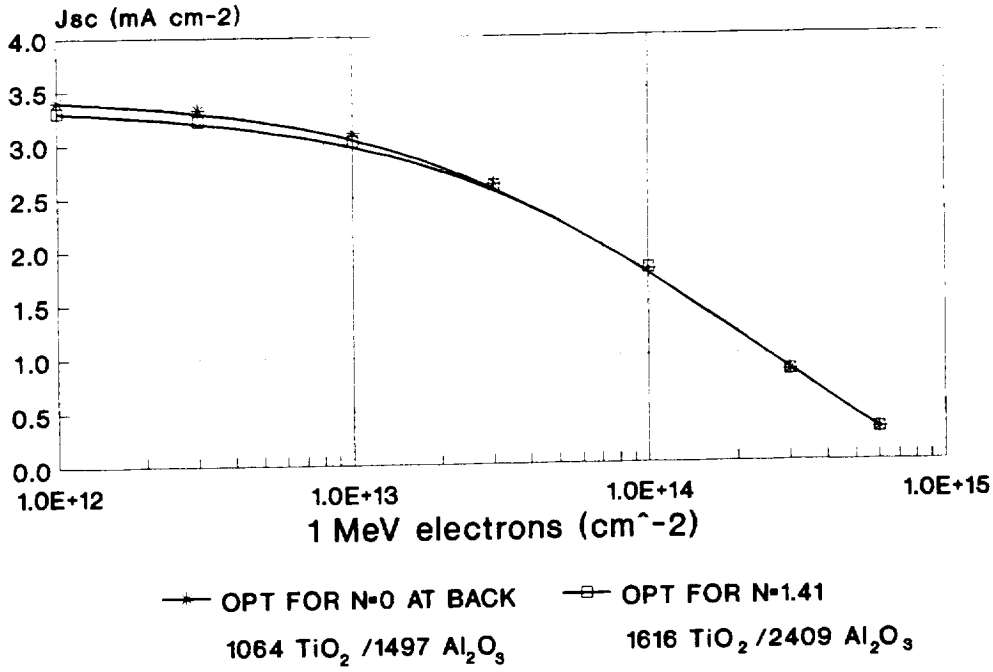

Figure 2-22 COMPUTED SHORT CIRCUIT CURRENT DENSITY UNDER BACK SIDE ILLUMINATION OF GRIDDED BACK 2 OHM-CM K6 CELL AS A FUNCTION OF 1 MeV ELECTRON FLUENCE

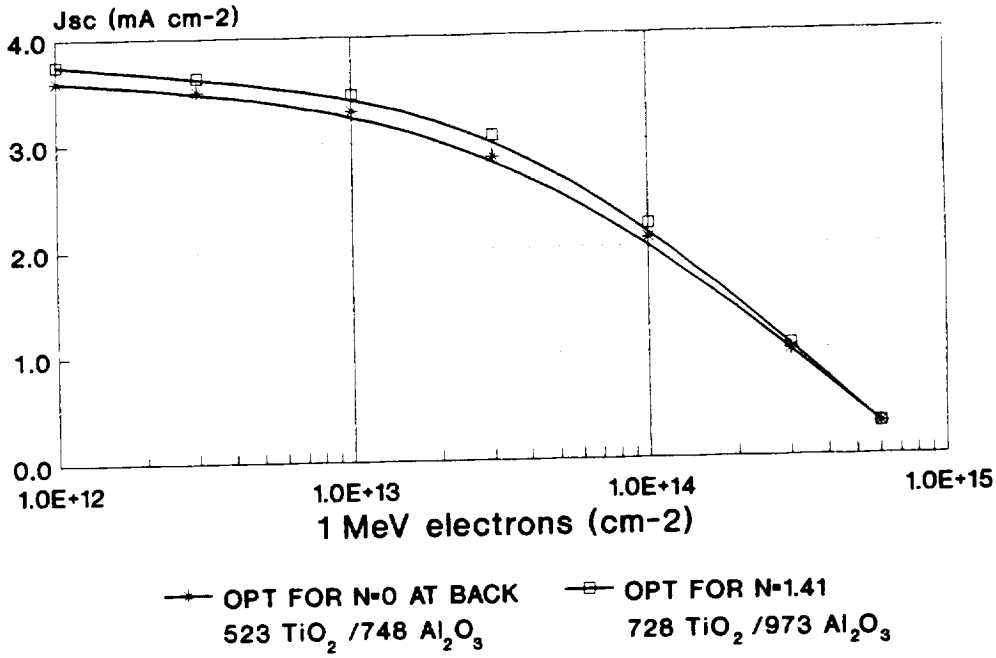

Figure 2-23 COMPUTED SHORT CIRCUIT CURRENT DENSITY, UNDER BACK SIDE ILLUMINATION, VS 1 MeV FLUENCE FOR CELL WITH "INFRA RED TRANSMISSION OPTIMIZED" AR COATING

albedo collection or IR transmission respectively. As expected, back illuminated J_{SC} falls rapidly with fluence since the current collecting junction is 200 microns from the light absorbing surface and the minority carrier diffusion length decreases rapidly with fluence. The difference in J_{SC} between cells optimized for albedo collection and IR transmission is small but significant however.

2.3.2.2 Experimental

In order to verify OCLI's modeling against empirical data a number of both 2 ohm-cm and 10 ohm-cm cells were measured under back illumination through a sample of the Kapton blanket coated with all relevant atomic oxygen coatings. Because there was a substantial difference in time frame between the fabrication of the 2 ohm-cm and 10 ohm-cm cells (which spanned a contract change) the 2 ohm-cm cells were fabricated with backside AR coatings optimized for I.R. transmission whereas the 10 ohm-cm cells had coatings optimized for albedo collection. Because of the need to work with space qualified AR coatings a decision was made to work with DAR coatings of TiO_2/Al_2O_3 only. Also it was decided to work with coatings optimized for BOL with a medium refractive index of n=1.0. Thus the DAR thicknesses as shown in Tables 2-5 and 2-6 were 746Å Al_2O_3/523Å TiO_2 for 10 ohm-cm cells 1497Å Al_2O_3/1064Å TiO_2 for the 2 ohm-cm cells. The spectral reflectance of DAR layers on silicon are shown in Figure 2-24 The difference in optical performance between the two layer designs is clear.

Measurements under simulated 35% AM1.5 were made at Spectrolab using an X25 solar simulator. Because of the difficulty in making adequate contact to the cell while illuminating through the Kapton blanket, only J_{SC} was measured. Also, because a

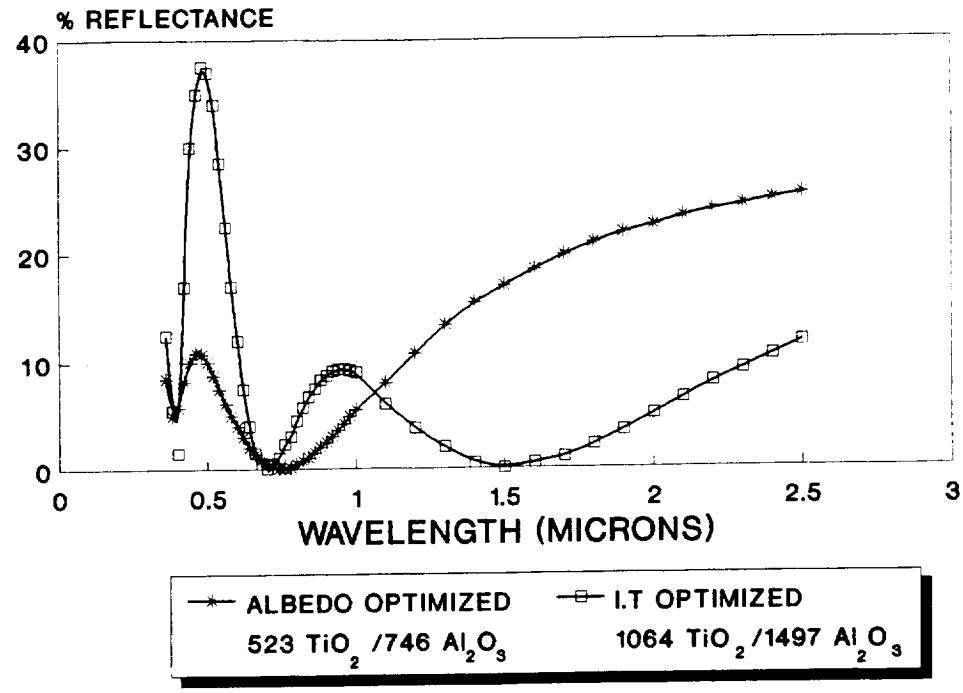

Figure 2-24 COMPUTED SPECTRAL REFLECTANCE FOR DUAL AR COATINGS OPTIMIZED FOR ALBEDO COLLECTION AND IR TRANSMITTANCE

simulator delivering an AM1.5 spectral content at 35% intensity was not readily available, measurements were made under 135.3 mW cm^{-2} intensity AM0 and a correction using standard spectral correction techniques for spectral mismatch and intensity was made. The intensity of the 35% AM1.5 spectrum used in our model was approximately 22.75 $mWcm^{-2}$.

In Figure 2-25 we show the empirical distribution of J_{SC} under back illumination through the Kapton blanket for both 2 ohm-cm and 10 ohm-cm cells using the above correction. The average corrected J_{SC} of the 2 ohm-cm cells, which had a backside

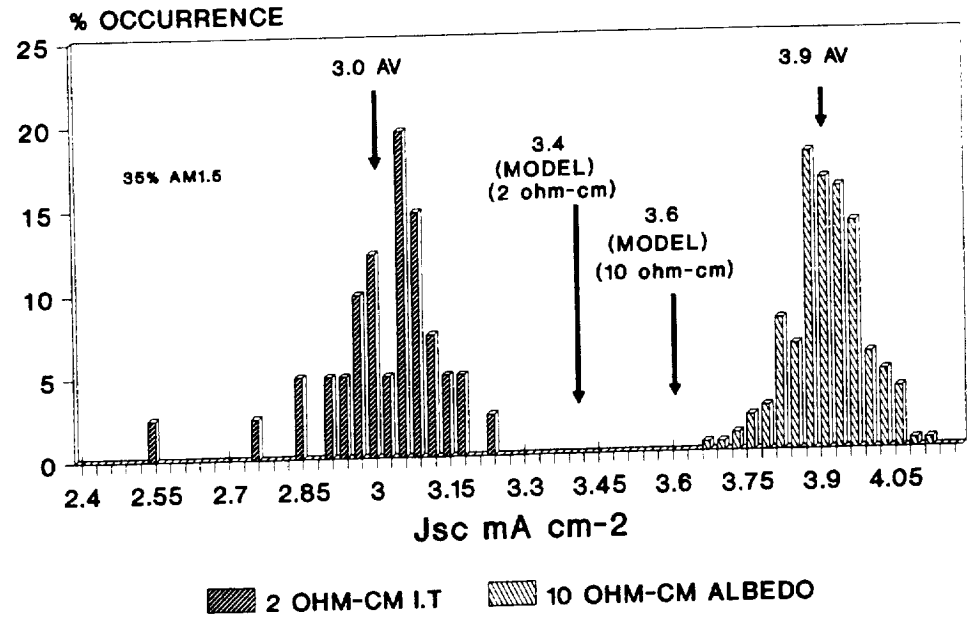

Figure 2-25 Jsc UNDER BACKSIDE ILLUMINATION (NORMALIZED TO 22.75 mW CM^{-2} AM1.5) FOR SPACE STATION FREEDOM CELLS OPTIMIZED FOR ALBEDO COLLECTION AND IR TRANSMITTANCE

coating optimized for IR transmission, was 3.00 $mAcm^{-2}$. This is slightly less than the 3.38 $mAcm^{-2}$ predicted by our model. The slight discrepancy is almost certainly due to small differences between empirical and computed internal QE. The average corrected J_{sc} of the 10 ohm-cm cells which had backside coatings optimized for collection of albedo radiation was 3.89 $mAcm^{-2}$ compared to 3.59 $mAcm^{-2}$ predicted by the model. In this case the slight increase over the predicted value is again almost certainly caused by small differences

between empirical and predicted internal QE. It should be noted that the QE data file used by OCLI in the computer model was for a 2 ohm-cm cell. The use of 10 ohm-cm material should produce an increase in QE due to the longer diffusion lengths in 10 ohm-cm material.

2.3.3 Cell Cover Optimization

The cost, power generation, thermal absorptance and emittance of various solar cell covers were calculated to show trades of performance versus cost. In Figure 2-26 we show the different designs considered. These designs reflected the types of cell cover available from OCLI at that time.

A proprietary model was used to calculate I_{sc} and solar absorptance for each cover type based on the transmission and absorption properties of each glass and using the Q.E. of a 2 ohm-cm silicon cell.

The adhesive was treated as a nonabsorbing material with refractive index 1.41 and arbitrary thickness. The cell was assumed to have a front surface DAR coating of 746Å Al_2O_3/ 523Å TiO_2.

The UV solar absorptance was calculated from the theoretical cover reflectance over the 280-350 nm wavelength range. The spectral region from 280-350 nm contains 4.27% of the total AM0 energy. Energy not reflected by the cover/cell assembly is absorbed in the cover, adhesive or cell. The results are summarized in Table 2-7 below.

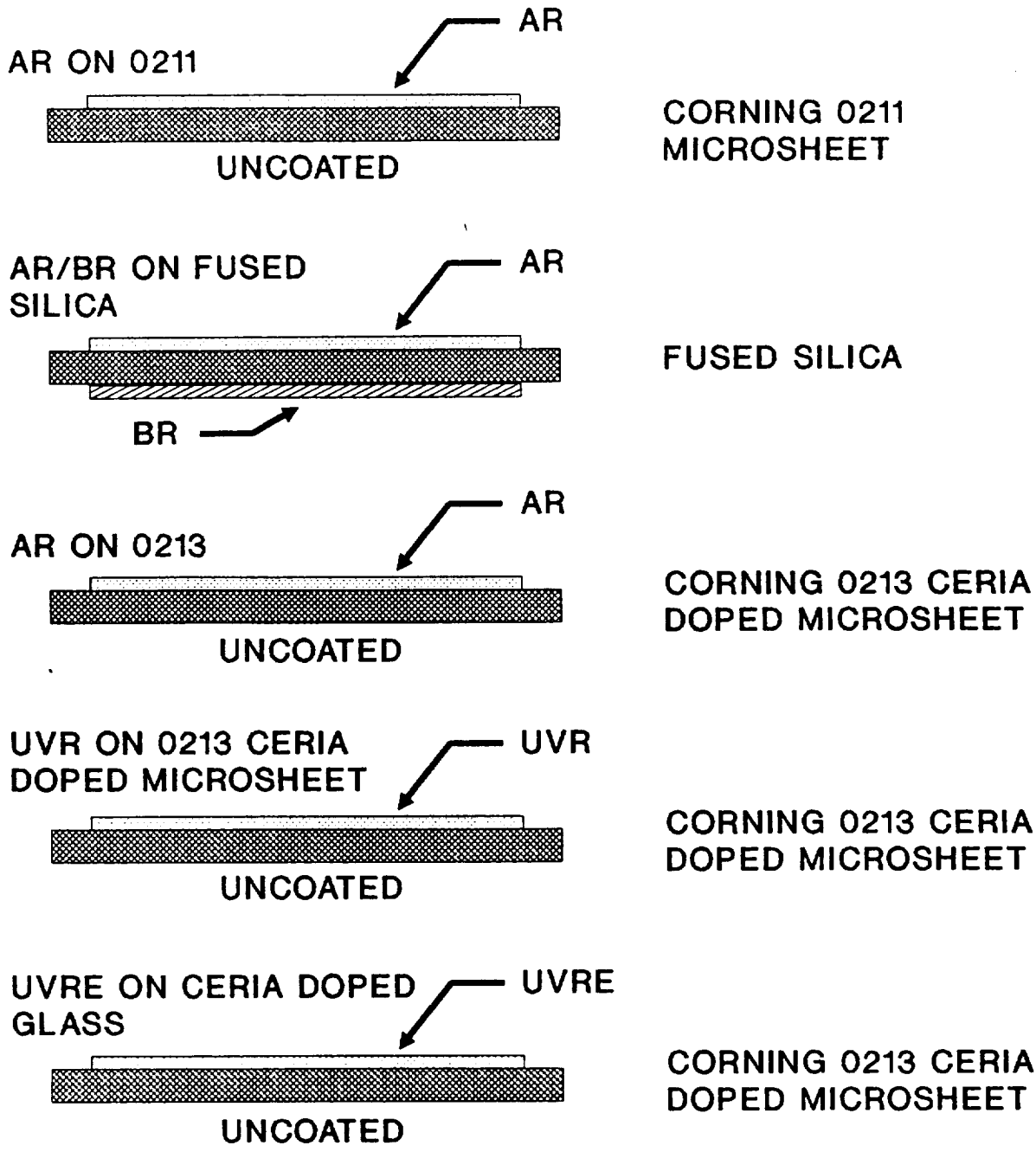

Figure 2-26 DIFFERENT TYPES OF CELL COVERGLASS CONSIDERED IN OCLI STUDY

Table 2-7 SOLAR CELL COVER PERFORMANCE TRADE-OFF

COVER DESCRIPTION	Jsc (mA/cm^2)	UV Solar Absorptance (%)	300K Emittance
Perfect cover (100% T)	43.62	0.00	1.00
AR on 0211	42.72	4.09	0.86
AR/BR on Fused Silica	42.19	0.39	0.82
AR on 0213	42.22	4.10	0.86
UVR on 0213	42.22	0.24	0.86
UVRE on 0213	42.25	0.80	0.89

The emittance values represent published values for the substrates and/or measurements on coated covers. Emittance is dominated by substrate properties for all covers except the UVRE on 0213. Measured values in the Table are derived from near normal infrared reflectance measurements (5-50 um) using standard techniques. The emittance values are total normal emittance at 300K.

The short circuit current of an ideal solar cell cover/cell assembly is shown in the first row of Table 2-7. This value represents the upper limit for short circuit current. All of the manufacturable designs fall short of the ideal design. I_{SC} is nearly identical for four of the designs and slightly higher for the AR on 0211. The higher I_{SC} at BOL for the AR on 0211 is due to higher transmittance in the 300-400 nm wavelength range. The other designs are purposely designed to have no transmittance below 350 nm to avoid darkening of the adhesive by incident ultraviolet radiation over time. The transmittance of these designs increases rapidly between 350-400 nm. Thus I_{SC} of the AR on 0211 design may drop below the other designs over time.

The UV solar absorptance is lowest for the UVR on 0213 and the AR/BR on fused silica, low for the UVRE on 0213 and high for the AR's on 0211 and 0213. The UVR on 0213 and the AR/BR on fused silica were optimized for minimum UV solar absorptance. The UV solar absorptance of the UVRE on 0213 is slightly higher because the UV rejection and emittance enhancement cannot both be optimized at the same time. The UVRE coating is a compromise between minimum UV solar absorptance and maximum emittance.

The emittance of the UVRE on 0213 is highest followed by the UVR and AR on 0213 and AR on 0211 and finally the AR/BR on fused silica. The emittance of the UVR and both AR designs are dominated by the emittance of the base borosilicate glass used in 0211 and 0213 Microsheet. The emittance of the AR/BR on fused silica is dominated by the emittance of fused silica, which is slightly lower than the emittance of borosilicate glass.

Relative costs for each of the products in 8cm x 8cm x 0.006" and 8cm x 8cm x 0.003" are tabulated in Table 2-8. Costs for the AR/BR on fused silica are indicated for 4cm x 4cm sizes. Fused silica is ground and polished from bulk "bricks". 4cm x 4cm represents the current largest size for covers made of this material. The costs for AR/BR on fused silica have been adjusted to cover equivalent area to the Microsheet (i.e. four 4cm x 4cm parts = one 8cm x 8cm part). Both 0211 and 0213 are drawn Microsheet glasses and may be fabricated in sizes up to 13"x 13". 8cm x 8cm is a reasonable dimension for large area covers made from 0211 or 0213.

Table 2-8 SOLAR CELL COVER RELATIVE COST TRADE-OFF

COVER DESCRIPTION	8cm x 8cm x .006"	8cm x 8cm x .003"	4cm x 4cm x .006" (Qty 4)	4cm x 4cm x .003" (Qty 4)
Uncoated 0213	1.00	1.10		
AR on 0211	1.25	1.37		
AR/BR on Fused Silica			4.95	6.19
AR on 0213	1.25	1.37		
UVR on 0213	1.65	1.82		
UVRE on 0213	2.38	2.61		

The relative costs do not include price reductions for large volumes. These numbers were intended to provide general information useful in comparison of performance/cost. Also the fused silica costs were for covers ground and polished on both sides. Fused silica covers with "frosted" surfaces are available at lower cost.

2.3.3.1 Cost/Performance Summary Discussion

The range of cell covers considered covered a wide range of cost/performance options, ranging from simple AR on 0211 or 0213 Microsheet to the UVRE on 0213 or AR/BR on fused silica. Each of these products may be appropriate for different applications. Systems designers must weigh the performance advantages of low UV solar absorptance, emittance, charged particle radiation resistance and cost to choose the best product for each unique application.

Cost considerations obviously eliminated the use of fused silica covers on Space Station FREEDOM. The UVR on 0213 provided extremely low absorptance, high efficiency (high transmittance) high emittance and good charged particle radiation resistance at moderate cost. The AR on 0213 also allowed excellent conversion efficiency but had a much higher UV solar absorptance due to UV absorption in the borosilicate glass.

For reasons of cost and delivery schedule a 6 mil borosilicate glass with AR (equivalent to AR on 0213) was therefore used for glassing the parts delivered in Task III of this contract. Some later cells were also delivered with a 5 mil thick cover.

2.4 OPTIMIZATION OF GRID DESIGN

In the case of the Space Station FREEDOM cell both the front and the back are gridded and it was important to be able to optimize both front and back grid designs.

The two top grid configurations considered on this program were for wraparound and wrapthrough contacts. These cases are shown schematically in Figures 2-27 and 2-28. At the time that this task was performed the wrapthrough design utilized two slots, laser scribed in the wafer. This was later changed to an array of four wrapthrough holes inboard on the wafer. In the wraparound case the contact was wrapped around the edges of the cell with a dielectric isolating the n+ contact from the p region. A similar method of dielectric isolation was used in both cell designs. The wrapthrough design afforded potentially lower series resistance since the average grid line length from the nearest bus-bar is shorter.

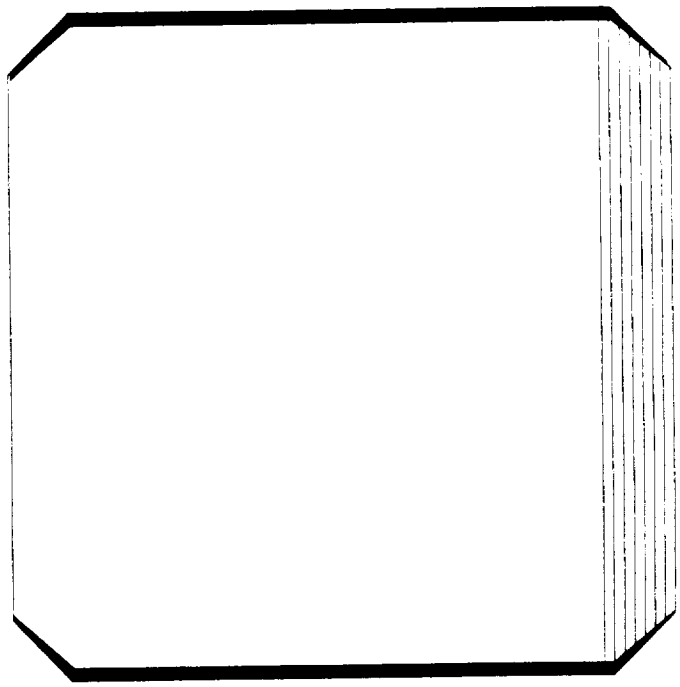

Figures 2-27 FRONT CONTACT "WRAPAROUND" OPTION

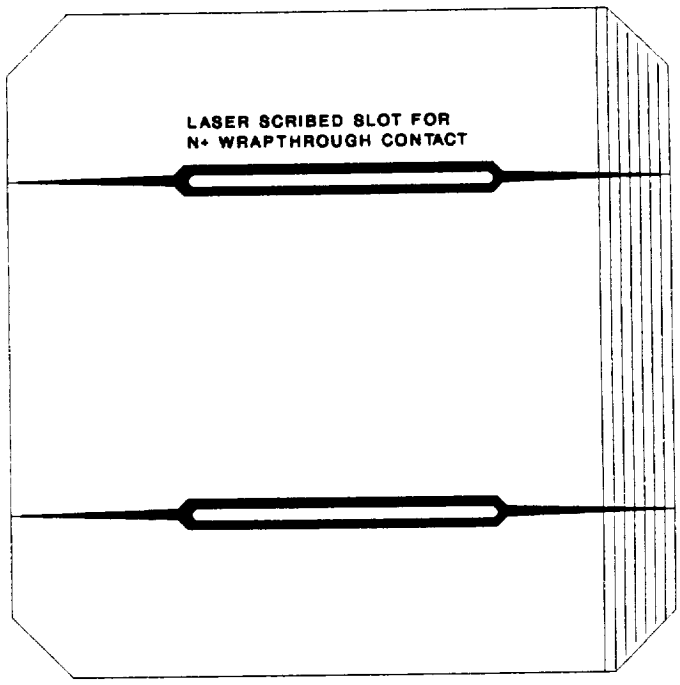

Figure 2-28 FRONT CONTACT "WRAPTHROUGH" OPTION

The back contact designs considered for each cell type are shown in Figures 2-29 and 2-30. There were eight P back contact weld points and four n+ contact weld points. For both wraparound and wrapthrough designs it was possible to assume a modular cell construction in order to simplify the analysis. Once the performance of a unit module was known, it was a simple matter to predict the performance of the complete cell.

The important parameters of the model used for grid-line optimization are the gridline dimensions, grid spacing, sheet resistance of the diffused region and the dimensions of the ohmic bus-bar. Tapering of the grid lines was also included in the model. It was also necessary to include the effects of base substrate resistivity, the ohmic contact resistance and also the effects of the gridded back structure. With respect to the latter the back grid structure was not a critical as for the front and it is possible to allow for back grid effects by the addition of a small multiplying factor to the base resistivity.

For each wrap design the data from previous computations for I_{sc}, V_{oc}, I_{01} and I_{02} were used together with the dimensions of the selected front grid module and other parameters such as emitter sheet resistance, base resistivity and contact resistance. The short circuit current density was adjusted to take into account the area of the module and the grid coverage factor and then an iterative nodal analysis was used to calculate the current-voltage relationship at nodes along each grid line. Finally an I-V output curve was drawn and a lumped series resistance parameter was calculated.

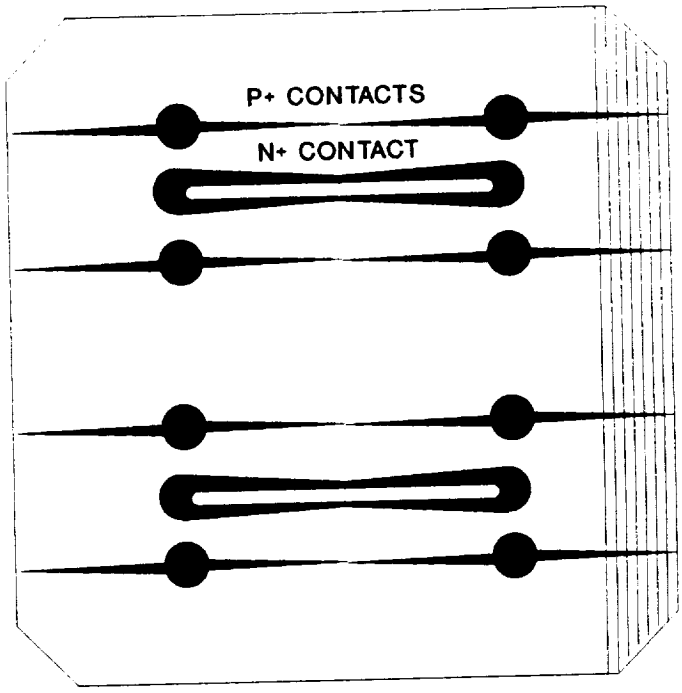

Figure 2-29 BACK CONTACT "WRAPAROUND" OPTION

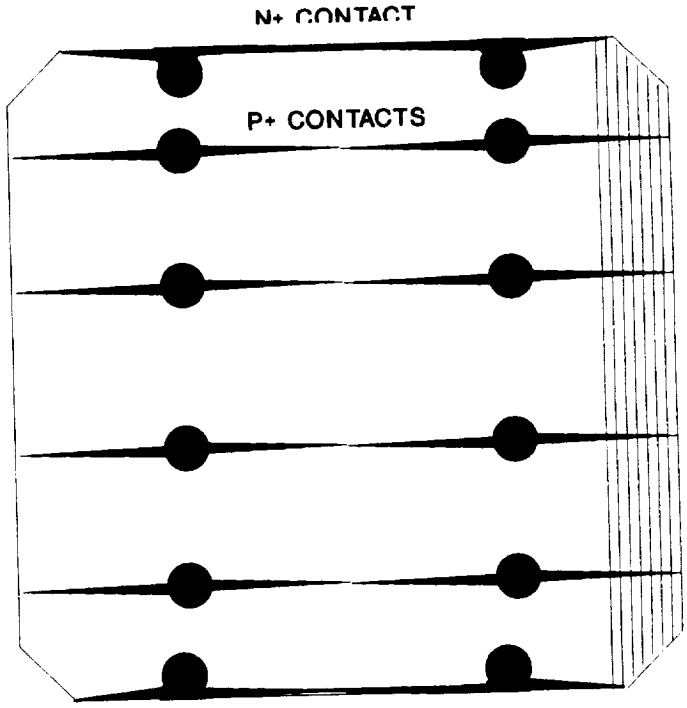

Figure 2-30 BACK CONTACT "WRAPTHROUGH" OPTION

In Table 2-9 we present the calculated data for selected cases which represented the optimum cell specification in each group. For the back contact design a grid height of 10 microns, was chosen with a grid spacing of 800 microns and a grid width of 25 microns. Because of the large number of weld points and bus bars on the back of the cell we calculated that this contributed a negligible 13 millohm-cm^{-2} to the overall series resistance of the cell.

For the front grid design we again chose a grid height of 10 microns, a width of 25 microns and an 800 micron grid spacing. A grid height of 10 microns was chosen to ensure the current carrying capability of the bus bars without making them unduly wide. (This thickness was easily achieved using a silver-plating technique.)

Considering Table 2-9 the results show, as expected, that the wrapthrough cells have a series resistance which is substantially lower then the equivalent wraparound cells. In either case however the series resistance was significantly lower than 800 milliohm-cm^2 used in earlier modeling. The performance of sculptured cells was not considered since it was concluded at this stage in the program that these structures had an excessive thermal absorptance which limited the on-orbit performance.

2.5 CRITICAL DESIGN REVIEW

A Critical Design Review (CDR) was held at Spectrolab on February 18, 1986 to which all prospective Space Station contractors were invited.

After consideration of available data at that time it was agreed that although the 4 mil K6 2 ohm-cm cell showed the highest predicted performance, the production of this cell, which was not demonstrated at the time, constituted an undue risk to the program.

There was concurrence however that the use of a back surface field and its effect on cell performance warranted further investigation.

Also the use of textured structures and oxide surface passivation were discounted based on experimental data.

The final conclusion was that the baseline cell for Task II manufacturing technology development should be a 8 mil, 2 ohm-cm K6 boron BSF cell with wrapthrough contact configuration.

3.0 TASK II: DEVELOPMENT OF CELL MANUFACTURING AND TESTING TECHNIQUES

The primary purpose of Task II was to develop the manufacturing processes to produce the wraparound solar cell, and to develop a process sequence that was both cost effective and workable for large volume production. Integral to this effort was performance characterization of the manufactured device and quality assurance planning that included in-line statistical process control, software management and product testing.

From Task I and experience in the development of the Spectrolab wraparound solar cell, we identified the processes and manufacturing techniques needing improvement or development. By scrutinizing the proposed process flow and the product performance requirements, all avenues were explored to reduce manufacturing costs.

During the time between the completion of Task 1 and the start of Task 2 some redesign of the front and back contact was made to reflect the requirements of LMSC who had been chosen as subcontractor to Rocketdyne for the photovoltaic power subsystem design.

In Figure 3-1 and 3-2 we show the modified front and back contact design. The two wrapthrough slots were replaced with four wrapthrough holes and a radial grid design. Modeling confirmed that since the average distance to the nearest n or p contact was essentially unchanged, the power output from the cell was unaffected.

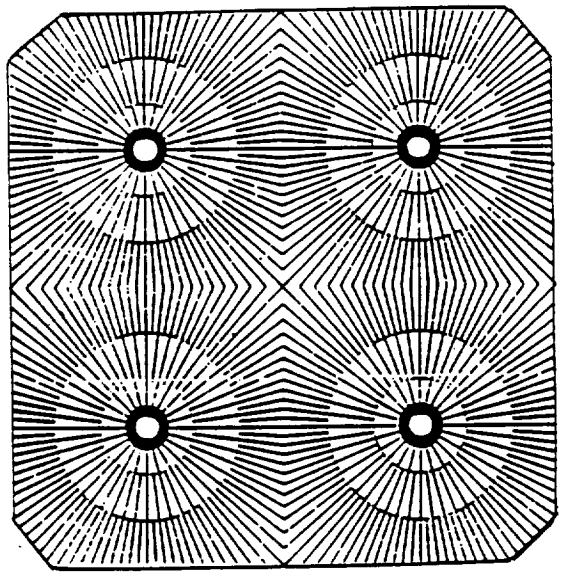

TOP

Figure 3-1 MODIFIED FRONT GRID DESIGN, INCORPORATING WRAPTHROUGH HOLE CONFIGURATION

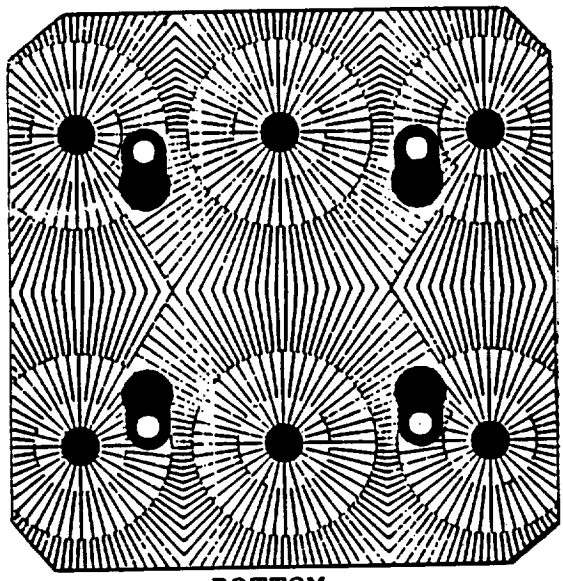

BOTTOM

Figure 3-2 MODIFIED BACK GRID DESIGN, INCORPORATING WRAPTHROUGH HOLE CONFIGURATION

3.1 STRAWMAN PROCESS SEQUENCE

A strawman process sequence was established, based on past and present experience with wraparound solar cells. This is shown in Figure 3-3.

The purpose of the initial wafer etch was to thin the wafer from an initial thickness of 14 mils to an intermediate thickness of about 10 mils.

Four holes were then laser scribed in the wafer using a pulsed Nd-YAG laser. Due to the pulsed nature of the laser the center of the holes remained attached to the edge by an area of badly damaged silicon.

A second wafer etch after laser scribing was then used to remove the hole center and to remove the amorphized material from around the hole edge.

Substantial process development was expended to arrive at a process which ensured well rounded holes. This is described in detail in Section 3.4.

A BSF formation process followed the hole formation. Both boron implantation and diffusion were investigated. This is described in Section 3.2.

After BSF formation the front junction was formed using SiO_2 masking to define the junction on the frontside only.

Following BSF and junction formation the dielectric was deposited around the wrapthrough hole using shadow masking techniques.

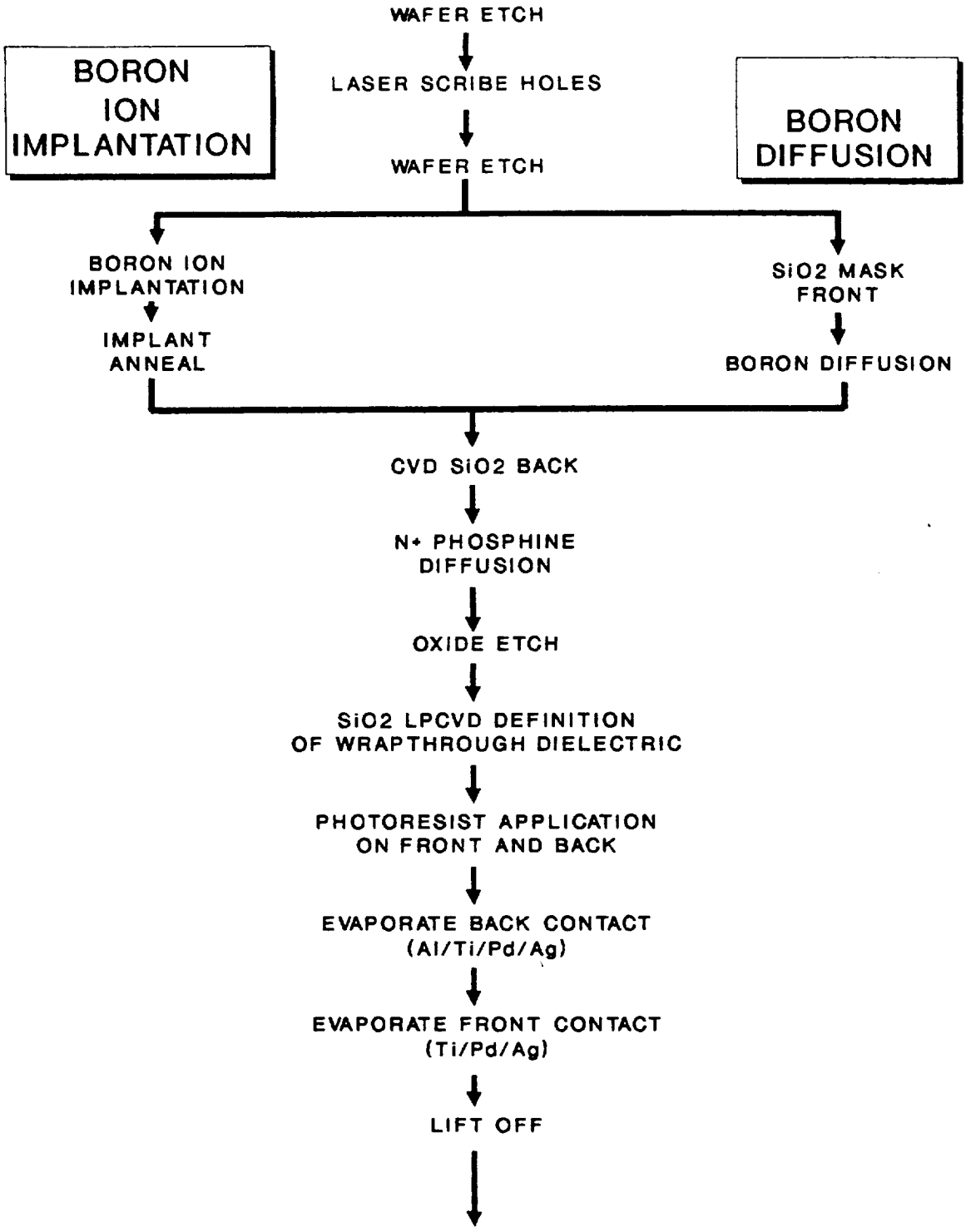

Figure 3-3 STRAWMAN PROCESS SEQUENCE FOR CELL PROCESSING

Experience with previous wraparound solar cells had clearly demonstrated that subtractive processes (i.e. depositing SiO_2 over the wafer and subsequently selectively etching away material) was inadvisable due to the formation of pinholes during etching. Pinholes provide points for Schottky barrier formation between the n contact and the p-type wafer and have been shown to be a serious loss mechanism in these cells.

Following dielectric deposition a photoresist process was used to define front and back grids. Because the wrapthrough holes eliminated the use of spin coating as a resist application method, various techniques including dipping, spray and roller coating were investigated. These experiments are described in Section 3.6.

After contact sintering a standard dual AR coating was applied to the front side. This was followed by a special purpose dual AR coating on the back side. In some cases the AR coating was optimized to maximize IR transmission out through the back of the cell. Later, as a result of the OCLI study, cells were coated with an albedo optimized coating consisting of 523Å TiO_2/746Å Al_2O_3.

Cells were cut to final size using standard Nd-YAG laser scribing and tested using a specially developed test fixture.

Cell covers (6 mil borosilicate glass with UVR) were applied on some cells using DC 93-500 adhesive.

3.2 BACK SURFACE FIELD (BSF) FORMATION PROCESS

A low cost boron BSF process was investigated using Boron Nitride (BN) disks, gaseous diffusion from diborane (B_2H_6), ion implantation and diffusion from a doped oxide. The results of these studies are described below.

3.2.1 BN Disk Diffusion

The work on BN disk diffusion was divided into two parts. During the first quarter of 1986, extensive tests were performed using solid source BN disks from Carborundum and Owens Illinois. At this time all wafers were 2 ohm-cm which was baseline for Task II development. Unknown at this time, boron oxygen complexes, formed during the high temperature processing prevented high quality devices from being produced. This work was repeated later in 1988 on 10 ohm-cm silicon wafers with much improved results. This work is described below.

3.2.1.1 Early Work on BN Diffusion (1986)

The process recommended by the disk manufacturer was to use a deposition step of 850°C for 1 hour to produce a boron rich oxide layer on the wafer surface. This was then followed by a 5 hour, 850°C drive-in anneal (without disks) in a N_2/O_2 atmosphere. Some wafers were also shipped to AG Associates for a rapid thermal anneal (RTA) at 1050°C in N_2 for 70-80 seconds. The rationale for performing the latter was to reduce the time at high temperature to reduce high temperature induced processing defects but still achieve 1 to 2 micron deep junctions with a surface concentration of $5 \times 10^{18} cm^{-3}$.

After boron diffusion, wafers were processed into nominal 2cm x 4cm top/bottom cells to eliminate confusion between BSF effects and other leakage problems at the wrapthrough hole. The actual cell area was 8.56 cm^2.

Persistent problems were encountered when trying to develop the BN disk diffusion process. Typically the spread in both Isc and Voc was very large as shown in Figures 3-4 and 3-5. The data shown are for parts diffused for a total of 6 hours at 850°C

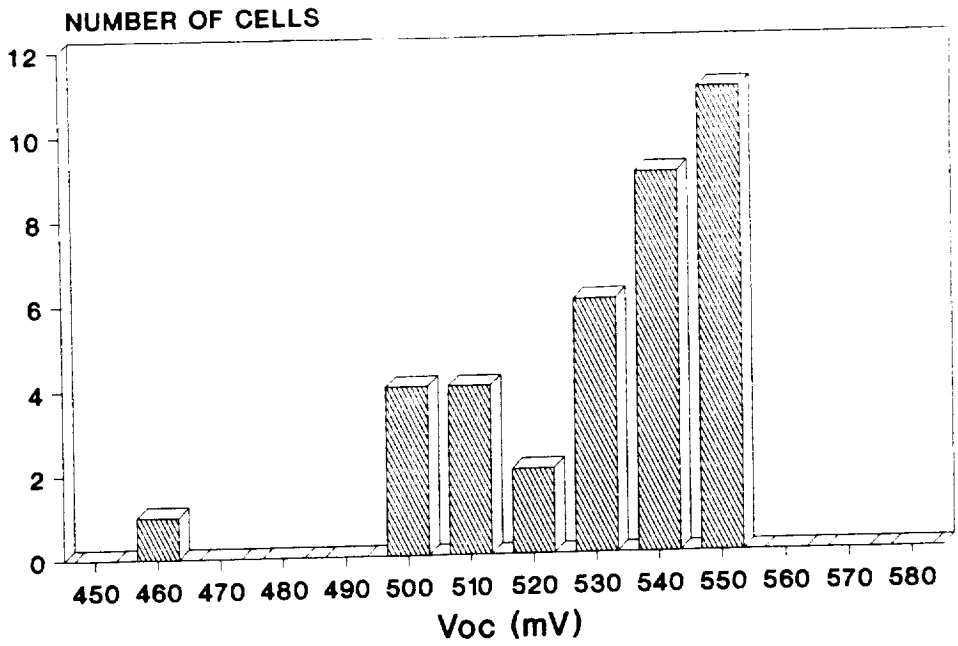

Figure 3-4 Voc DISTRIBUTION FOR CELLS WITH BSF PRODUCED BY BN DISK BORON DIFFUSION FOR 6 HOURS AT 850°C

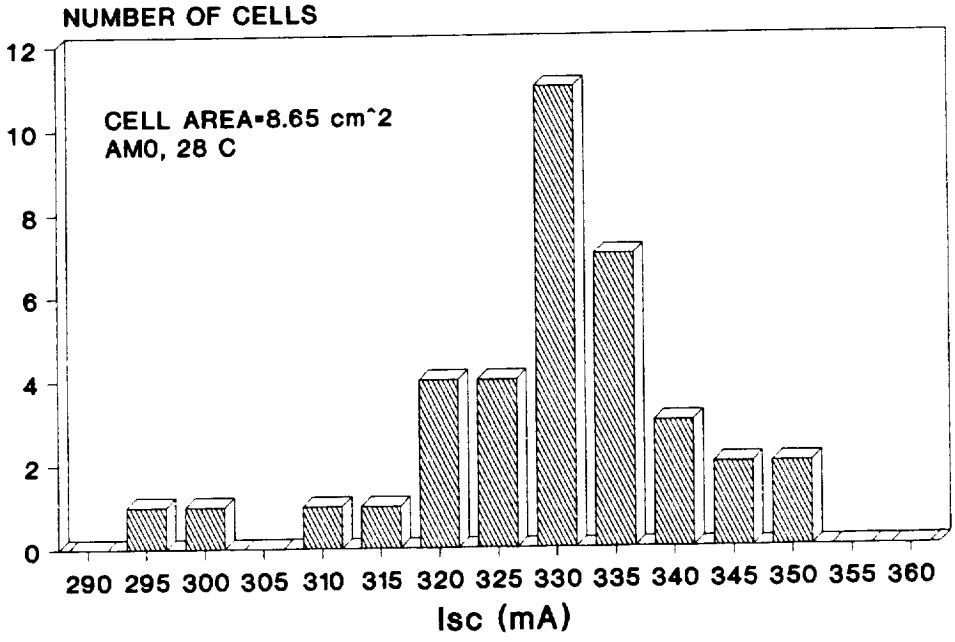

Figure 3-5 Isc DISTRIBUTION FOR CELLS WITH BSF PRODUCED BY BN DISK BORON DIFFUSION FOR 6 HOURS AT 850°C

although similar characteristics were obtained for parts which were rapidly thermal annealed. Some wafers were sent to Owens Illinois and Carborundum for diffusion and returned to Spectrolab for processing but the spread in data was always the same.

Further analysis using dark I-V and spectral response measurements indicated that the wide range in Voc and Isc was due to large degradations in diffusion length in some wafers. Figure 3-6 shows the dark I-V curves measured on cells picked from the top and bottom of the Voc distribution.

First and second diode saturation currents I_{01} and I_{02} were determined to be 3.2E-11 A cm^{-2} and 1.27E-8 A cm^{-2} for cell # 20 and 6.14E-11 A cm^{-2} and 1.76E-6 A cm^{-2} for cell # 39. This compared to approximately 1 x 10^{-12} A cm^{-2} and 3 x 10^{-8} A cm^{-2} for a good BSF device.

Because little progress was being made on BN disk diffusion at this point in time the diffusion process was abandoned in favor of ion implantation which was showing more encouraging results.

3.2.1.2 Later Work on BN Disk Diffusion (1988)

In the first quarter of 1988 the contract was modified to re-evaluate the use of solid source BN disk diffusion using 10 ohm-cm wafers. It should be noted here that interim work had shown this sensitivity of low resistivity (2 ohm-cm) silicon to high temperature processing and 10 ohm-cm wafers had become baseline.

In Table 3-1 we show the process matrix used for evaluation. Wafers and disks were inserted into the chamber at 800°C using an automated boat loading system. This was followed by a 30

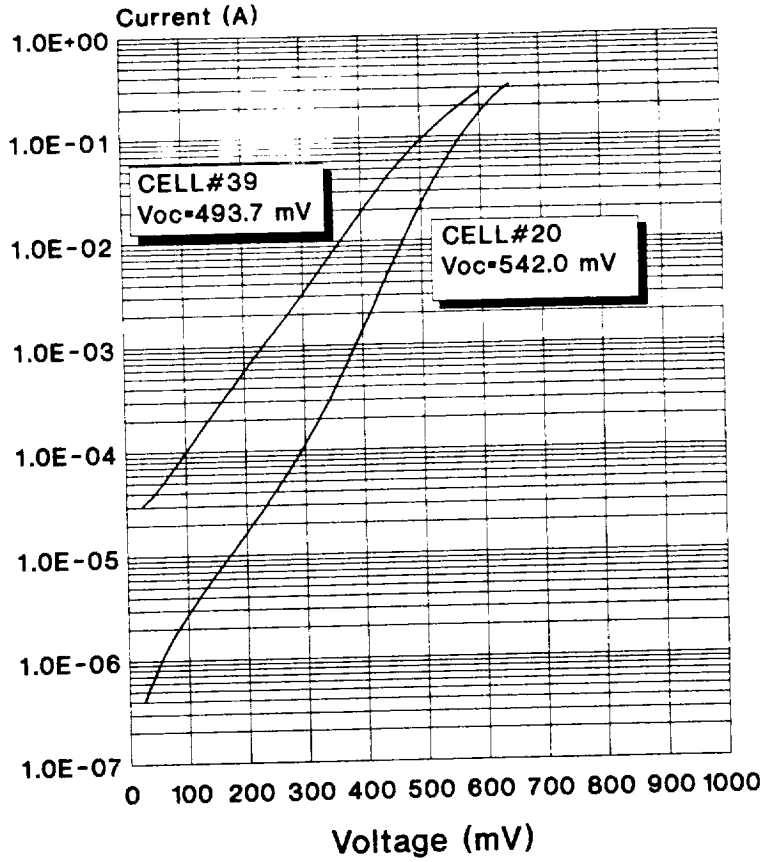

Figure 3-6 TYPICAL DARK IV CURVES FOR CELLS SELECTED FROM TOP (CELL #20) AND BOTTOM (CELL #39) FROM Voc DISTRIBUTION

Table 3-1 PROCESS MATRIX FOR BACK SURFACE FIELD FORMATION USING BN DISKS

Process Sequence	LOT NUMBER B1	B2	B4	B6
Insert (T deg C)	800C	800C	800C	800C
Stabilize (time mins)	30	30	30	30
Ramp to: (T deg C)	1000	1000	1000	985
Soak (time mins)	60	90	90	35
Reinsert	NO	NO	800C	800C
Drive in temp (T deg C)	N/A	N/A	1070	1070
Drive in time (mins)	N/A	N/A	105	90
LTO Time (time mins)	45	45	45	45
(T deg C)	750	750	800	750

minute stabilization period during which time, temperature equilibrium was established. The wafers were then ramped to 985 or 1000°C and soaked for between 35 and 90 minutes in a forming gas (4% H_2/96% N_2) atmosphere. During this time a boron rich glass was deposited onto the surface. At this point some of the lots (B4 and B6) were removed from the furnace and inserted into another clean tube without disks for a further drive-in sequence. (The BN disks only withstood a maximum temperature of 1000°C).

Prior to removal, all wafers, regardless of whether or not a drive in sequence was performed, were subjected to a low temperature oxidation (LTO) process which facilitated subsequent removal of the boron glass.

Following boron diffusion all wafers were made into nominal 2cm x 4cm cells.

In Table 3-2 we summarize the data. Lots B1 and B2 had shallow junctions of 0.72 and 0.8 microns respectively as determined by spreading resistance and generally showed low Voc and Isc values. They were therefore rejected at this stage prior to AR coating. (Lot B4 was not metallized due to the very low voltage probe measurements). Lot B6 was completed and cells were characterized. The data is summarized in Table 3-3. The best cell I-V curve is shown in Figure 3-7. The efficiency was 14.8% (AM0, 28°C).

A phenomenon which was consistently observed on all BN diffused cells was a dynamic increase in Voc over a period of approximately 20 seconds continuous illumination. This was also reflected by a small decrease in Isc also.

Table 3-2 JUNCTION DEPTH, VOLTAGE PROBE AND KEY CELL DATA FOR BN DISK MATRIX EXPERIMENT

Parameter Measured	LOT NUMBER B1	B2	B4	B6
Junction Depth (microns)	0.72	0.80	2.50	2.40
Voltage Probe (mV)	575-600	590-600	297-505	575-609
Cell Voc (mV)	579 best	584 best	not processed further	600-613
Cell Jsc (mA cm^-2)	29.6 best (no DAR)	30 best (no DAR)		42.5 best (with DAR)

Note: The Jsc and Voc on a K4 control cell processed simultaneously were 38.5 mA cm^-2 and 544 mV respectively

Table 3-3 SUMMARY DATA FOR 2cm X 4cm CELLS PRODUCED USING BN DISK DIFFUSION

Initial Voc (mV)	Initial Voc (mV)	Jsc (mA cm^-2)	J @495 mV (mA cm^-2)	FF @ Load	EFF @ Load %	I01 Amp cm^-2	I02 Amp cm^-2
611	612	42.5	40.1	0.76	14.7	*	*
609	613	42.3	40.4	0.77	14.8	9.3E-13	7.4E-8
600	608	41.9	39.3	0.76	14.4	*	*
606	612	42.3	40.1	0.77	14.7	*	*
613	613	42.6	40.1	0.76	14.7	*	*
601	611	42.3	39.7	0.76	14.5	*	*

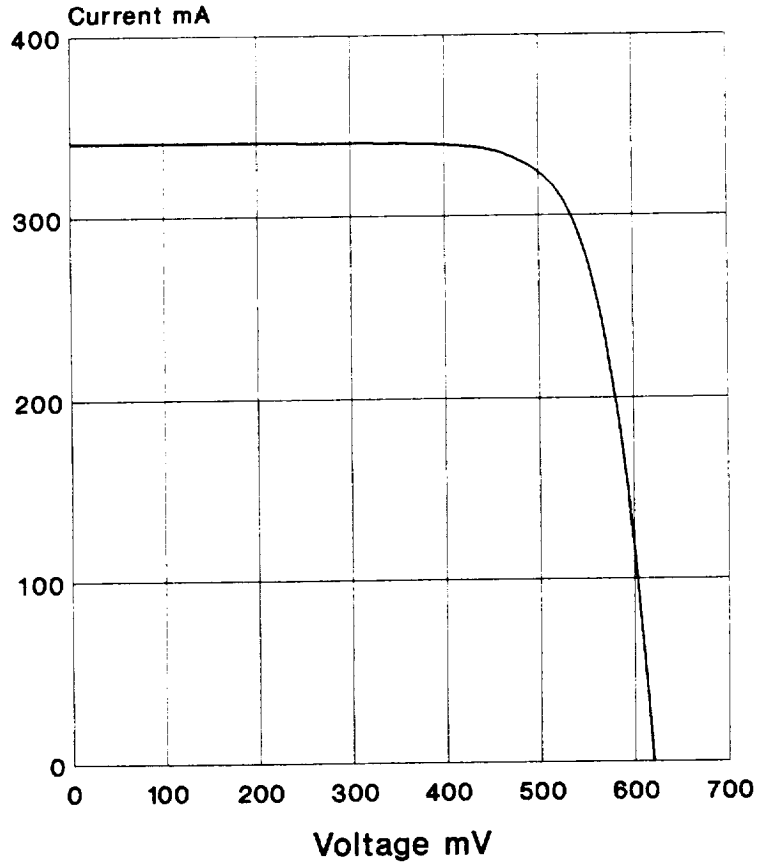

Figure 3-7 BEST 2cm X 4cm CELL PRODUCED USING BN DISK DIFFUSION

The increase was seen to be more pronounced on lower efficiency, low voltage cells. The increase in Voc and decrease in Isc was found to persist even after storage in the dark for up to 30 minutes after illumination.

This process could be repeated many times indicating the process of filling and emptying of very slow traps or recombination centers in relatively poor communication with the semiconductor. A detailed discussion appears in Section 3.4.

While the BN disk diffusion process was matured to a sufficiently advanced state to enable 15% efficiency cells to be produced it was not pursued further due to the persistence of the "dynamic response" phenomenon (which would make LAPSS testing impossible)and also due to the success of the alternative method of field formation by ion implantation.

3.2.2 Diffusion From Borosilicate Glass

Part of the Task II development effort was to investigate the use of boron doped silicon dioxide as a low cost BSF diffusion source.

Doped oxides were procured externally from Thermco, ASM and Tempress. The doped oxide thickness was 0.5μm and the boron composition was approximately 4 atomic %.

Table 3-4 shows the process matrix which was performed. As with the BN disk diffusion, the wafers were inserted into the tube at 800°C and allowed to equilibrate for 30 minutes. The temperature was then ramped up to between 1050 and 1100°C and then a drive in was performed in N_2 for up to 2.5 hours. The wafers were then quenched to room temperature by rapid removal from the furnace.

Table 3-5 shows the data on 2cm x 4cm cells which resulted from the matrix. The process producing the most consistent performance was achieved using a drive in for 2 hours at 1050°C.

As with the BN disks some dynamic response of Voc was seen.

Although BSG was shown to be an effective method of BSF formation the persistent occurrence of the dynamic Voc response caused the process to be rejected in favor of ion implantation.

Table 3-4 PROCESS MATRIX FOR BSG BACK SURFACE FIELD FORMATION

Process Sequence	40.1 B3	LOT NU B5	14.7 B7	* B8
42.3	40.1	0.77	14.7	*
Insert	800C	800C	800C	800C
(T deg C)	39.7	0.76	14.5	*
Stabilize (time mins)	30	0	15	20
Ramp to: (T deg C)	1100	1050	1070	1100
Drive in tim (mins)	150	120	120	120

Table 3-5 SUMMARY DATA FOR 2cm X 4cm CELLS PRODUCED USING BSG FOR BACK SURFACE FIELD FORMATION

PERFORMANCE AVERAGE EACH WAFER

Wafer#	Voc (mV)	Jsc (mA cm^-2)	J @495 mV (mA cm^-2)	FF @ Load	EFF @ Load %
A1	612	42.75	40.63	0.769	14.9
A2	610	42.88	40.88	0.771	14.9
A3	607	42.63	40.38	0.770	14.8
A4	607	42.38	40.00	0.770	14.6
Best	613	43.13	41.25	0.772	15.1

3.2.3 Ion Implantation

Back surface field formation by boron ion implantation was developed on 2 ohm-cm and 10 ohm-cm wafers at both Spire Corporation and Ion Implant Services.

Wafers were procured at 14 mils thickness and etched to 8 mils using 30% NaOH followed by a standard 3-1-2 $HNO_3/HF/CH_3COOH$ polish etch. Several optically polished wafers always accompanied the polish etched wafers to implant so that spreading resistance doping profile measurements could be made. Two implant doses were investigated, 5×10^{15} ions cm^{-2} at 50 keV which was designed to produce a 1 micron junction with a surface concentration of approximately 10^{20} electrically active atoms per cm^2 and 5×10^{14} ions cm^{-2} at 10 keV, designed to produce a surface concentration of 5×10^{18} cm^{-2} and a junction depth of approximately 0.5 microns.

After implantation the wafers were damage annealed in dry nitrogen for 2 hours (5×10^{15} ions cm^{-2}) or 30 minutes (5×10^{14} ions cm^{-2}) to electrically activate the dopant.

After being returned to Spectrolab the implanted wafers were cleaned using standard silicon cleaning procedures. The backs were diffusion masked using atmospherically deposited CVD SiO_2 and a phosphorus diffusion was performed to create a 0.15 micron deep N^+ emitter. Following removal of the diffusion oxide and back oxide mask the backs of the wafers were metallized using a standard Ti/Pd/Ag metallization. A similar metallization was used to produce the front grid metallization using a lift off process. Wafers were finally dual AR coated with TiO_2/Al_2O_3 and scribed to final size (8.65 cm^2) using a laser scriber.

In Figures 3-8 and 3-9 we show the measured spreading resistance profile of the high and low dose implants as measured at Solecon Labs. The technique measured electrically active concentrations of impurities as a function of depth into the substrate. The profiles were close to those expected and which have been found previously to produce high efficiency solar cells.

In Figures 3-10, 3-11, and 3-12 we show the distribution of Voc, Isc and efficiency for the cells implanted at 5×10^{14} ions cm^{-2} at 10 keV. It was concluded poor performance resulted from the fact that the diffusion was too shallow and further work was confined to 5×10^{15} cm^{-2} 50 keV implants.

In Figures 3-13, 3-14, and 3-15 we show the distribution of 10 ohm-cm parts implanted with $5 \times 10^{15} cm^{-2}$ boron and annealed for 2 hours in N_2. The poor performance was due to defects generated during the high temperature processing. These defects, described in Section 3.2.5, reduce the base diffusion length and the cell performance.

It should be noted here that Voc for a 10 ohm-cm non fielded cell with a base diffusion length of approximately 600 microns is typically 545 mV. The fact that very low voltage parts were associated with low Isc supports the fact that the base diffusion length was also probably degraded. This was confirmed by spectral response measurements showing very poor response in the red region.

Later work on boron implantation using $5 \times 10^{15} cm^{-2}$ 50 keV boron annealed 2 hours resulted in much better cell characteristics; Voc = 598 mV, Isc = 40.7 ma/cm^2, eff. = 13.9%. Because this process was reproducible on 10 ohm-cm silicon it was baselined for all further SSP Task II development and Task III pilot production work.

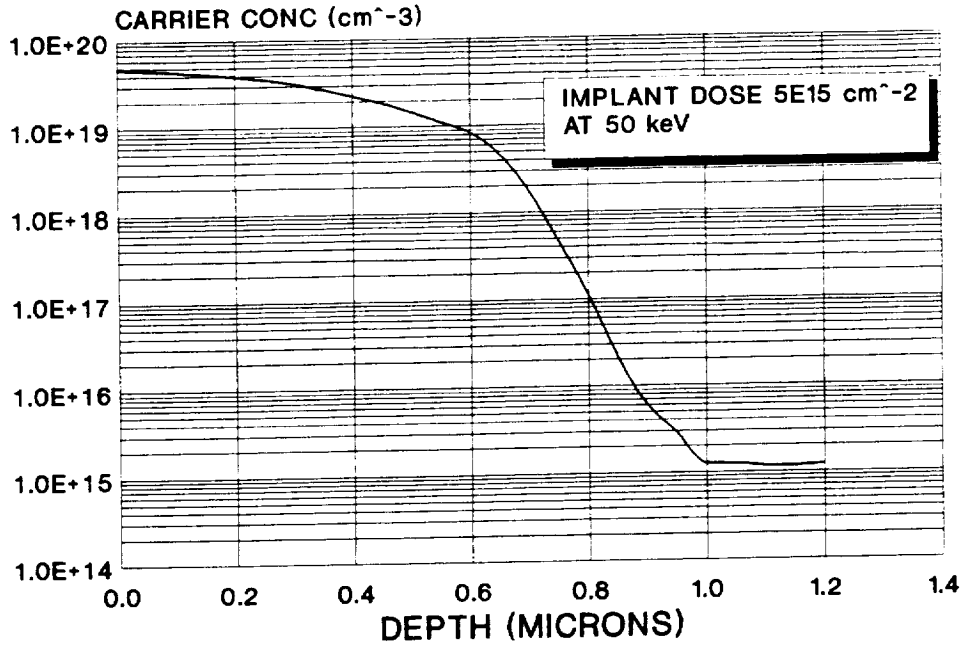

Figure 3-8 SPREADING RESISTANCE PROFILE OF HIGH ENERGY, HIGH DOSE IMPLANT

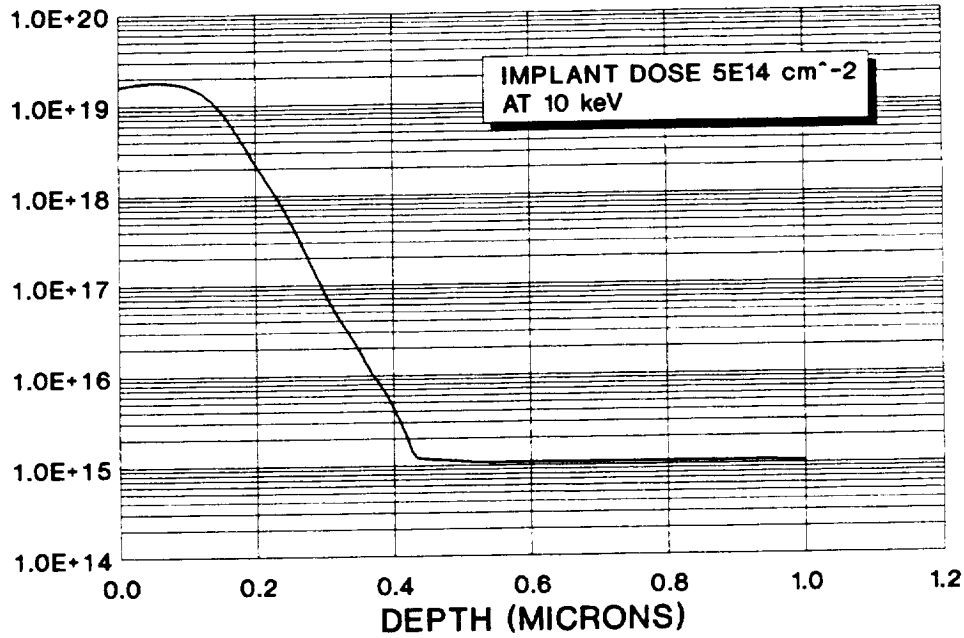

Figure 3-9 SPREADING RESISTANCE PROFILE OF LOW ENERGY, LOW DOSE IMPLANT

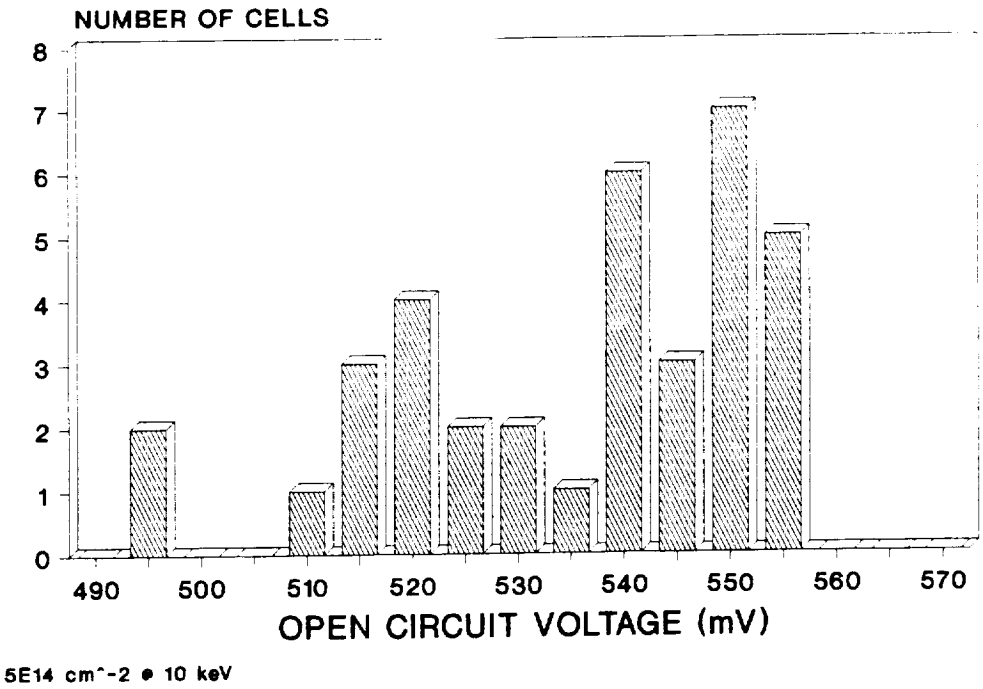

Figure 3-10 Voc DISTRIBUTION OF CELLS PRODUCED BY ION IMPLANTATION OF $5x10^{14}$ CM^{-2}, 10 keV B IONS

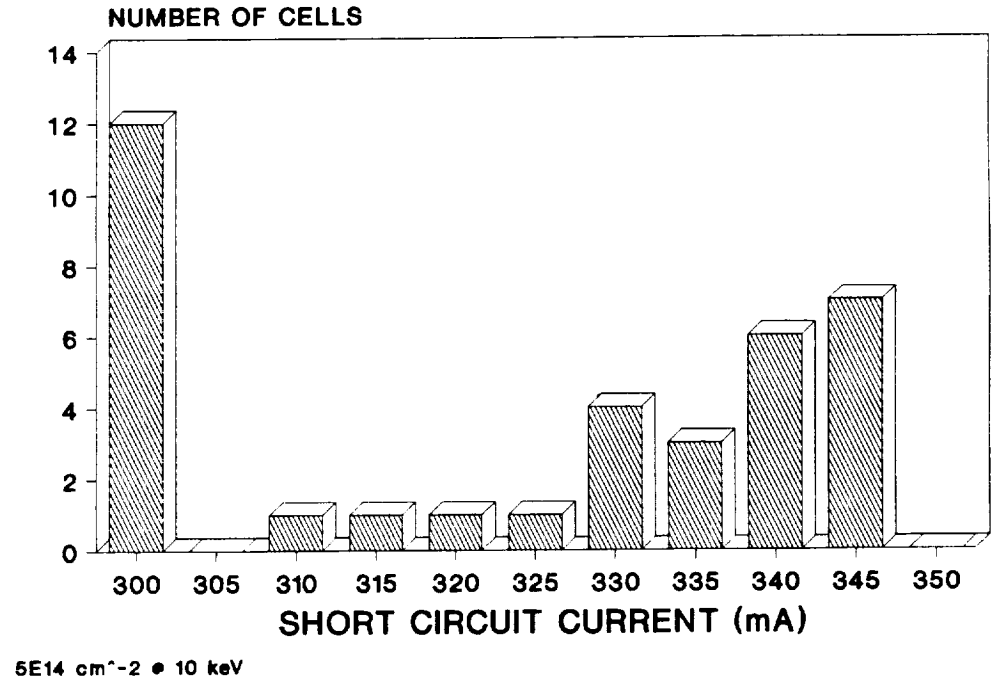

Figure 3-11 Isc DISTRIBUTION OF CELLS PRODUCED BY ION IMPLANTATION OF $5x10^{14}$ CM^{-2}, 10 keV B IONS

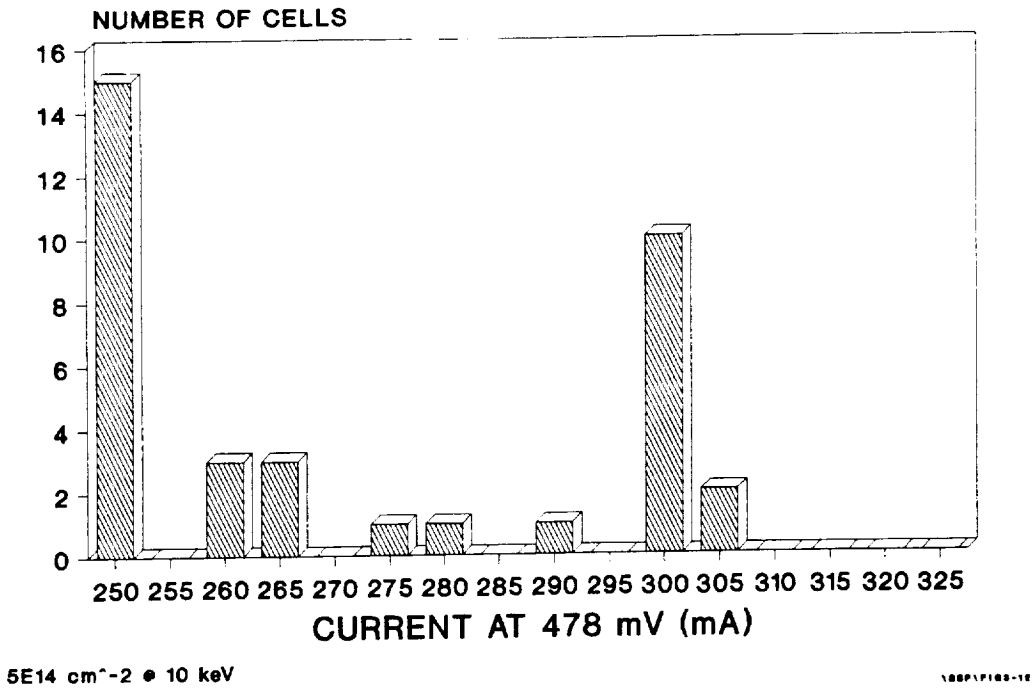

Figure 3-12 I @ 478 mV DISTRIBUTION OF CELLS PRODUCED BY ION IMPLANTATION OF $5x10^{14}$ CM^{-2}, 10 keV B IONS

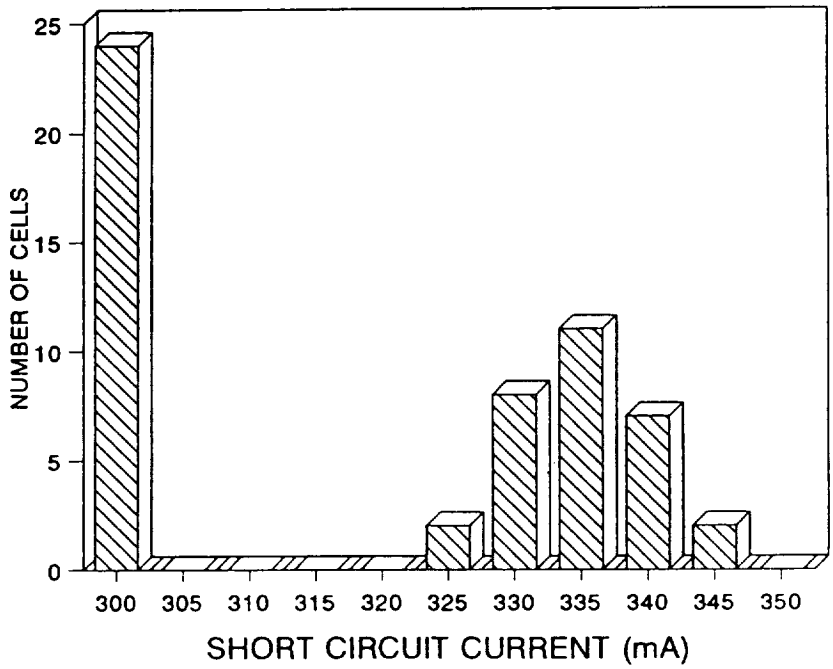

Figure 3-13 Isc DISTRIBUTION OF CELLS WITH BSF IMPLANTED WITH $5x10^{15}$ B IONS @ 50 keV. IMPLANT ANNEAL 2 HOURS AT $985^{o}C$

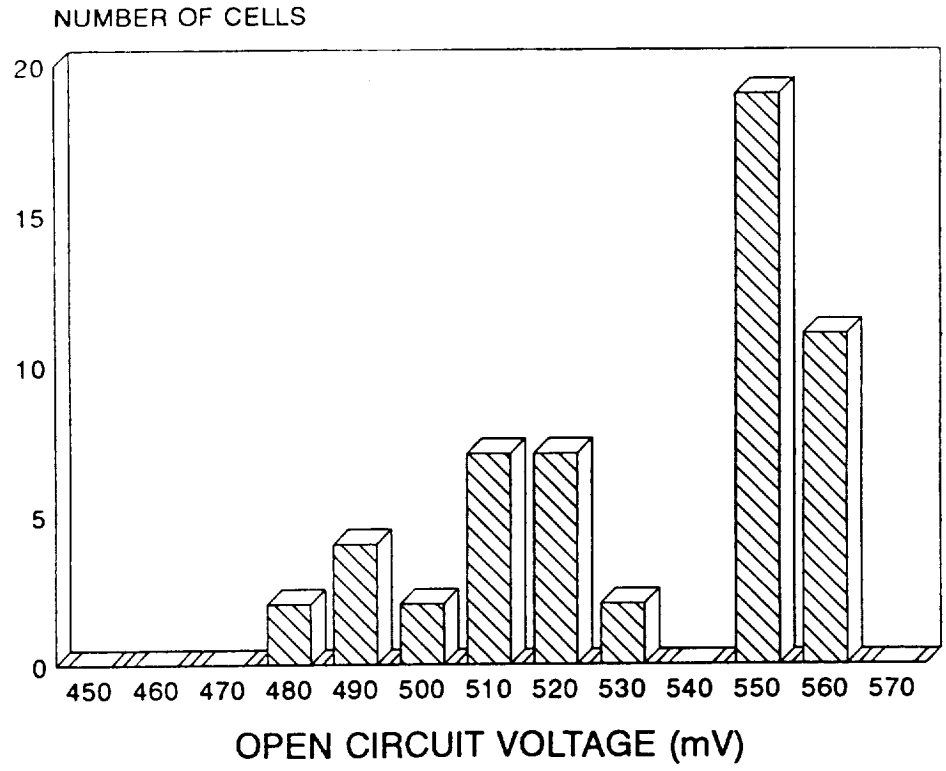

Figure 3-14 Voc DISTRIBUTION OF CELLS SHOWN IN FIGURE 3-13

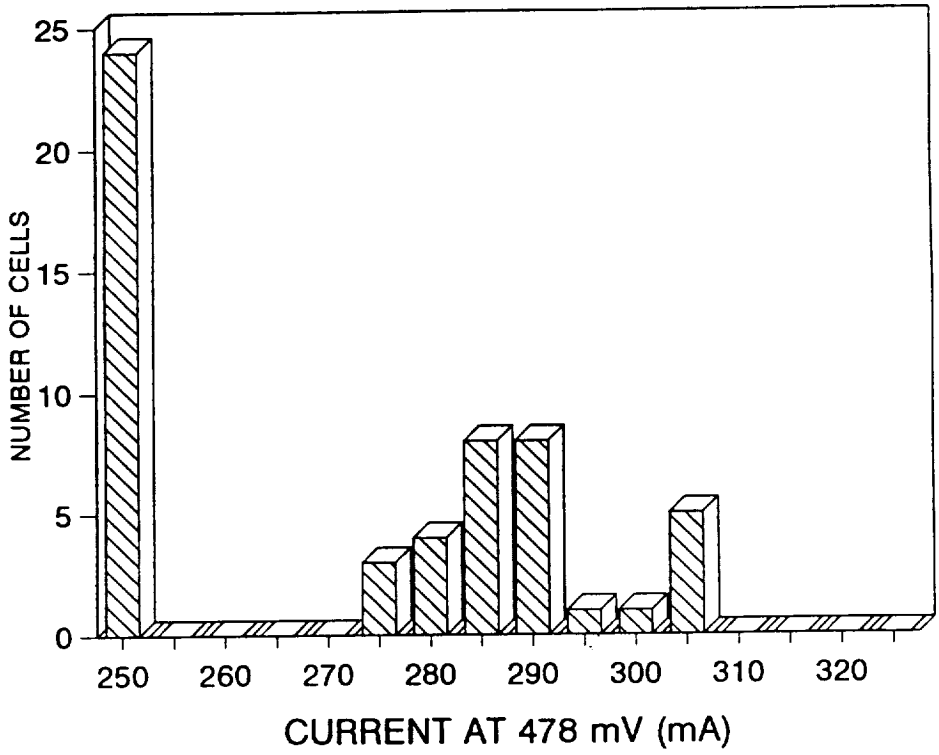

Figure 3-15 I@478 mV DISTRIBUTION OF CELLS SHOWN IN FIGURE 3-13

3.2.4 Time Dependence of Voc and Isc

An unusual phenomenon noticed during illuminated testing of many of the BSF development cells (BN, doped oxide and implanted) was the time dependence of Voc and Isc. On parts that possessed Vocs of typically 550 mV it was noticed that Voc would increase over a period of about 5 minutes to typically 570 mV or more. The rate of increase in Voc could be increased by illuminating the cell to about 6X concentration, whereupon the effect would take place in a matter of seconds. Concurrent with this increase in Voc a decrease in Isc was observed. After several hours of dark storage the cells would revert to their original electrical state whereupon the effect could be repeated. This behavior is typical of the presence of deep, slow traps within the silicon base produced as a result of processing. Typical illuminated AM0 I-V characteristics obtained at the beginning of illumination and after an extended period are shown in Figure 3-16. The increase in Voc was only significant on parts with initial Voc values above approximately 540 mV (i.e., with base diffusion lengths on the order of approximately 300 microns or greater). This points very strongly to the existence of deep, slow trapping states at the boron P^+/P interface. One would not expect these states to affect Voc with, for example, a 50 micron diffusion length since they would be out of electrical communication with the minority carriers emitted into the base. However, a decrease in Isc was observed on all parts after prolonged illumination.

It is difficult to explain the simultaneous increase in Voc and decrease in Isc by any simple, single recombination process. The increase in Voc implies a reduction in J_{01}, the first diode recombination current, presumably by flooding and immobilization of the deep level recombination centers by electrons or holes produced by illumination. One would

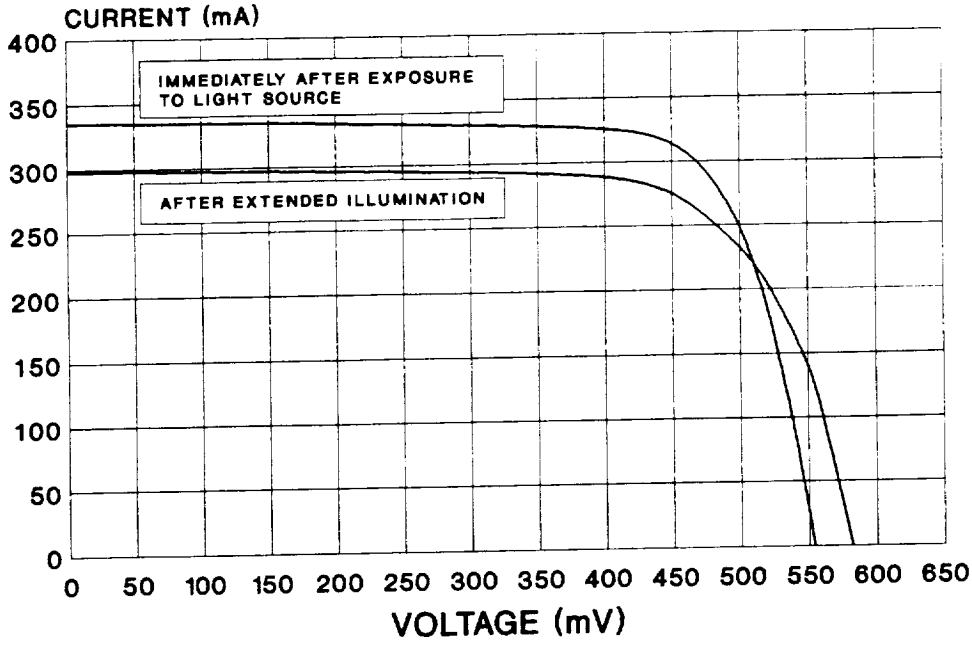

Figure 3-16 TIME DELAYED EFFECT OF ILLUMINATION OF IV CHARACTERISTIC OF EARLY IMPLANTED CELLS

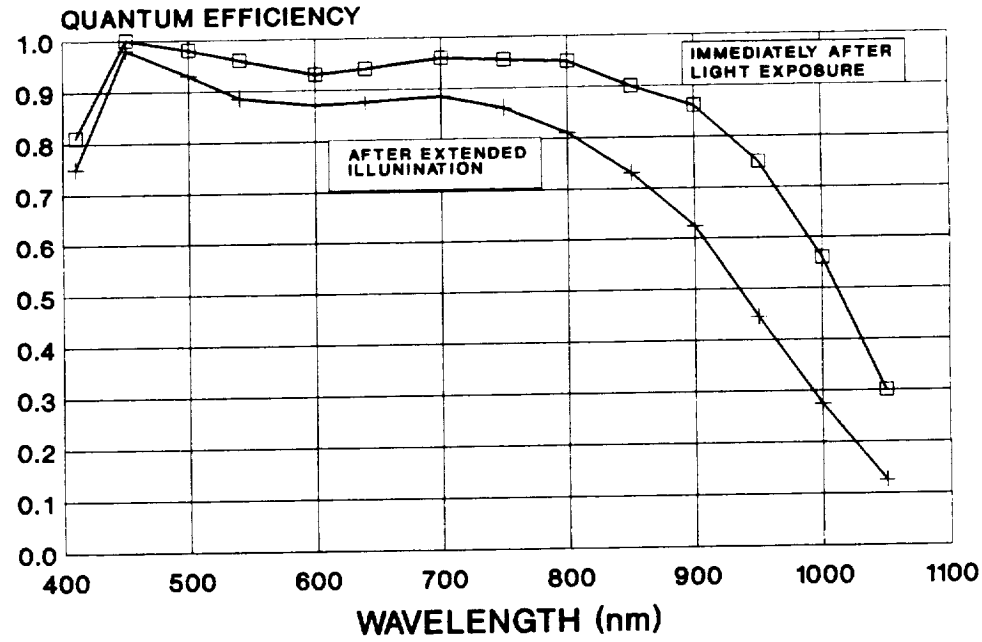

Figure 3-17 TIME DELAYED EFFECT OF ILLUMINATION ON QE OF EARLY IMPLANTED CELLS

intuitively expect this also to increase the red response through immobilization of these recombination centers and hence increase Isc. In Figure 3-17 we show the external Q.E. measured before and after extended illumination and it is clear that the reverse is true.

This lead us to believe that there were two processes in operation, one involving a large number of traps at the back P/P^+ interface which become immobilized upon illumination (which tended to increase Voc and Isc) and another set of traps approximately uniformly distributed throughout the base which became activated by illumination. These would decrease minority carrier lifetime and diffusion length (which would decrease red response and also slightly decrease Voc). One could then envisage a certain distribution of traps which simultaneously increased Voc and decreased Isc. There was indeed conclusive evidence from spectral response data that a bulk recombination process existed which reduced the base diffusion length to approximately 50 microns on some samples. We did not expect this to be due to any effect of the ion implantation since damage extended only a few microns, at most, into the samples.

One possible cause for the phenomenon was the formation of boron-oxygen or boron-carbon complexes or precipitates (which are known to be active recombination centers in silicon) during the high temperature damage annealing process. This is described further in the following section.

3.2.5 Process Related Defect Generation

Intermittent problems were encountered during the first two years of the program when processing cells with ion implanted, or diffused boron BSFs. Cells typically showed severely

depressed Voc and Jsc whereas K4 (no BSF) controls showed no degradation. This lead us to conclude that there were no problems associated with the N^+ junction formation process.

Over a period of many months intensive investigation it became clear that the problem was correlated more frequently with the use of 2 ohm-cm wafers although it was still sometimes apparent when 10 ohm-cm wafers were used.

In Figure 3-18 we show the external quantum efficiency of a 2 ohm-cm cell which showed severe Voc and Isc degradation. By comparison we also show in the same figure the quantum efficiency for an undergraded cell made from 10 ohm-cm. There was clearly substantial diffusion lengths degradation in the 2 ohm-cm cell.

In order to understand the effects more clearly, defect etching using a modified Sirtl etch was initiated. In Figures 3-19 and 3-20 we show optical microscopy cross-sections after defect etching of the same cells shown in Figure 3-18.

Samples from the badly defected wafer together with unannealed control samples were also sent to Dr. Al Hassim at SERI for TEM microscopy. Thorough TEM plan view examinations of control wafers showed no crystallgraphic defects, segregation or precipitates.

However 2 ohm-cm samples which had been subjected to anneals of 985°C for 2 hours showed a high density of dislocation loops and precipitates. In Figures 3-21 and 3-22 we show TEM micrographs of dislocation loops (Figure 3-21) and a precipitate (Figure 3-22).

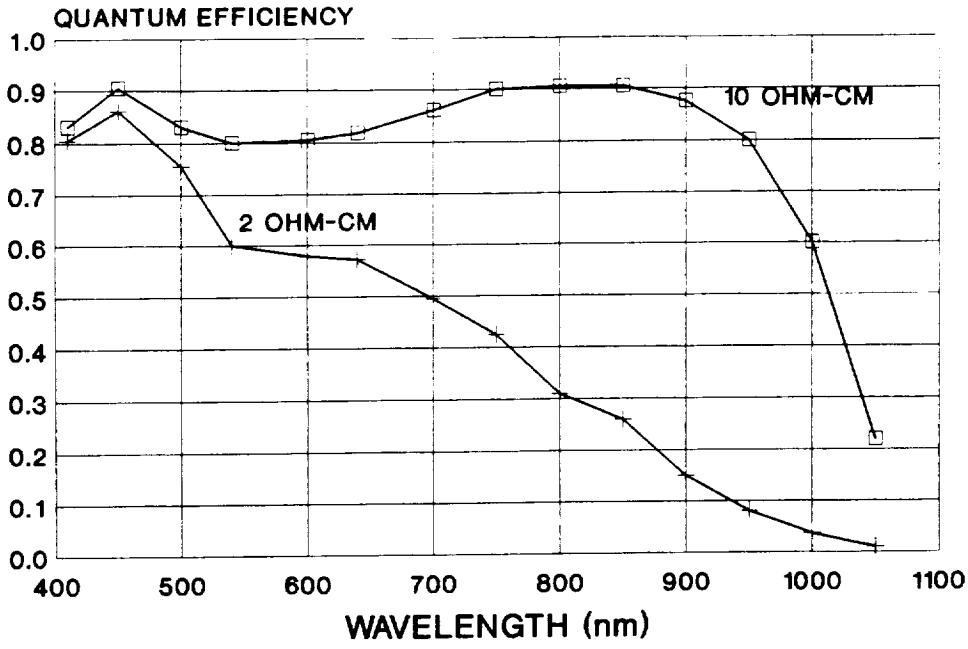

Figure 3-18 EFFECT OF THERMALLY INDUCED DEFECTS ON QE

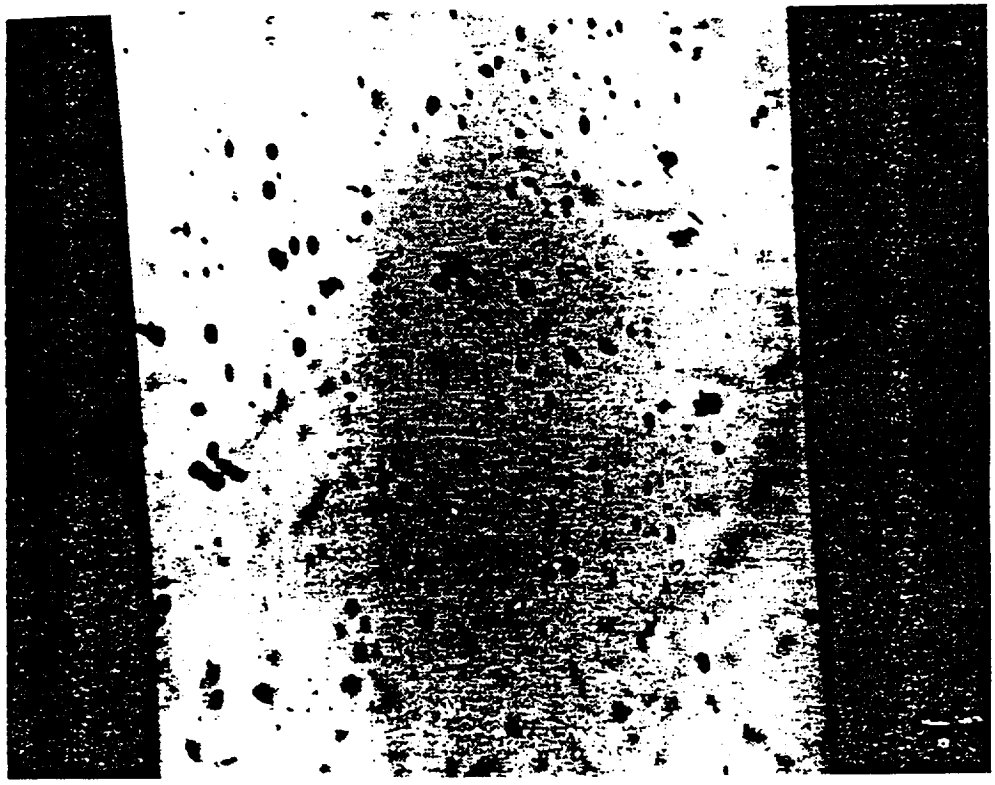

Figure 3-19 CROSS-SECTION OF SIRTL ETCHED 2 OHM-CM WAFER AFTER PROCESSING AT 985°C FOR 2 HOURS

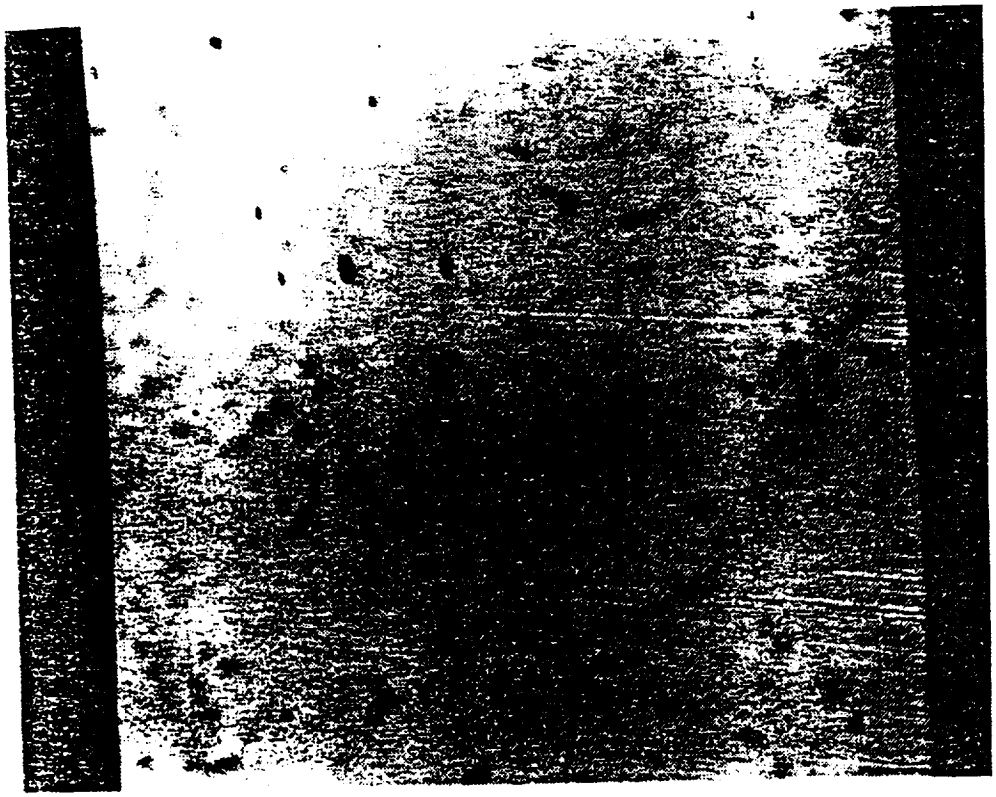

Figure 3-20 CROSS-SECTION OF SIRTL ETCHED 10 OHM-CM WAFER AFTER PROCESSING AT 985°C FOR 2 HOURS

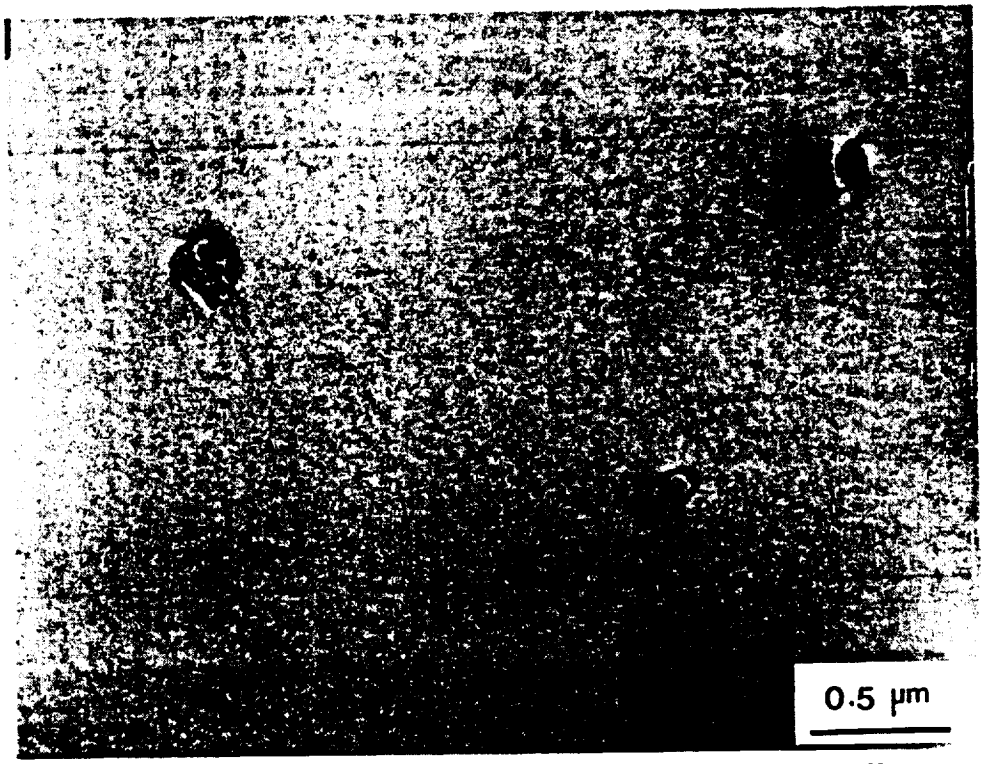

Figure 3-21 TEM MICROGRAPH OF A THERMALLY GENERATED DISLOCATION LOOP

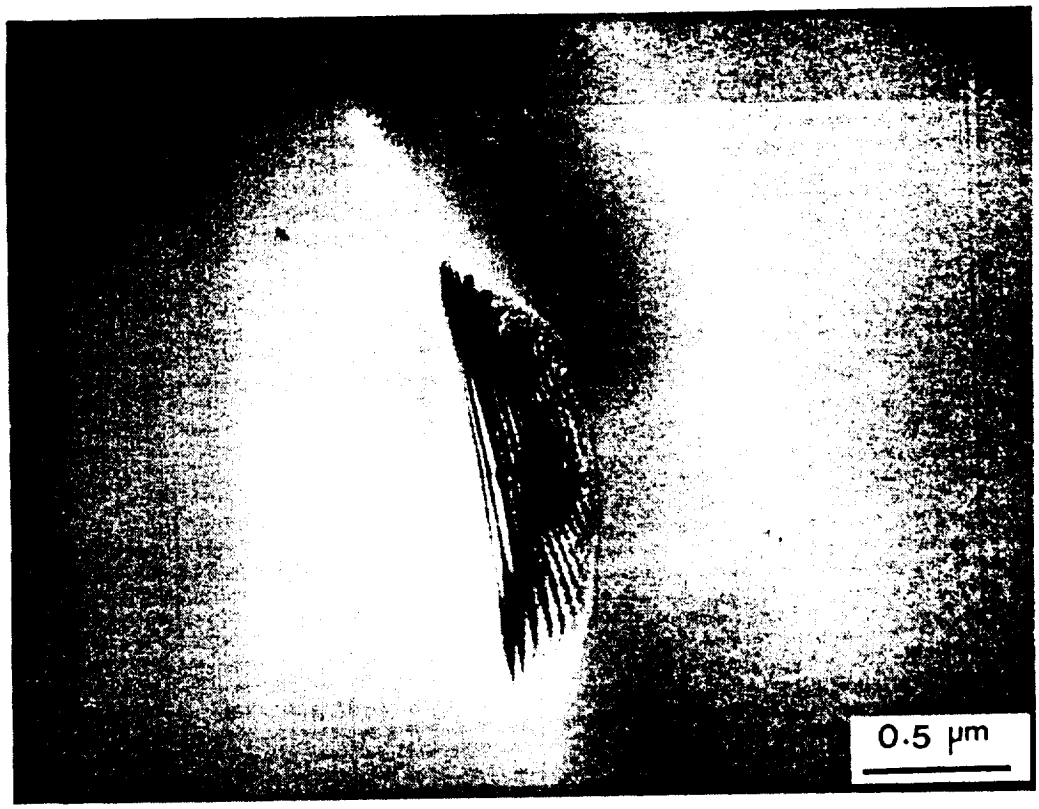

(C)

Figure 3-22 TEM MICROGRAPH OF A THERMALLY GENERATED PRECIPITATE

X-ray analysis (EDS) on some of the precipitates also showed the presence of oxygen. This led us to believe that the precipitate and defect formation might be caused by interaction between high levels of oxygen and the relatively high boron levels in 2 ohm-cm silicon, compared to 10 ohm-cm.

A survey of the literature indicated that boron and oxygen form a level 0.27 eV below the silicon conduction band. The capture cross-sections for electrons and holes determined by DLTS were found to be $O_n = 3 \times 10^{-13}$ cm^2 and $O_p = 8.5 \times 10^{-16}$ cm^2 respectively. Furthermore it was found that the concentration of this defect and the radiation induced degradation of boron doped cells increases markedly with boron concentration[2].

On the basis of these data and analysis a request was made to NASA LeRC to change the baseline cell resistivity from 2 ohm-cm to 10 ohm-cm.

The timeframe of this request was such that the 50 Task II deliverable cells were made from 2 ohm-cm silicon but all Task III deliverables were manufactured from 10 ohm-cm silicon.

3.3 FRONT JUNCTION FORMATION

Front junction formation was performed using a standard phosphine diffusion.

The junction depth was 0.15 microns with a surface concentration of 7×10^{19} cm^{-3}.

In order to eliminate junction leakage at the wrapthrough hole the n+ junction was terminated approximately 10 mils from the hole edge.

No problems were experienced on this particular process module.

3.4 WRAPTHROUGH EDGE DEVELOPMENT

The profile of the wrapthrough hole played an important role in determining the electrical characteristics of the cell. Edge profiles which were jagged were easily damaged during processing and lead to localized damage to the wrapthrough dielectric and subsequently caused shorting of the N^+ contact to the base of the cell.

The method of forming the hole in wrapthrough cells was to laser scribe at discrete points along the wafer until light could be seen through a dotted line of pinholes along the scribe line.

The center of the hole was then removed by etching the wafer in NaOH which readily dissolved the laser damaged material around the hole. However, the type of hole profile produced by this technique was extremely ragged as shown in Figure 3-23 and resulted in poor electrical characteristics through the creation of shunt paths as mentioned earlier. It was determined that the ragged edges were caused primarily by differences in the etch rate of damaged material along the laser scribe lines. Badly damaged amorphous material etched much faster than crystalline material, thus resulting in a perforated edge. This was rectified by cutting at a slower rate. When etched, this material was removed at a constant rate, resulting in a clean hole profile.

A dependence of the edge profile on the type of etchant used was also noted. NaOH based etchants were anisotropic on different crystal planes and resulted in faceted hole edges. An edge profile typical of that etched in NaOH only is shown in Figure 3-24. The edge facets are clearly visible.

In contrast, acid etchants based on 3-1-2 etch were generally isotropic but gave rise to knife edges if over etching occurred. These edges were extremely brittle and chipped during processing as shown in Figure 3-25.

A number of experiments were therefore performed to optimize the laser cutting parameters and also a matrix of NaOH and 3-1-2 based etching procedures was investigated. It was found that the optimum procedure was to etch the wafers to within a few mils of final thickness, etch in NaOH to within about 1 mil of final thickness and then to etch to final thickness in 3-1-2 etch. This procedure eliminated both faceting and knife- edging of the wafer and results in the rounded edge profile shown in Figure 3-26. This provided an ideal base on which to form the dielectric isolation layer for the wrapthrough contract.

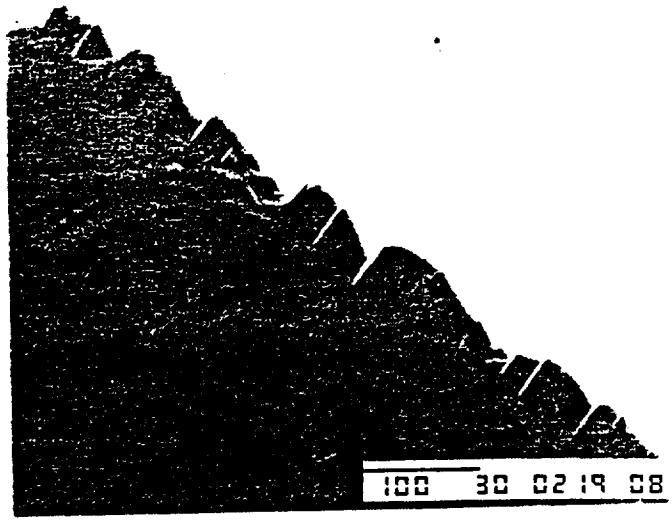

Figure 3-23 RAGGED WRAPTHROUGH EDGE CAUSED BY IMPROPER LASER SCRIBING

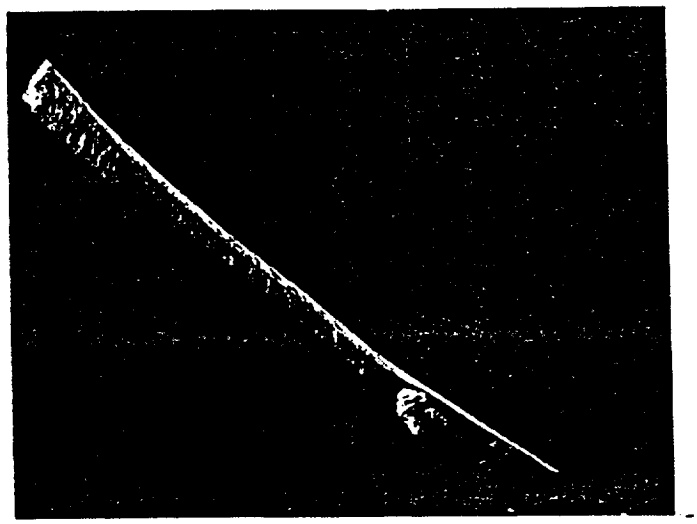

Figure 3-24 FACETED ETCHTHROUGH SLOT CAUSED BY BASIC TECH ONLY

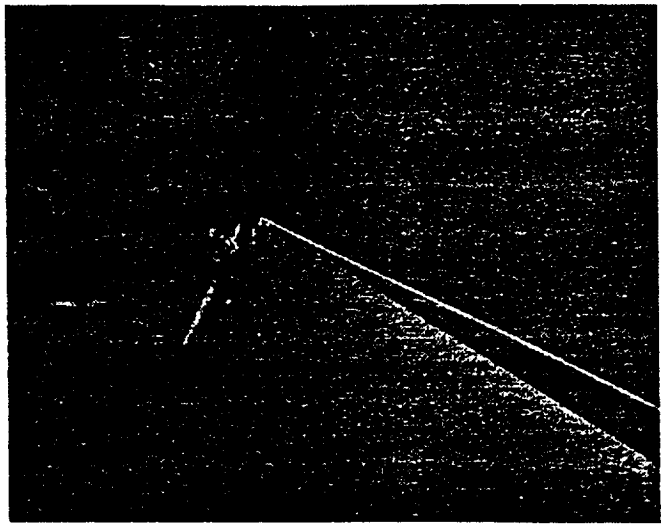

Figure 3-25 RAZOR EDGE CAUSED BY ACID 3-1-2 ETCH ONLY

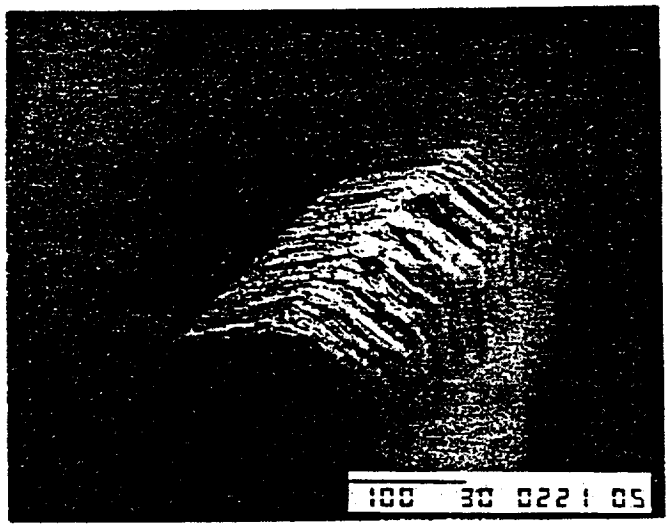

Figure 3-26 OPTIMIZED EDGE PROFILE PRODUCED BY COMBINATION OF ACID AND BASIC ETCHING

3.5 DIELECTRIC DEPOSITION

Deposition of SiO_2 around the wrapthrough hole was performed using approximately 1 micron of LPCVD SiO_2.

The oxide was deposited by shadow masking using shadow masks on either side of the wafer. It was found that only a slight amount of penumbra deposition occurred under the mask. This was removed using a short 1% HF penumbra etch, prior to metallization to eliminate series resistance effects caused by the presence of an insulator underneath the contact.

3.6 PHOTORESIST APPLICATION AND MASKING

Because a wrapthrough design was pursued it was necessary to develop a special technique for photoresist applications.

Perforated wafers could not successfully be spin coated because photoresist crept through the holes and into the vacuum chuck assembly.

Three different photoresist application methods were investigated, namely spraying, dry film lamination and dipping.

3.6.1 Spraying

Spray application was investigated at Hughes Aircraft Company, Solid State Products Division in Newport Beach using a Zicon spray application system. Photoresist application in this system took place by moving the wafers on a translation stage under a spray head which itself oscillated in a direction normal to that of the wafers. Up to approximately 30 wafers were coated at one time. Photoresist thickness was controlled by the

speed of the translation stage, the velocity of the spray head across the wafers and by the type of spray nozzle and spray pressure used.

While this system appeared to be very flexible and performed well, there was the inherent disadvantage that only one side was coated at one time. This necessitated the removal of the wafers from the stage for drying followed by reapplication of the resist on the other side. This was found to compromise to some extent the photoresist surface which was in contact with the stage surface.

Also, it was found necessary to plug the holes during resist application to prevent excessive build-up of resist within the slots which would subsequently cause problems during mask exposure and development.

Despite some shortcomings, which could probably be resolved, it was felt that the technique and equipment used were viable for the manufacture of the wrapthrough cell. The technique was not pursued further however due to the success of the dipping process described in Section 3.6.3 below.

3.6.2 Dry Film Photoresist Application

Samples were sent to MacDermitt for application of 0.5 mil thick dry film positive photoresist by lamination.

Efforts to define a grid pattern were initially hampered because of the incompatibility between Spectrolab's standard photoresist developer and the photoresist.

Subsequent use of MacDermitt developer produced lines with very ragged edges after developing. Since the silicon surface prior to lamination had a somewhat orange peel effect it was felt that small air pockets were being laminated between the dry film and the silicon. This gave rise to wide spots in the photoresist upon exposure and subsequent development. This technique was therefore not pursued further.

3.6.3 Photoresist Application By Dipping

The preferred method of photoresist application was found to be by dipping and uniform coatings 5 microns thick were produced with minimal disruption of the photoresist uniformity at the wrapthrough holes.

In Figure 3-27 we show a cross-section of a wrapthrough edge on a part which had been dip coated in positive photoresist. It is clear that a reasonably uniform layer of photoresist was produced in and around the slot edge. In Figure 3-28 we show the definition of the photoresist after exposure and development using the grid mask . The photoresist edges were well defined and no photoresist remains in the area around the slot which will subsequently form the wrapthrough contact metallization. However, a small residue of photoresist was found to remain inside the slot which could subsequently compromise metal adhesion during thermal cycling.

A suitable UV exposure energy was subsequently identified to achieve minimal residue but achieve well defined photoresist line widths of approximately 1 mil.

3.7 ANTIREFLECTION (AR) COATING DESIGN

The front AR coating used for all cells was 570Å TiO_2/870Å Al_2O_3.

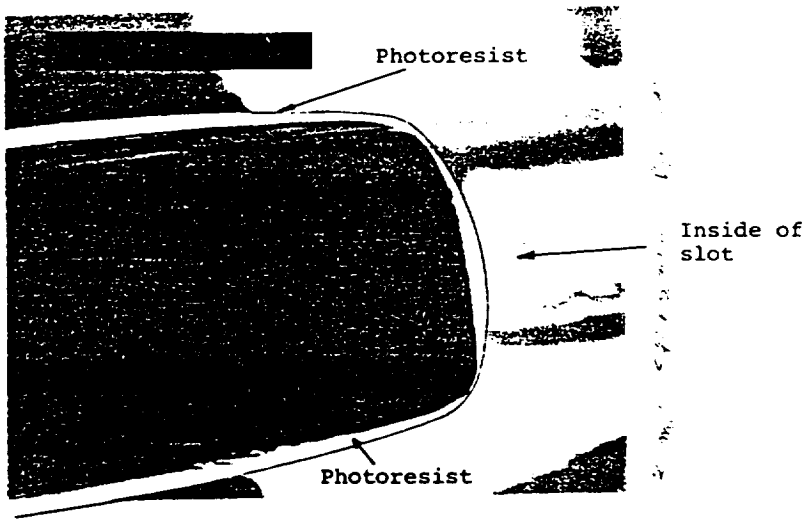

Figure 3-27 CROSS-SECTION OF DIP COATED 8 MIL WAFER

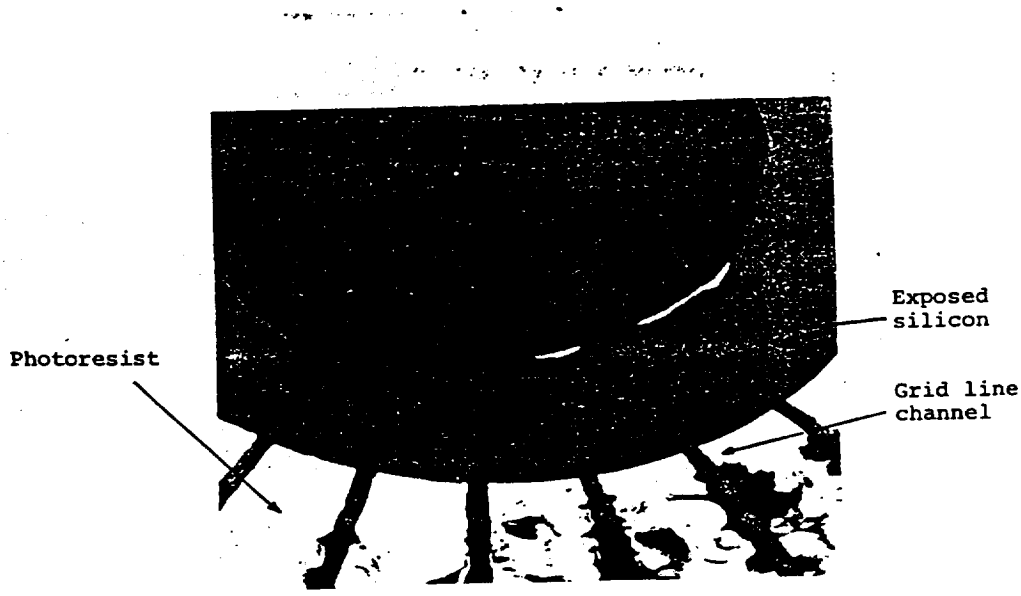

Figure 3-28 PHOTORESIST RESIDUE IN HOLE AFTER RESIST EXPOSURE

However two different designs for the backside AR coating were utilized.

Initially, Spectrolab optimized the cell for maximum transmission of IR wavelengths at 1.5 microns. This resulted in a backside AR coating of 1064Å TiO_2/1497Å Al_2O_3.

Later however, at the direction of the NASA LeRC program manager the backside AR coating was optimized for albedo illumination. This resulted in a backside AR coating of 523Å TiO_2/746Å Al_2O_3 nominal thickness.

The chronological sequence of events was such that the 50 cells delivered at the end of Task II was the backside coating optimized for IR transmission.

The majority of cells delivered in Task III had the backside coating designed for albedo collection although some had the IR transparent design.

A full discussion of the backside AR coating optimization appears in Section 2.3.1.

3.8 COVERGLASS APPLICATION DEVELOPMENT

The conventional method of coverglass application is not optimum for large area cells with wrapthrough contacts. The reason for this is that during front coverglass application a significant amount of excess DC 93-500 adhesive can pass through the wrapthrough holes and around the perimeter of the cell and cure on the front and back of the cell as well as the n+ contact pads. This necessitates highly labor intensive adhesive clean up prior to final test which adds to the cell assembly cost and contributes to cell breakage.

In this task, a previously developed proprietary bonding process was modified for application to Space Station solar cells. First the process was evaluated for its effectiveness on large area cells. This evaluation resulted in designing and purchasing the tools necessary to facilitate coverglass application using the proprietary technique.

The bonding process was applied to filtering assemblies for delivery under task 3. The new bonding techniques reduced the labor and time required to apply the coverglass.

3.9 PRODUCTION VERIFICATION

At this point in time the intermittent problem of high temperature process induced defects was not fully understood and so the 50 cells were fabricated from 2 ohm-cm silicon. Process induced defects were not noticed on these lots however and high efficiency cells were delivered.

The electrical performance is given in Section 3.8.2 below.

3.9.1 Test Fixture Fabrication

The electrical testing of wrapthrough gridded back cells required a special purpose test fixture.

In order to reduce the reflection of IR radiation from the test block we designed the test fixture to include a non-reflecting 'black' coating on its front surface. This reduced reflection from the block to less than 4% over the spectral range of interest.

3.9.2 Cell Electrical Test Data

Tables 3-6, 3-7, and 3-8 summarize the data on the 134 cells fabricated from the 150 wafer starts (3 lots). Light intensity was set to AM0 using a handheld standard which we believed most closely approximated the spectral response of the gridded back 2 ohm-cm K6 cell. Due to an oversight the standard cell was set up to produce a test block temperature of 28 ± 0.5°C compared with the NASA specification of 25°C. The result was that the tabulated value of Voc in Tables 3-6, 3-7, and 3-8 were about 6.6 mV too low.

Also the efficiency shown the Tables was calculated from the load point current measured at 490 mV using the equation:

$$\text{Efficiency} = \frac{I_{(490)} \times 0.49}{1.353 \times A} \times 100\%$$

where $I_{(490)}$ is the current at 490 mV load and A is the cell area of 62.4 cm^2

Since the maximum power point was significantly more than 490 mV on some of the cells the efficiency calculated was very conservative. The 50 deliverable cells were in fact re-tested at 25°C and the true efficiency at the maximum power point was calculated. This data is summarized in Tables 3-9 and 3-10. The average AM0, 25°C efficiency was 14.5%.

Table 3-6 TABULATED DATA FOR 134 CELLS PRODUCED FROM 150 WAFER STARTS IN TASK 2. LOT #01

CELL ID	VOC	ISC	I @ 490	% @ 490
1	610	2582	2403	13.9
2	609	2570	2376	13.8
3	606	2547	2275	13.2
4	569	2225	1788	10.3
5	597	2550	2262	13.1
6	604	2552	2308	13.4
7	602	2418	2174	12.6
8	563	2196	1054	6.1
9	605	2511	2200	12.8
10	591	2459	2300	13.3
11	607	2540	2359	13.7
12	594	2456	2178	12.6
13	594	2482	2137	12.4
14	603	2540	2187	12.7
15	602	2554	2289	13.3
16	607	2577	2334	13.5
17	596	2496	2138	12.4
18	610	2526	2228	12.9
19	600	2479	2559	13.0
20	601	2580	2191	12.7
21	608	2557	2326	13.5
22	604	2521	2273	13.2
23	597	2423	2133	12.4
24	609	2588	2304	13.4
25	597	2454	2211	12.8
26	610	2545	2309	13.4
27	606	2560	2331	13.5
28	571	2318	1937	11.2
29	601	2554	2226	12.9
30	601	2555	2332	13.5
31	600	2554	2209	12.8
32	607	2534	2334	13.5
33	607	2578	2353	13.7
34	604	2465	2233	13.0
35	605	2577	2270	13.2
36	606	2522	2262	13.1
37	603	2561	2354	13.7
38	563	2280	1455	8.4
39	590	2450	2099	12.2
40	605	2537	2324	13.5
41	607	2558	2296	13.3
42	602	2544	2259	13.1
43	592	2419	2044	11.6
44	611	2588	2249	13.1
45	603	2552	2277	13.2

Average I @ 490 = 2207mA *

Average % @ 490 = 12.8%

*Exluding cells #4, 8, 28 and 38.

Table 3-7 TABULATED DATA FOR 134 CELLS PRODUCED FROM 150 WAFER STARTS IN TASK 2. LOT #02

CELL ID	VOC	ISC	I @ 490	% @ 490
1	597	2539	2323	13.5
2	601	2558	2247	13.0
3	611	2563	2346	13.6
4	601	2526	2200	12.8
5	607	2524	2330	13.5
6	607	2547	2353	13.7
7	595	2447	2110	12.2
8	592	2416	2175	12.6
9	557	2099	1002	5.8
10	605	2560	2188	12.7
11	595	2562	2118	12.3
12	605	2574	2222	12.9
13	610	2576	2410	14.0
14	604	2546	2283	13.3
15	603	2550	2358	13.7
16	610	2576	2354	13.7
17	601	2508	2228	12.9
18	607	2574	2310	13.4
19	609	2590	2369	13.7
20	602	2564	2117	12.3
21	610	2592	2406	14.0
22	608	2081	2372	13.8
23	606	2515	2182	12.7
24	604	2564	2230	12.9
25	580	2310	1970	11.4
26	611	2585	2435	14.1
27	610	2581	2397	13.9
28	604	2555	2371	13.8
29	607	2572	2317	13.4
30	602	2503	2219	12.9
31	584	2325	1979	11.5
32	597	2518	2210	12.8
33	599	2537	2094	12.2
34	596	2548	2037	11.8
35	609	2596	2338	13.6
36	597	2529	2245	13.0
37	598	2545	2195	12.8
38	602	2558	2266	13.2
39	607	2478	2243	13.0
40	608	2548	2263	13.1
41	603	2553	2175	12.6
42	607	2511	2223	12.9
43	610	2507	2309	13.4
44	603	2553	2278	13.2

Average I @ 490 = 2211 mA*

Average % @ 490 = 12.82%*

*Excluding cells #9, 25, 31

Table 3-8 TABULATED DATA FOR 134 CELLS PRODUCED FROM 150 WAFER STARTS IN TASK 2. LOT #03

CELL ID	VOC	ISC	I @ 490	% @ 490
1	601	2560	2335	13.6
2	599	2479	2232	13.0
3	589	2411	2116	12.2
4	607	2543	2244	13.0
5	605	2547	2243	13.0
6	560	2147	1036	6.0
7	607	2552	2341	13.6
8	552	2070	1466	8.5
9	606	2469	2128	12.4
10	570	2253	1756	10.2
11	603	2532	2295	13.3
12	590	2407	2073	12.0
13	611	2576	2360	13.7
14	607	2555	2096	12.2
15	609	2574	2277	13.2
16	606	2570	2364	13.7
17	613	2576	2380	13.8
18	608	2560	2324	13.5
19	611	2586	2388	13.9
20	610	2573	2387	13.9
21	604	2547	2288	13.3
22	608	2582	2373	13.8
23	607	2555	2353	13.7
24	609	2545	2355	13.7
25	608	2572	2388	13.9
26	596	2463	2210	12.8
27	608	2587	2397	13.9
28	611	2579	2400	13.9
29	610	2588	2348	13.6
30	609	2576	2338	13.6
31	602	2480	2290	13.3
32	603	2518	2309	13.4
33	606	2570	2392	13.9
34	603	2566	2288	13.3
35	587	2399	2248	13.0
36	606	2563	2388	13.9
37	479	2530	001	-
38	590	2368	2127	12.3
39	609	2566	2382	13.9
40	598	2566	1479	8.6
41	605	2550	2384	13.8
42	201	2360	002	-
43	584	2356	1650	9.6
44	599	2517	2190	12.7
45	608	2576	2387	13.9

Average I @ 490 = 2227 mA*

Average % @ 490 = 12.92%*

*Excluding cells #6, 8, 10. 37, 42, 43.

Table 3-9 TABULATED DATA ON CELLS DELIVERED TO NASA LeRC FROM LOT #02 (25°C TEST TEMP)

LOT 02

CELL #	V_{oc}	I_{sc}	I_{490}	M_9Max Power %
1	602	2526	2443	14.7
2	606	2563	2387	14.0
3	613	2552	2413	14.5
5	612	2514	2436	14.0
6	613	2538	2463	15.0
13	614	2560	2492	15.2
14	611	2541	2440	14.6
15	608	2549	2469	14.8
16	614	2563	2456	14.8
18	611	2574	2425	14.6
19	614	2581	2441	14.8
21	615	2570	2493	15.1
22	613	2566	2481	15.0
24	609	2567	2330	13.7
26	615	2570	2479	15.0
27	614	2573	2460	14.8
28	610	2538	2463	14.7
29	611	2547	2425	14.4
35	614	2582	2476	15.0
36	603	2520	2356	13.9
38	606	2543	2370	14.4
39	612	2461	2348	13.9
40	612	2528	2325	13.9
43	614	2487	2409	14.6
44	610	2527	2422	14.7

Average efficiency measured at max power point, 25°C AMO = 14.6%.

Table 3-10 TABULATED DATA ON CELLS DELIVERED TO NASA LeRC FROM LOT #03 (25°C TEST TEMP)

LOT 03

CELL #	V_{oc} mV	I_{sc} mA	I_{490} mA	M_9Max Power %
1	606	2553	2421	14.7
4	611	2550	2320	13.9
5	609	2550	2345	13.8
7	611	2542	2436	14.7
13	615	2558	2403	14.3
15	613	2551	2457	14.8
16	609	2553	2474	15.2
18	612	2557	2429	14.4
19	615	2577	2487	15.0
20	614	2560	2451	14.5
21	608	2534	2406	14.6
22	613	2573	2452	14.6
23	611	2545	2438	14.7
25	612	2560	2498	15.4
27	612	2565	2446	14.5
28	614	2564	2475	15.0
29	614	2571	2436	15.1
30	613	2564	2412	14.3
32	609	2570	2427	14.7
33	611	2560	2413	14.3
34	607	2553	2399	14.6
36	611	2550	2479	15.1
39	612	2523	2376	14.2
41	609	2528	2413	14.0
45	612	2557	2308	13.2

Average efficiency measured at max power point, 25°C AMO = 14.5%

4.0 TASK III PILOT PRODUCTION

A total of five hundred and eighty seven solar cell assemblies were fabricated in Task III to demonstrate the production capability of the process. The finalized process flow is shown in Figure 4-1. The cell coverglass was 5 mil thick ceria doped microsheet with MgF_2 front surface AR coating.

The first step was the generation of the wrapthrough holes and thinning of the wafer. The four holes were formed using a laser scribe. A final selective etch as then performed to round the inside of the holes.

A back surface field, BSF, was produced by implanting the back side of the wafers with boron and annealing. The front junction was formed using a phosphine diffusion process. SiO_2 was used as the dielectric layer to isolate the n+ contact from the p+ BSF.

Photolithography processing was employed to define the grid pattern on the front and the back of the cells. Antireflective coatings, TiO_2/Al_2O_2, were deposited on both the front and back of cells. The coating on the back of the cells was optimized for transmission of albedo light into the back of the cell as described earlier.

The completed cells were cut to size using a Nd-YAG laser scribe. Cells were filtered with the 5 mil ceria doped microsheet coverglass using DC93-500 adhesive and standard filtering procedures.

THIN TO 10 MILS

LASER SCRIBE HOLES

ETCH TO 8 MILS
(HOLE SMOOTHING)

ION IMPLANTATION

ION IMPLANT ANNEAL

PHOSPHORUS DIFFUSION

LPCVD SiO2

PHOTOLITHOGRAPHY

(DIP PHOTORESIST)

PLATING

DUAL AR COATING
FRONT AND BACK

LASER SCRIBE

TEST

COVERGLASS ATTACHMENT

TEST

Figure 4-1 PROCESS SEQUENCE FOR PILOT PRODUCTION CELLS

4.1 ELECTRICAL PERFORMANCE

Two groups of cells were processed sequentially. All assemblies were tested under a X-25 solar simulator at 25°C. The simulator was calibrated using a 4 mil gridded back BSF silicon balloon flown standard.

The cells were tested using a computer test set up that was modified for use with the large area Space Station cells. Space Station cell characteristics required that both software and hardware changes were made to the existing set up. The programmable power supply was modified to enable it to reach the higher current of the Space Station cell. In addition, software was written to save and convert 100 data pairs from each I-V curve to a lotus spread sheet format. These changes made possible the delivery of floppy disks with IV curves for the first 382 cells fabricated.

The average performance and standard deviations of the first 382 assemblies is summarized in Table 4-1 below:

Table 4-1 AVERAGE PERFORMANCE OF THE FIRST 382 SOLAR CELL ASSEMBLIES

	Average	Standard Dev.
Voc	614 mV	5.8 mV
Isc	2611 mA	18.8 mA
Vmp	495 mV	10.6 mV
Imp	2302 mA	54.8 mA
FF	71.2%	1.9 points
Eff.	13.5%	.5 points
I@495 mV	2299 mA	8.4 mA

The distributions for these parameters are shown in Figures 4-2 through 4-8. The fill factor is the primary parameter that was found to depress the performance of the cells. The distributions show that there was a large spread of measured values for Voc and for the fill factor. Shunting of the junction at the wrapthrough hole was found to be depressing both Voc and the fill factor. Measurements on later cells, with the same grid configuration showed that series resistance also played an important role in depressing performance.

An additional 205 filtered assemblies were also fabricated using the process flow described earlier. Because of the tight time schedule to fabricate and test these assemblies, measurements were only performed at a load voltage of 495 mV. The distribution of I at 495 mV is shown in Figure 4-9. These assemblies had an average I@495 mV of 2336 mA. The performance of this second group has improved relative to the first. The broad distribution of performance seen earlier was tightened up through minor process refinements and operator familiarity with the processing.

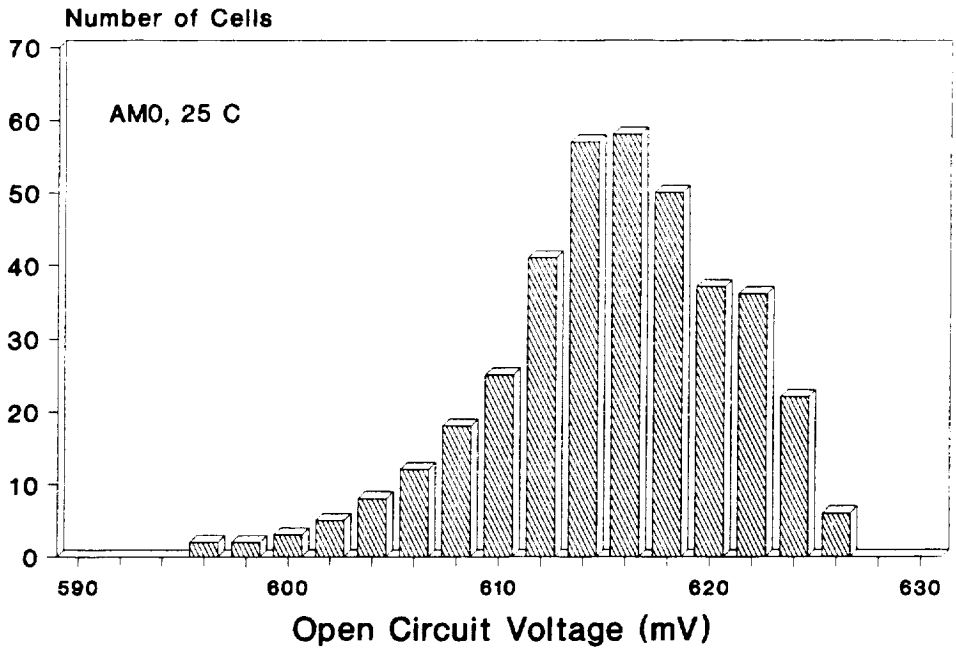

Figure 4-2 Voc DISTRIBUTION OF FIRST 382 FILTERED CELL ASSEMBLIES DELIVERED TO NASA LeRC

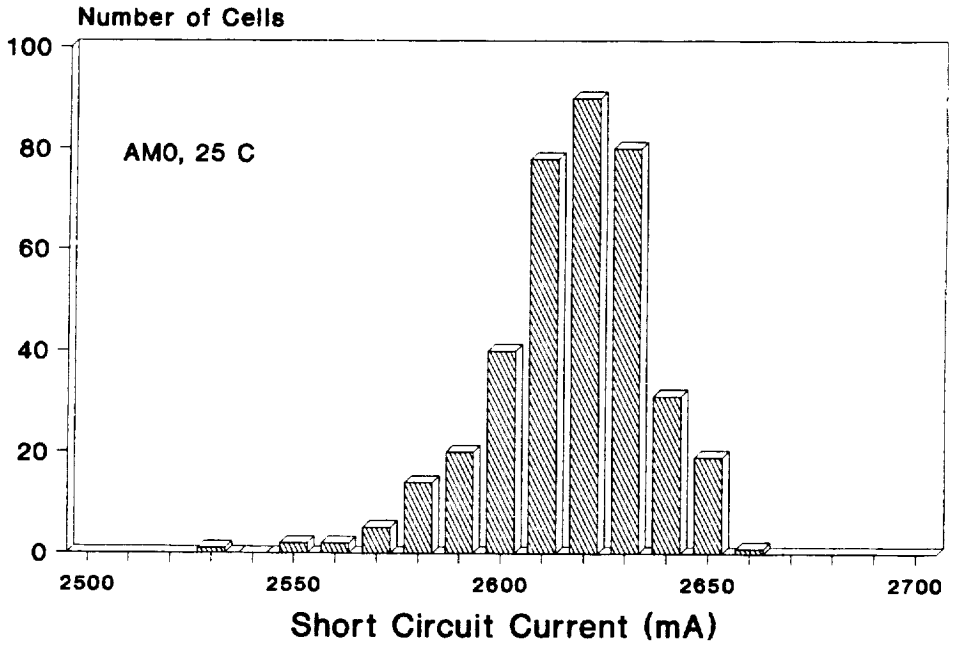

Figure 4-3 Isc DISTRIBUTION OF FIRST 382 FILTERED CELL ASSEMBLIES DELIVERED TO NASA LeRC

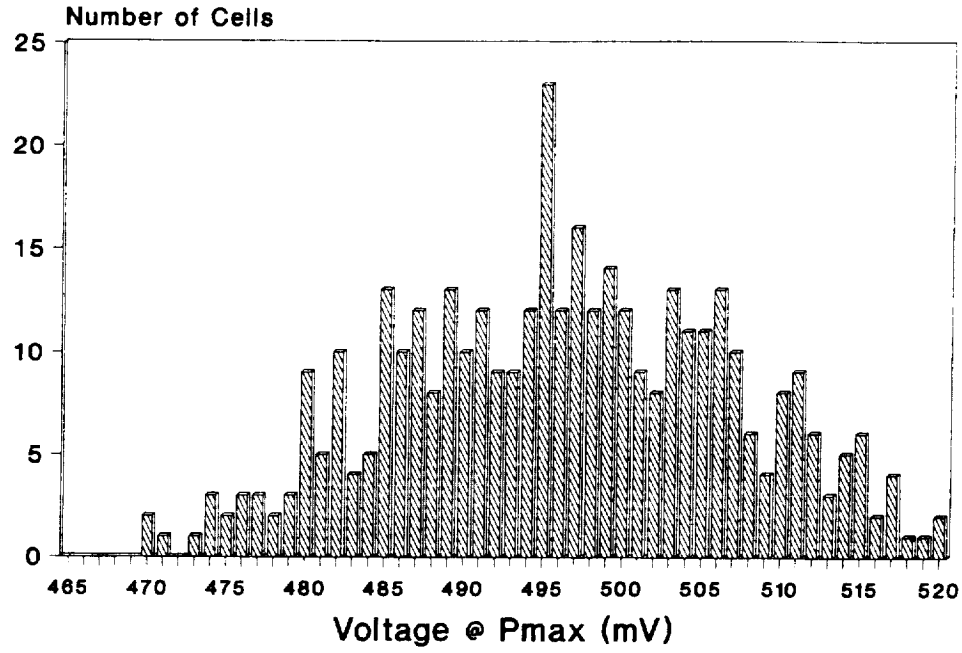

Figure 4-4 Vmp DISTRIBUTION OF FIRST 382 FILTERED CELL ASSEMBLIES DELIVERED TO NASA LeRC

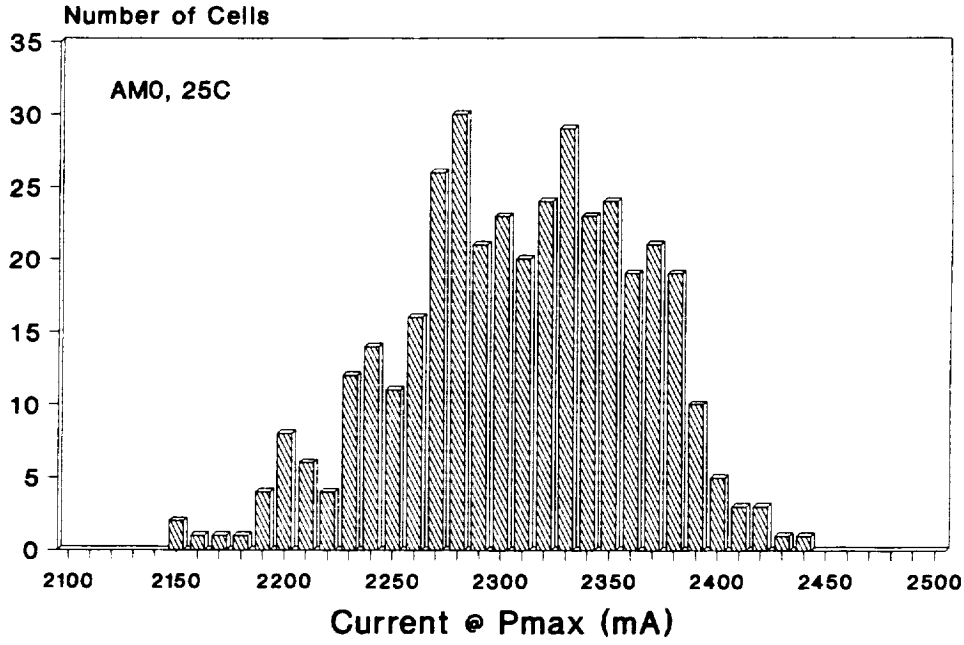

Figure 4-5 Imp DISTRIBUTION OF FIRST 382 FILTERED CELL ASSEMBLIES DELIVERED TO NASA LeRC

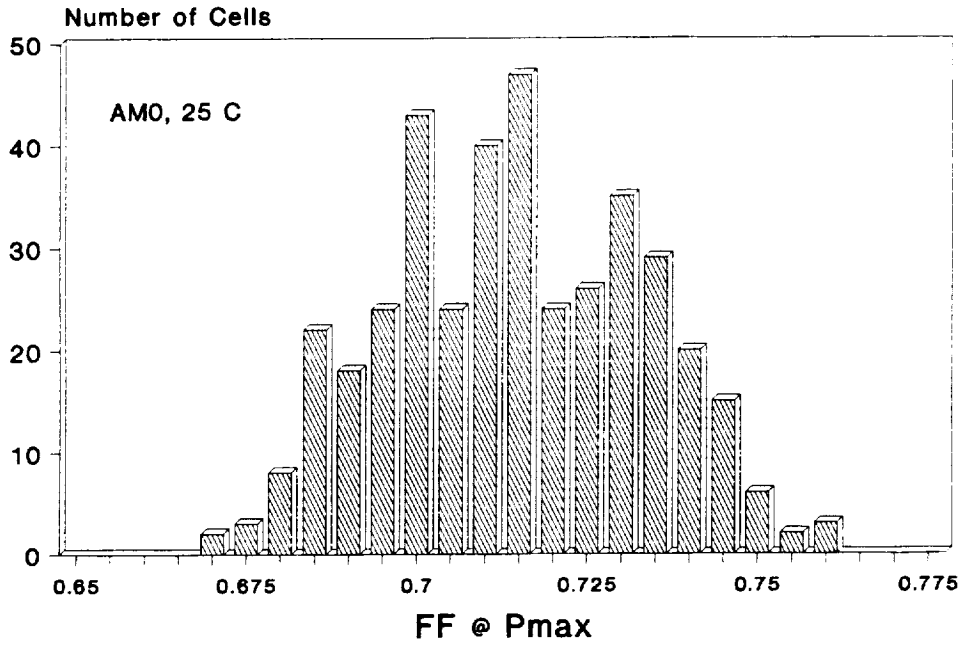

Figure 4-6 FF DISTRIBUTION OF FIRST 382 FILTERED CELL ASSEMBLIES DELIVERED TO NASA LeRC

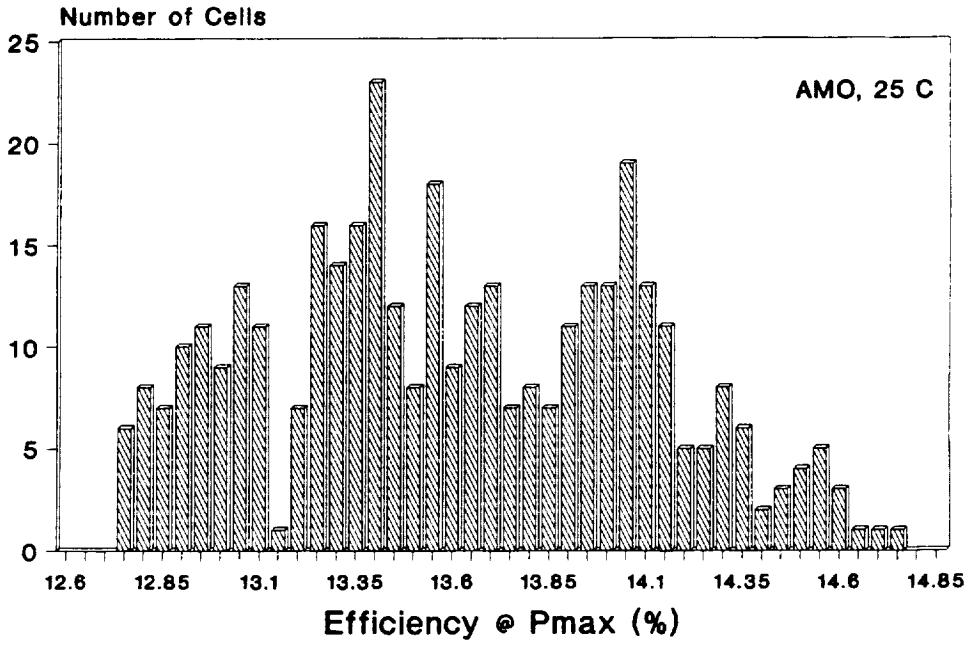

Figure 4-7 EFFICIENCY @ Pmax DISTRIBUTION OF FIRST 382 FILTERED CELL ASSEMBLIES DELIVERED TO NASA LeRC

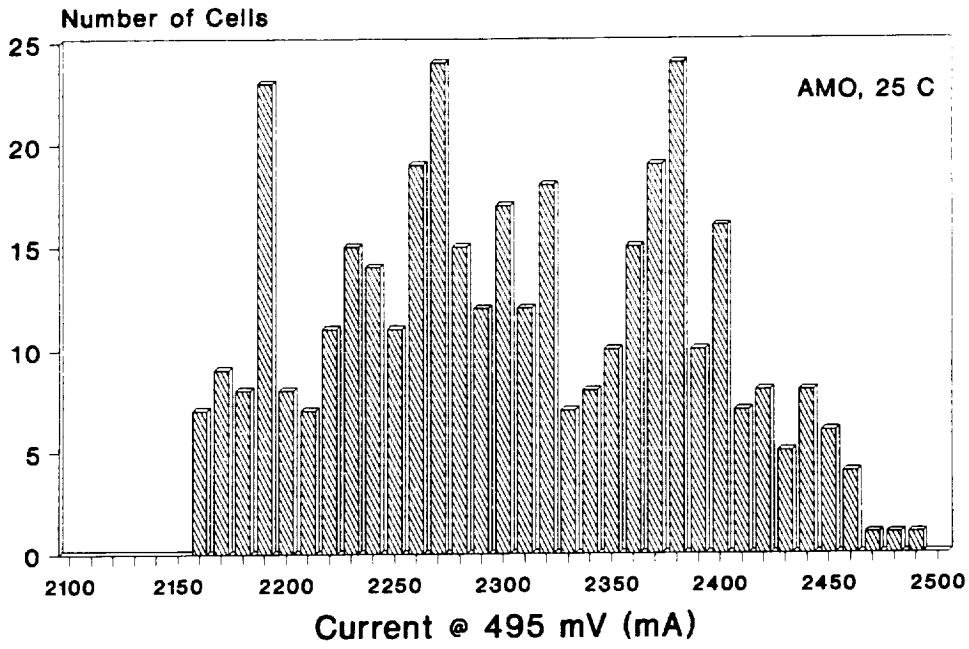

Figure 4-8 I @ 495 mV DISTRIBUTION OF FIRST 382 FILTERED CELL ASSEMBLIES DELIVERED TO NASA LeRC

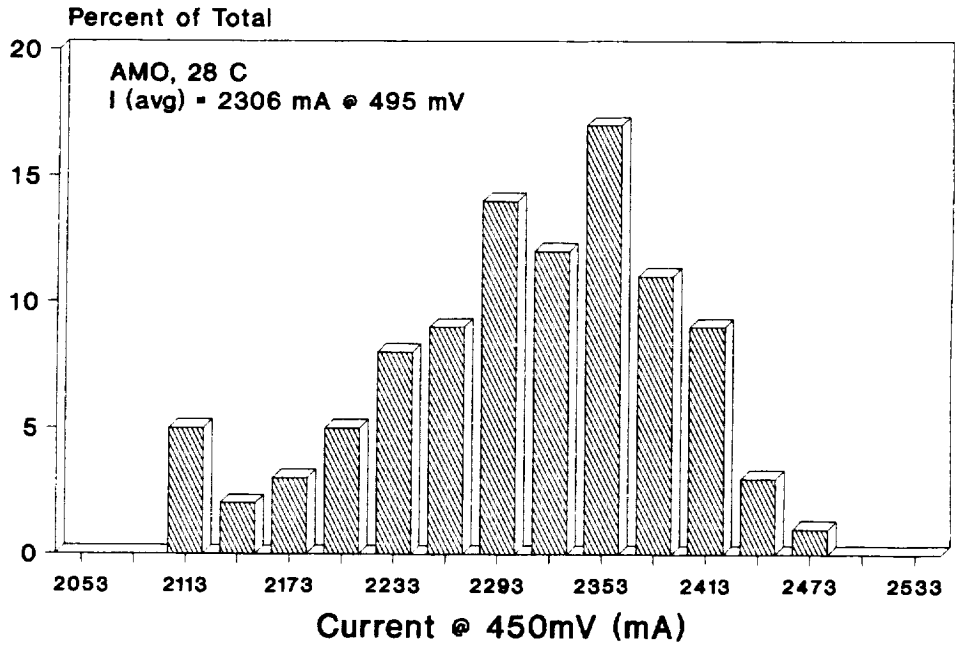

Figure 4-9 I @ 495 mV DISTRIBUTION OF FINAL 205 FILTERED CELL ASSEMBLIES DELIVERED TO NASA LeRC